Earth-Science Reviews 217 (2021) 103609

Contents lists available at ScienceDirect

Earth-Science Reviews

journal homepage: www.elsevier.com/locate/earscirev

Review Article

Cenozoic uplift and erosion of the Norwegian Barents Shelf – A review

Amando P.E. Lasabuda [a,*], Nora S. Johansen [b,1], Jan Sverre Laberg [c,a], Jan Inge Faleide [a,d,e], Kim Senger [f,a], Tom Arne Rydningen [c], Henry Patton [g], Stig-Morten Knutsen [h,a], Alfred Hanssen [c,a]

[a] ARCEx – Research Centre for Arctic Petroleum Exploration, Department of Geosciences, UiT – The Arctic University of Norway, Tromsø, Norway
[b] Department of Geoscience and Petroleum, Norwegian University of Science and Technology (NTNU), Trondheim, Norway
[c] Department of Geosciences, UiT – The Arctic University of Norway, Tromsø, Norway
[d] Department of Geosciences, University of Oslo, Oslo, Norway
[e] CEED – Centre for Earth Evolution and Dynamics, Department of Geosciences, University of Oslo, Oslo, Norway
[f] Department of Arctic Geology, The University Centre in Svalbard (UNIS), Longyearbyen, Norway
[g] CAGE – Centre for Arctic Gas Hydrate, Environment and Climate, Department of Geosciences, UiT – The Arctic University of Norway, Tromsø, Norway
[h] The Norwegian Petroleum Directorate (NPD), Harstad, Norway

ARTICLE INFO

Key words:
Cenozoic
Uplift
Erosion
Barents Shelf
Tectonic
Glacial

ABSTRACT

Uplift and erosion are complex phenomena in terms of their governing processes, precise timing and exact magnitude. The intricate relationship between different geodynamic processes leading to uplift may increase uncertainties in estimating spatial and temporal patterns. Sediment distribution from uplifted (and eroded) topography and the corresponding paleoenvironmental reconstructions require reliable constrains. The Barents Shelf provides a unique arena to study uplift and erosion due to extensive seismic and well data attributed to high petroleum activity. This particular interest has led to a voluminous literature about this topic over the last three decades. Here, we present the current status of the Cenozoic uplift and erosion on the Norwegian Barents Shelf by reviewing the key terminology, its tectonic history and paleoenvironment, methods in quantifying uplift and erosion, as well as timing and possible mechanisms. Our new erosion maps show an increase in net erosion to the north and northeast that represents key underlying concepts, including tectonic (compression, rift-flank uplift, thermo-mechanical coupling, mantle dynamics, flexural/isostatic response) as well as magmatic and glacial processes. We have integrated pre-glacial and glacial net erosion using the mass balance method and added our results from sonic velocity, interval velocity and sandstone diagenesis methods to the new maps. This review shows that discrepancies of net erosion estimates from different methods are on the order of 500 m. Finally, we identify research gaps for future studies, with implications for the Barents Shelf and other uplifted basins worldwide.

1. Introduction

Uplift and erosion are complex phenomena across geological time-scales in terms of their governing processes, precise timing and exact magnitude. Their simplified relation is linked to the creation of topography and removal of sediments (Fig. 1). Orogenic processes are considered as the primary driving forces for km-scale uplift (e.g. the Alps and the Himalayas). Larger-scale regional uplift may result from mantle dynamic topography (e.g. Carminati et al., 2009; Carminati and Doglioni, 2010). Formation of intraplate inversion structures is still debated. They may be associated with plate kinematics (e.g. Gac et al., 2020; Stephenson et al., 2020), far-field stresses attributed to mid-oceanic ridge formation (e.g. Mosar et al., 2002), metamorphic phase changes (e.g. Indrevær et al., 2018), mantle dynamics or a combination of different processes. Glacial dynamics play a role in isostatic uplift, specifically through processes of repeated high-magnitude crustal loading and unloading, i.e. glacial erosion on the shelf and glacial sediment deposition in the basins.

In the source-to-sink framework, uplifted topographic structures are regarded as source areas for erosional products, which are transported to

* Corresponding author:
E-mail address: amando.lasabuda@uit.no (A.P.E. Lasabuda).
[1] Present address: AkerBP, Oslo, Norway.

https://doi.org/10.1016/j.earscirev.2021.103609
Received 11 October 2020; Received in revised form 18 March 2021; Accepted 19 March 2021
Available online 23 March 2021

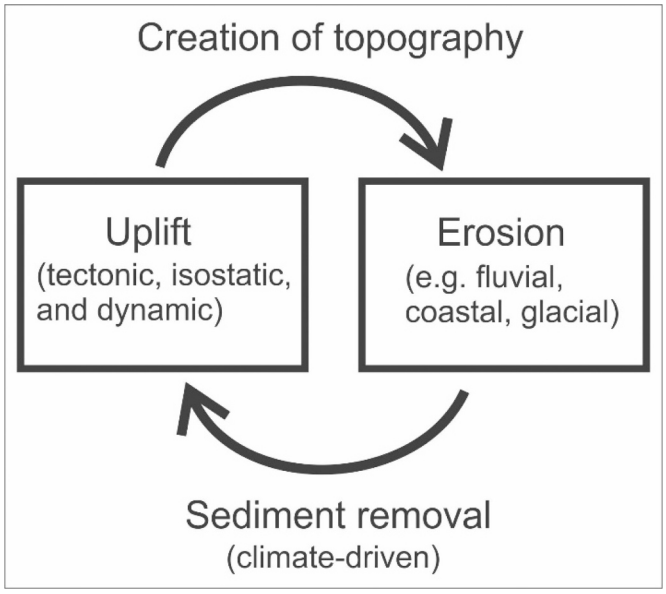

Fig. 1. Conceptual relationships between uplift and erosion. The creation of topography driven by tectonics, isostatic compensation or mantle dynamics is subjected to erosion through fluvial, coastal, or glacial processes. The corresponding sediment removal regulated by climate variations may lead to tectonic, isostatic and dynamic uplift.

sedimentary basins along the continental margin as well as adjacent oceanic basins. Erosion occurs by fluvial, coastal or glacial processes (Fig. 1), whose rates are often linked to the tectonic setting (e.g. Sømme et al., 2009a), bedrock character of the source area (e.g. Dowdeswell et al., 2010b) and climatic variations (e.g. Cook et al., 2020). On the Barents Shelf, the main challenge of Cenozoic source-to-sink analyses is the reconstruction of the likely source areas due to active plate movements. Landscape evolution resulting from uplift and erosional processes has had important paleoclimatic implications in Scandinavia, including the creation of topographic highlands, interpreted to have acted as ice-sheet nucleation areas (e.g. Kleman and Stroeven, 1997; Knies and Gaina, 2008; Medvedev and Hartz, 2015). Moreover, uplift of the Tibetan plateau and the positive feedbacks initiated by this event may have influenced global cooling and the growth of large continental ice sheets in the Cenozoic (Raymo and Ruddiman, 1992).

Numerous sedimentary basins worldwide have experienced uplift and many of them hold significant petroleum potential (e.g. the Barents Shelf basins offshore Norway and Russia (Fig. 2a), the Porcupine Basin in Ireland, the Western Canada Basin in Canada, the Permian Basin in the USA, the Maracaibo Basin in Venezuela, the Zagros Foreland Basin in Iran, the Junggar Basin in China and the Timan-Pechora Basin in Russia) (Doré and Jensen, 1996; Bird et al., 2008; Henriksen et al., 2011a). Major challenges for petroleum exploration in these areas, including the Barents Shelf, have been attributed to the effects of uplift and erosion on the petroleum system elements. These include hydrocarbon (re)migration to shallower traps, lower sealing capacity due to thinner overburden, fault re-activation, poor reservoir quality due to previous deep burial, and changes in hydrocarbon phase, i.e. from oil to gas as shown from the predominance of gas discoveries on the Barents Shelf (e.g. Doré and Jensen, 1996; Japsen et al., 2010; Henriksen et al., 2011a; Fjeldskaar and Amantov, 2018; Løtveit et al., 2019).

The Barents Shelf, with an average water depth of ~200 m, also includes the exposed Svalbard archipelago (Fig. 2a). The Barents Shelf experienced episodic uplift and erosion as a result of early – middle Cenozoic tectonism, followed by repeated glaciations during the late Cenozoic (e.g. Eldholm et al., 1987; Vågnes and Amundsen, 1993; Breivik et al., 2003; Faleide et al., 2008; Ohm et al., 2008; Henriksen et al., 2011b; Piepjohn et al., 2016; Fjeldskaar and Amantov, 2018; Lundin and Doré, 2018; Medvedev et al., 2018). Although research on uplift and erosion of the Barents Shelf is relatively well-established (e.g. Vorren et al., 1991; Nyland et al., 1992; Riis, 1992; Løseth et al., 1993; Richardsen et al., 1993; Faleide et al., 1996; Fiedler and Faleide, 1996; Hjelstuen et al., 1996; Dimakis et al., 1998; Cavanagh et al., 2006; Dörr et al., 2013; Zattin et al., 2016; Zieba et al., 2016; Ktenas et al., 2017; Hjelstuen and Sejrup, 2020), there are still large variations in the magnitude of predicted uplift and erosion between different methods, including their main source of errors (e.g. Riis and Fjeldskaar, 1992; Ohm et al., 2008; Henriksen et al., 2011a; Laberg et al., 2012; Baig et al., 2016; Amantov and Fjeldskaar, 2018; Lasabuda, 2018; Ktenas et al., 2019). There is also uncertainty on the controlling mechanisms responsible for the uplift episodes on the Barents Shelf, as well as the greater NE Atlantic and the circum-Arctic region (e.g. Japsen and Chalmers, 2000; Doré et al., 2002; Anell et al., 2009; Green and Duddy, 2010; Doré et al., 2016; Nikishin et al., 2019).

The Barents Shelf is a data-rich example of an uplifted petroleum province. Seismic data acquisitions are rather continuous and exploration drilling activities are relatively high in the area opened for petroleum activities on the Barents Shelf. This has added valuable insights to the subsurface structural mapping, patterns of basin infilling, and regional stratigraphic control on the evolution of the region. By integrating observations from new data, we may refine the magnitude of uplift and erosion as well as calibrate existing knowledge. For example, pre-glacial and glacial uplift and erosion concepts can be used to better constrain the episodes and possible mechanisms of uplift and erosion, which can be applied in glaciated basins with Cenozoic uplift elsewhere. Moreover, apart from the traditional methods for estimating uplift and erosion on the Barents Shelf (e.g. sonic velocity, vitrinite reflectance and mass balance), there are also a few emerging methods, such as using porosity and resistivity data derived from logs. A better quantification of uplift and the magnitude of net erosion, as well as their spatiotemporal variations, will lead to better constraints for basin modelling and reduced uncertainties related to petroleum exploration.

The aims of this study are the following:

(1) Review the current state of research into the topic of Cenozoic uplift and erosion on the Barents Shelf, by comparing the various methods applied and their uncertainties.
(2) Combine the Cenozoic pre-glacial and glacial net erosion from the mass balance method to calculate the total Cenozoic net erosion.
(3) Present and evaluate three methods based on physical properties to quantify net uplift and erosion, i.e. the sonic velocity, interval velocity and sandstone diagenesis methods based on the studied wells (Fig. 2b). The results from these three methods are combined and averaged.
(4) Create an updated compilation map of the spatial pattern and magnitude of net erosion and review the possible mechanisms of uplift and erosion, as well as their timing and changing rates through time.
(5) Identify critical research directions to address remaining uncertainties in this field.

2. Terminology

The terminology related to uplift and erosion, as adopted here, follows Riis and Jensen (1992), Doré et al. (2002) and Corcoran and Doré (2005). The term *uplift* is commonly preferred for a positive change in surface elevation (increasing height) relative to a datum, and *subsidence* for the opposite effect (Riis and Jensen, 1992; Doré and Jensen, 1996). *Exhumation* can be used more loosely to describe uplift by any means and is often associated to loss of mass or volume (Doré et al., 2002). *Surface uplift* is defined as the positive difference between the paleoelevation of a surface from the onset to the termination of uplift, and can occur due to relatively 'shallow' tectonics (e.g. thin-skinned deformation). On the other hand, *crustal uplift* focuses on the upward movement of volumes of

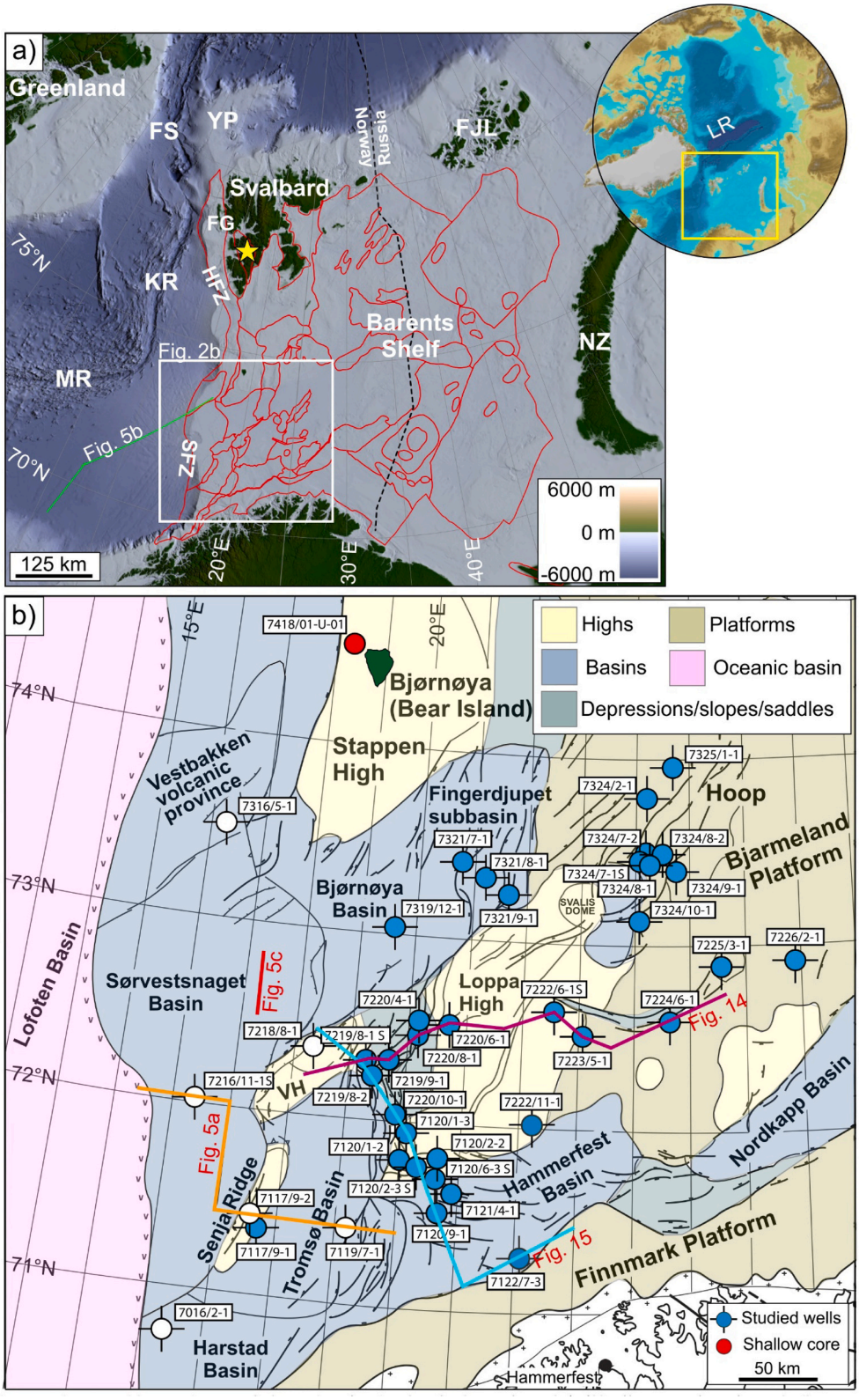

Fig. 2. a) Regional map of the Barents Shelf. Bathymetry is modified from IBCAO v.4.0 Jakobsson et al. (2020). Structural elements as shown in red lines are adapted from the Norwegian Petroleum Directorate (NPD, 2020). The dashed line marks the political boundary between Norway and Russia. The star marks the location of the outcrop in Fig. 6c. b) Structural elements (coloured according to Henriksen et al., 2011b) and the location of well data used in this study are shown. Transects 1 and 2 are shown in violet and blue, respectively. We follow the formal nomenclature of structural elements on the Barents Shelf by the Norwegian Petroleum Directorate (Gabrielsen et al., 1990). Abbreviations used: FG: Forlandsundet Graben; FJL: Franz Josef Land; FS: Fram Strait; HFZ: Hornsund Fault Zone; KR: Knipovich Ridge; LB: Lofoten Basin; LR: Lomonosov Ridge; MR: Mohn Ridge; NZ: Novaya Zemlya; SFZ: Senja Fracture Zone; VH: Veslemøy High; YP: Yermak Plateau.

rocks and may be related to deeper tectonic processes (i.e. thermal effects including thinning of the lithosphere and isostasy associated with glacial rebound or the effect of sediment removal) (Doré et al., 2002).

Crustal uplift is somewhat synonymous to *net uplift* in the context of hydrocarbon exploration. *Net uplift* is regarded as the difference between the maximum burial depth of a marker horizon and its present depth (Riis and Jensen, 1992; Doré and Jensen, 1996) (Fig. 3). Meanwhile, *gross uplift* is the difference between the maximum burial depth and the depth prior to reburial.

It is important to note that maximum burial does not always correspond to maximum subsidence. Maximum burial is the maximum overburden over a marker bed, while maximum subsidence is the

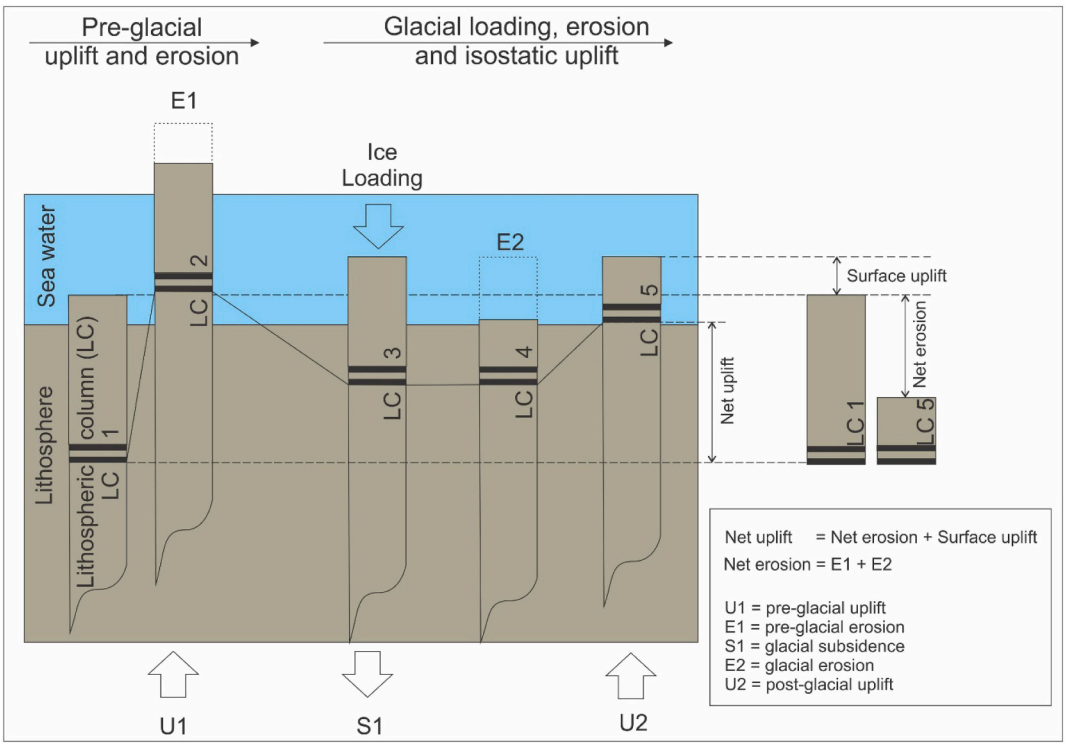

Fig. 3. Concepts of pre-glacial and glacial uplift and erosion in terms of lithospheric columns. The double black lines represent a reference point. LC: Lithospheric column; U: Uplift; E: Erosion; S: Subsidence. In this figure, the lithosphere is overlain by sea water. LC1 represents the initial condition. LC2 shows the occurrence of pre-glacial uplift (U1) resulting in pre-glacial erosion (E1). LC3 represents the glacial conditions where ice loads the column. This condition results in glacial subsidence (S1). Note that the glacial part repeats itself in several cycles. LC4 shows the corresponding glacial erosion (E2). LC5 represents the present-day condition after isostatic uplift (U2) took place. Figure is modified from Dimakis et al. (1998).

maximum depth of the bed (Riis and Jensen, 1992). A given marker bed may be presently at maximum subsidence, but not at maximum burial depth due to erosion, which may take place without major uplift. An example for this erosion is subglacial erosion (erosion that occurs below an ice sheet). In contrast, a given marker bed may be at maximum burial but not at maximum subsidence, due to the fact that uplift may occur without (or very little) erosion, such as uplift of the seabed in the marine realm (i.e. under water).

Erosion is defined as a decrease in the thickness of overburden, which can occur under water, subaerially or subglacially, and it may be episodic or constant (England and Molnar, 1990). The term *erosion* may be used when only considering surface sediment removal, while *denudation* is often used to consider mass lost due to surface and subsurface sediment removal processes (i.e. including chemical dissolution such as karstification) and commonly used in a thermal frame of reference (Doré et al., 2002). *Net erosion* is the difference between net uplift and surface uplift (Fig. 3) and does not consider individual episodes of erosion or deposition (Riis and Jensen, 1992; Henriksen et al., 2011a).

The relation between net uplift, net erosion and surface uplift is described in Eq. (1) below:

$$\text{Net uplift} = \text{Net erosion} + \text{Surface uplift} \quad (1)$$

Both types of uplift may be contemporaneous to erosion. The net effect and magnitude of the episodes of surface uplift of sediment source areas, subsidence of the area(s) of deposition (the sink), and ice loading/unloading and its spatial and temporal variation on the Barents Shelf and surrounding land areas are, however, still poorly constrained.

In this study, we use the term *uplift* to avoid confusion with other, more specific, terms of uplift. We also prefer the term *net erosion* to reflect the final amount of erosion considering the complex Cenozoic erosion history on the Barents Shelf. When applicable, we use the term *erosion* to express the process *per se*. Note that some workers use the term *exhumation* to 'integrate' both processes, i.e. uplift and erosion on the Barents Shelf (e.g. Baig et al., 2016; Ktenas et al., 2019). This review highlights the importance of both of these processes, including the two periods of pre-glacial and glacial uplift as well as the corresponding mean erosion rates.

3. Summary of geological history of the Barents Sea including episodes of uplift and erosion and possible mechanisms

3.1. Pre-breakup period (Cretaceous – Paleocene)

3.1.1. Major tectonic event(s)

In the Early Cretaceous, rifting and subsequent thermal subsidence were responsible for the formation of major basins and the deposition of thick sediment packages along the western margin of the Barents Shelf (Faleide et al., 1993; Kairanov et al., 2018). The northern Barents Shelf was uplifted during this period, associated with thermal doming and the High Arctic Large Igneous Province (HALIP) (Maher and Harmon, 2001; Senger et al., 2014). The Loppa High (see Fig. 2b for location of the structural elements) is also interpreted to have been uplifted in the Early Cretaceous, and this was earlier believed to have been a result of footwall uplift due to a failed episode of rifting (Wood et al., 1989). However, more recent studies show that other mechanisms than footwall uplift (e.g. metamorphic phase changes) are needed to explain the uplift processes of the high (Indrevær et al., 2017, 2018).

The Eurekan Orogeny was initiated during the Late Cretaceous–Paleocene (De Paor et al., 1989; Piepjohn et al., 2016). This megatectonic event incorporated the area from the Canadian Arctic to the Barents Shelf. In the Late Cretaceous, a major episode of uplift and erosion affected a wide part of the Barents Shelf, including Bjørnøya and Svalbard where the Paleocene overlies Aptian–Albian (Lower Cretaceous) strata (Ritter et al., 1996). On Svalbard, apatite fission track

(AFT) studies show that an early period of cooling due to exhumation started in the Late Cretaceous (c. 70 Ma) (Blythe and Kleinspehn, 1998; Dörr et al., 2019).

This regional uplift may be related to tectonic compression of Greenland towards the Barents Shelf (Fig. 4a). These compressions must have caused shortening/inversion of Upper Cretaceous strata in offshore basins, for example in the southwestern Barents Sea (e.g. Sørvestsnaget Basin) or in NE Greenland (the Wandel Sea Basin). Nevertheless, it is not straightforward to trace the evidence of contractional deformation from the Late Cretaceous due to the subsequent prominent Eocene contraction. Compressional signatures of Paleocene age (prior to breakup) have, however, been recorded in East Greenland (Guarnieri, 2015). We highlight the possible role of Late Cretaceous magmatism that may have affected the thermal and vertical movement in a regional scale. This mechanism may be considered as a second phase of HALIP magmatism, which has been documented elsewhere in the circum-Arctic, for example in the North Greenland (Tegner et al., 2011), the Ellesmere Island in Canadian Arctic (e.g. Estrada et al., 2016; Naber et al., 2020) and further north on the Alpha Ridge, Arctic Ocean (e.g. Døssing et al., 2017; Williamson et al., 2019).

3.1.2. *Paleoenvironment*

The sedimentary response to the Early Cretaceous HALIP magmatism is exemplified by the prograding system southwards from Svalbard terminating in the Hoop area (Grundvåg et al., 2017; Kairanov et al., 2018; Marín et al., 2018; Faleide et al., 2019; Midtkandal et al., 2019b). The main source area must have been located north of Svalbard, since Lower Cretaceous sediments are preserved there (Grundvåg and Olaussen, 2017; Grundvåg et al., 2019; Midtkandal et al., 2019a). Thick Lower Cretaceous strata are also observed in the northwest flank of the Bjørnøya Basin, suggesting that the Stappen High was initially part of a sediment depocenter in the Early Cretaceous before being uplifted later in the Paleogene (Blaich et al., 2017). The Loppa High was also an important sediment source area, as represented by the development of

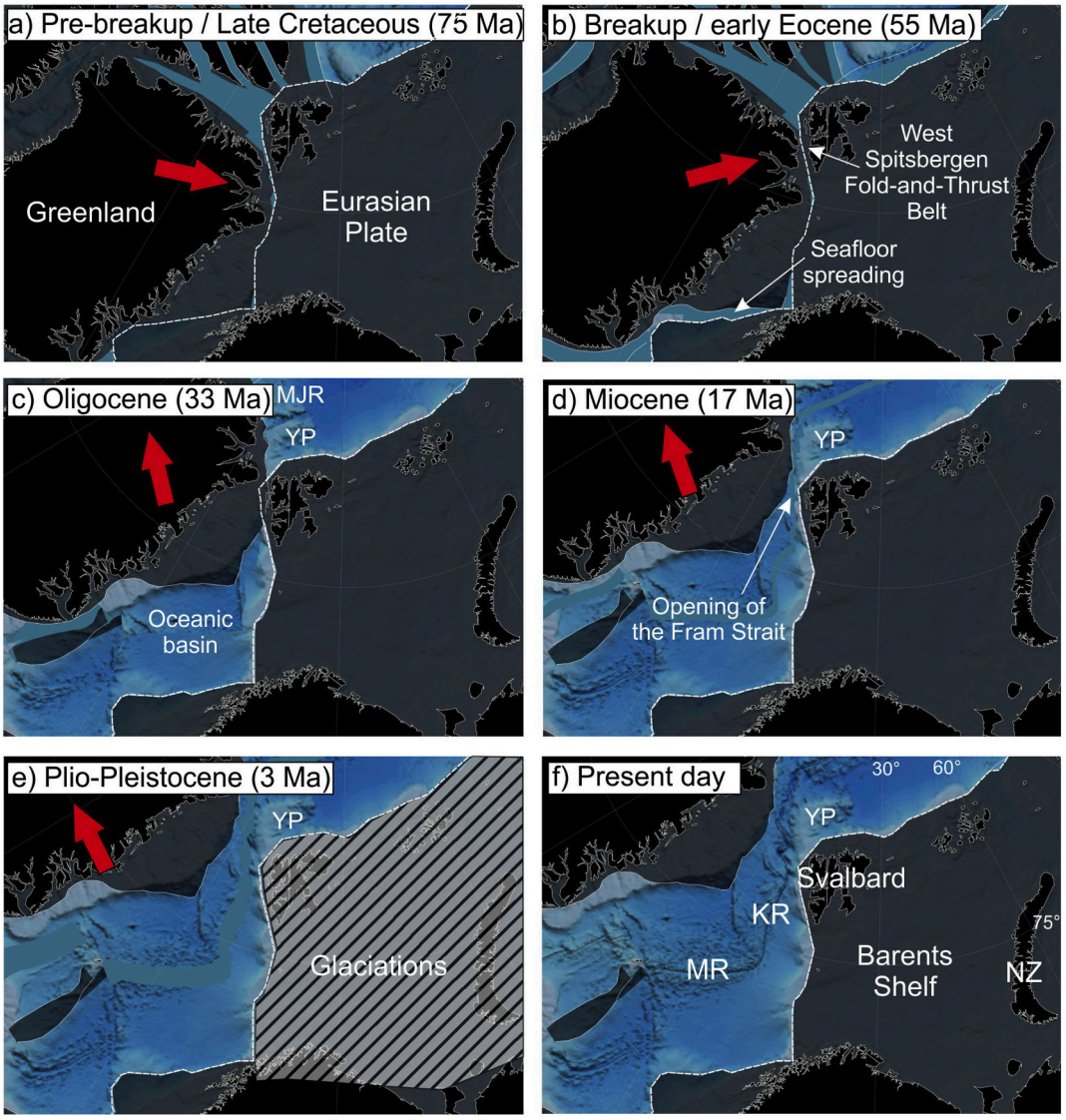

Fig. 4. Plate reconstruction in the study area from the Late Cretaceous to present day. Red arrows represent the overall direction of Greenland relative to a fixed Eurasian Plate, which is used as a reference frame (shown in white dashed line). a) Pre-Cenozoic breakup represented by a plate configuration in the Late Cretaceous (75 Ma). b) Cenozoic breakup/early Eocene (55 Ma) marks the onset of seafloor opening and the formation of the West Spitsbergen Fold-and-Thrust Belt. c) The Oligocene (33 Ma) marks a major plate reorganization. d) The Miocene (17 Ma) plate configuration showing the opening of the Fram Strait, thus allowing ocean circulation between the North East Atlantic and Arctic oceans. e) The Plio-Pleistocene (3 Ma) marks the period of glaciations represented by dashed areas. Note that ice sheets varied spatially and temporally. e) The present day. Abbreviations are as follows; KR: Knipovich Ridge; MJR: Morris Jesup Rise; MR: Mohn Ridge; NZ: Novaya Zemlya; YP: Yermak Plateau. Plate reconstructions are derived from GPlates 2.2 (Matthews et al., 2016; Müller et al., 2019).

canyons, that acted as conduits for submarine slides/fans in the Hammerfest Basin (e.g. Sattar et al., 2017; Harishidayat et al., 2018). Upper Cretaceous strata are mainly observed in the basins along the western continental margin of the Barents Shelf (Fig. 5a) and in the corresponding Wandel Sea Basin in the NE Greenland.

Exploration well data indicate a deep-marine paleoenvironment in the southwestern Barents Sea in the Paleocene (Eidvin et al., 1993; Ryseth et al., 2003; Lasabuda et al., 2018a). The area north of Bjørnøya and NE Greenland may have been a key Paleocene source area based on a recent paleogeographical reconstruction (Lasabuda et al., 2018b). Some low-angle clinoforms are observed prograding into the Hammerfest Basin (Knutsen and Vorren, 1991; Prøis, 2015) leaving two possible sediment routing scenarios; from the northern, uplifted paleo-Svalbard-northern Barents Shelf area or from a more local source on the Loppa High and the adjacent Bjarmeland Platform (Fig. 2b).

3.2. Breakup period (Eocene)

3.2.1. Major tectonic event(s)

The rifting and sea-floor spreading following breakup in the Norwegian–Greenland Sea may have initiated tectonic (rift-flank) uplift and flexure of the crust, i.e. uplift during this period has been attributed to the geodynamic evolution between the Greenland and the Eurasian plates (Fig. 4b). The onset of spreading has been estimated based on magnetic polarity reversals and is correlated to Magnetic Anomaly 24, c. 55 Ma (Talwani and Eldholm, 1977). The western margin of the Barents Shelf shows a segmented transform development as part of the broad scale *De Geer Zone* development (Faleide et al., 1993). The development of this mega-shear zone appears to be concurrent with the main Eurekan deformation in this period which also affected Greenland and the Ellesmere Islands (Doré et al., 2016; Piepjohn et al., 2016).

Rifting and sea-floor spreading was also initiated in the Arctic Ocean in the Eocene (Karasik, 1968; Vogt et al., 1979; Minakov et al., 2012; Berglar et al., 2016; Lutz et al., 2018), and here it has been suggested to have started somewhat earlier, corresponding to Magnetic Anomaly 25 at c. 57 Ma (Brozena et al., 2003). The continuous rifting led to the separation of the Lomonosov Ridge (Fig. 2a) from the northern Barents Shelf continental margin (Jokat et al., 1992), leaving a very sharp transition between the near-normal thicknesses of continental and oceanic crust (Minakov et al., 2012; Berglar et al., 2016; Lundin and Doré, 2018). The spreading and tectonic uplift including flexure of the crust may have initiated uplift of the whole segment from Svalbard to Franz Josef Land. Magmatic activity has been observed in the stretched continental margin such as the Yermak Plateau and onshore Svalbard,

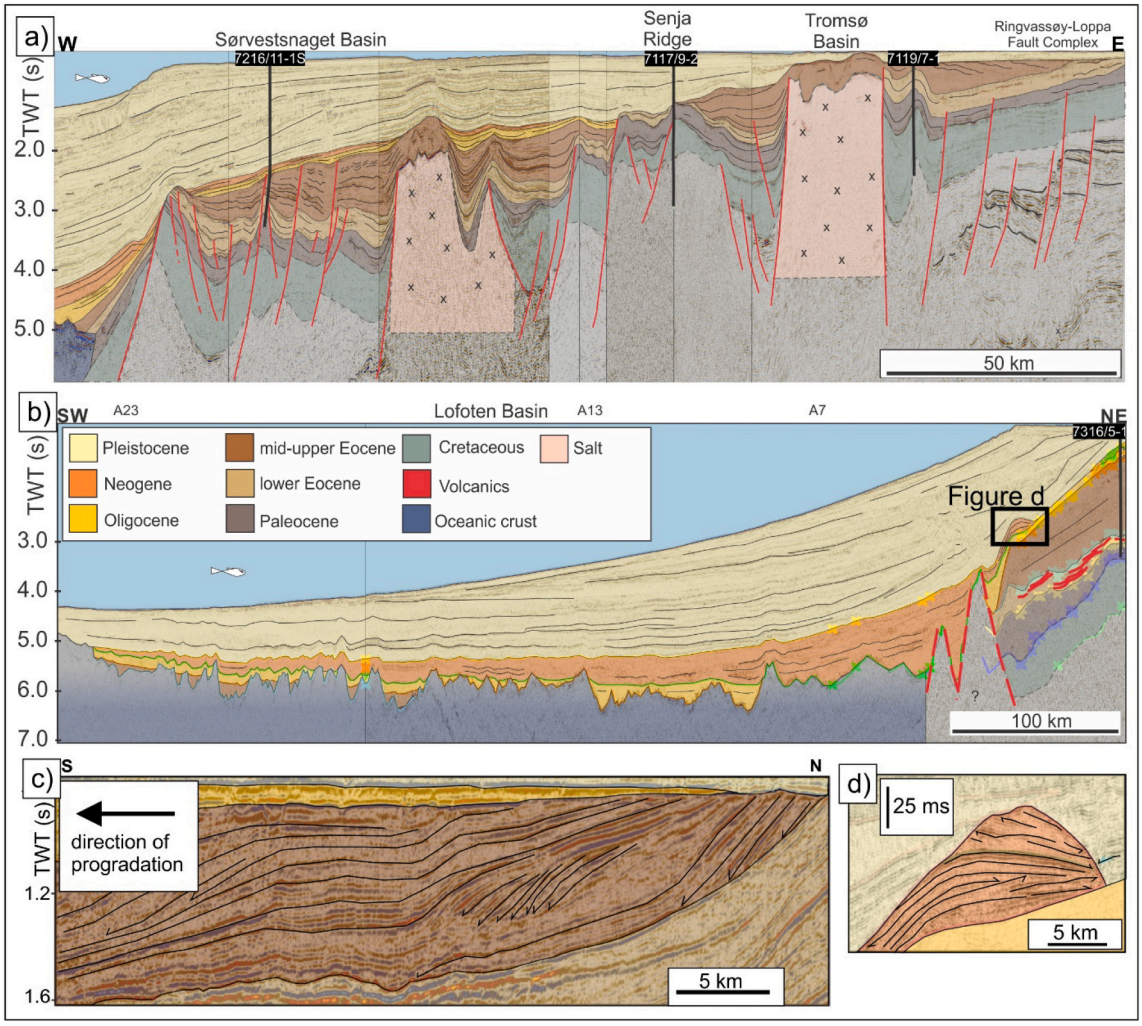

Fig. 5. a) E-W geoseismic profile showing the Cenozoic strata in the southwestern Barents Sea area (modified from Lasabuda et al., 2018b). b) NE-SW geoseismic profile showing pre-glacial Cenozoic strata directly deposited on the oceanic crust and overlain by the thick glacigenic sediments of the Bjørnøyrenna TMF (modified from Lasabuda et al., 2018b). c) N-S Geoseismic profile showing the middle Eocene sediment progradation in the Sørvestsnaget Basin (modified from Safronova et al., 2014). AAPG © (2014). Reprinted by permission of the AAPG, whose permission is required for further use. d) Zoom-in geoseismic in figure (b) showing the interpretation of contourites (modified from Rydningen et al., 2020). See Fig. 2a and b for location.

although more precise dating is needed for the Cenozoic volcanism (Senger et al., 2014).

The western Barents Shelf continental margin was governed by transpression, extension and transtension (Nøttvedt et al., 1988; Faleide et al., 2008). The northern part of the margin is characterized by the shear-dominated Hornsund Fault Zone (Fig. 2a). The southern part of the margin, the Senja Fracture Zone, is a shear-dominated segment with evidence of transtension (e.g. Kristensen et al., 2018). Between these two segments, the Vestbakken volcanic province formed as a pull-apart basin (Faleide et al., 2008).

Seismic data from the western margin of Svalbard show a complex tectonic development, including the formation of the Forlandsundet Graben (Steel et al., 1985; Gabrielsen et al., 1992; Blinova et al., 2009). The early Cenozoic breakup, linked to the Eurekan deformation, also included a transpression-compression component that was responsible for the West Spitsbergen Fold-and-Thrust Belt development (Braathen et al., 1995; Bergh et al., 1997; Leever et al., 2011; Blinova et al., 2012, 2013; Dallmann, 2015; Piepjohn et al., 2016), which possibly extends further south towards the Stappen High (Bergh and Grogan, 2003; Lasabuda et al., 2018b). The main uplift event of the Stappen High (southwest of Bjørnøya forming the northwest flank of Bjørnøya Basin) was in the Paleogene (Blaich et al., 2017) and may have been affected by the igneous activity in the Vestbakken volcanic province (Fig. 5b). Modelling results incorporating thermo-mechanical coupling are best explained by uplift along the Senja Fracture Zone (Vågnes, 1997).

Northern Scandinavia was also affected by a phase of uplift in the Late Cretaceous to Paleogene time (Hendriks and Andriessen, 2002), from rift-flank (Torske, 1972) or footwall uplift (Redfield and Osmundsen, 2013) during the initial development of a passive continental margin. Maximum uplift is estimated to be almost 1500 m (Riis, 1996) and was probably continuous throughout the Cenozoic (Carminati et al., 2009).

3.2.2. Paleoenvironment

The western Barents Sea was characterized by deep-marine conditions surrounded by coastal to shelf areas. Sandy turbidite fans are reported at the distal part of a sediment progradation system in the Sørvestsnaget Basin (Fig. 5c; Ryseth et al., 2003; Safronova et al., 2012, 2014). These fans are the product of sediment transport by turbidity currents that transported coarse-grained sediments to the basin-floor (Fig. 6a). A series of sandy fans has also been encountered in well 7316/5-1 (Eidvin et al., 1998), though such features are absent in the area of well 7016/2-1 in the Harstad Basin (Blaich et al., 2017). Conglomerates are documented from a shallow core northwest of Bjørnøya by Eikelmann (2017), suggesting the sediment source area was in close vicinity (Fig. 6b). The Stappen High and the Loppa High might have been prominent sediment source areas, with a possible contribution also from mainland Norway, which was affected by uplift at this time (Torske, 1972; Redfield and Osmundsen, 2013). The uplifted western Svalbard margin acted as the main sediment source for the Central Basin on Svalbard (Helland-Hansen, 2010; Petersen et al., 2016), where a sandy turbidite succession overlies predominantly shale deposits as reported by Helland-Hansen and Grundvåg (2020) (Fig. 6c).

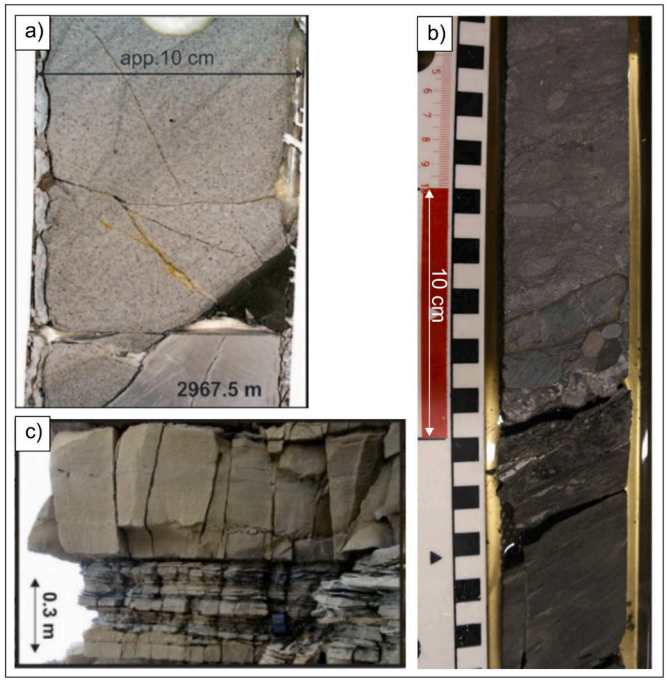

Fig. 6. Eocene rocks from the Barents Shelf. a) Middle Eocene turbidite sand from well 7216/11-1S in the Sørvestsnaget Basin (adapted from Safronova et al., 2014). AAPG © (2014). Reprinted by permission of the AAPG whose permission is required for further use. See Fig. 2b for location. b) Upper Paleocene–lower Eocene conglomerates at 89.2 m depth from shallow borehole 7418/01-U-01, northwest of Bjørnøya (adapted from Eikelmann, 2017). See Fig. 2b for location. c) Eocene turbidite succession from the Central Basin, Svalbard showing thick, massive sands overlying predominantly shale deposits (adapted from Helland-Hansen and Grundvåg, 2020). See Fig. 2a for location.

3.3. Post-breakup period

3.3.1. Oligocene

3.3.1.1. Major tectonic event(s). The post-Eurekan is defined from the Oligocene onwards (Piepjohn et al., 2016) when a major plate reorganization occurred in the earliest Oligocene (at Magnetic Anomaly 13, c. 33 Ma) (Talwani and Eldholm, 1977). The most likely preconditioning factor for uplift during this period was when Greenland started to move in the same direction as the North American plate (Fig. 4c). This event marked the onset of passive and oblique spreading after the occurrence of transform margin along the whole length of the western Barents Shelf. To the north, the Yermak Plateau separated from its counterpart, the Morris Jesup Rise, sometime in the Oligocene, probably also at Magnetic Anomaly 13, c. 33 Ma (Fig. 4c; Jackson et al., 1984; Kristoffersen et al., 2020).

On Svalbard, a period of cooling/exhumation (35–25 Ma) is indicated based on AFT data (Blythe and Kleinspehn, 1998). Mantle rise and lithospheric thinning contributed to the exhumation of Svalbard at around this period (Vågnes and Amundsen, 1993). Paleobathymetry modelling suggests that the western part of Barents Shelf was uplifted in the Oligocene (Straume et al., 2020). Moreover, volcanism has been reported in the Vestbakken volcanic province (Faleide et al., 1988). The main controlling mechanisms of uplift in the Oligocene remain unclear, although it may be related to deeper mantle processes (*sensu* Vågnes and Amundsen, 1993; Minakov, 2018). The eastwards shifting of depleted asthenosphere beneath continental Europe (Carminati et al., 2009) may have also affected the Barents Shelf. Some local inversion structures and domes in other parts of the Norwegian continental shelf have been attributed to ridge push and far-field stresses from the mid-oceanic ridge during this plate reorganization (e.g. Mosar et al., 2002).

3.3.1.2. Paleoenvironment. A major plate reorganization in the Oligocene was likely responsible for structural inversion observed in the Sørvestsnaget Basin and Vestbakken volcanic province (Blaich et al., 2017; Lasabuda et al., 2018b). Further north along the margin, the onset of rifting may have caused footwall uplift that affected offshore and onshore areas (Svalbard). The paleoenvironment of the Barents Shelf in the Oligocene is likely to have mainly been a lowland (i.e. low-lying areas such as alluvial plain and fluvial terrace) (Lasabuda et al., 2018b) with a significant marine shallowing in the southwestern Barents Sea area (Fig. 7; Ryseth et al., 2003). The Oligocene source area for the

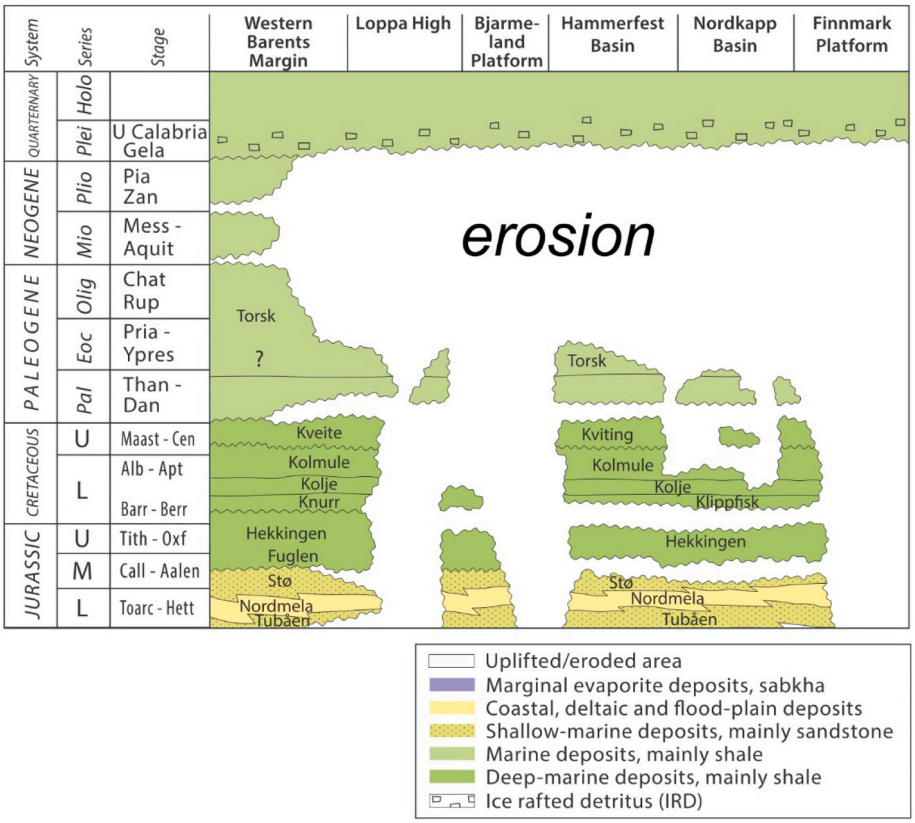

Fig. 7. Lithostratigraphy from the Norwegian Petroleum Directorate (NPD, 2014) for major structural elements in the Barents Sea. Note the Cretaceous Kolmule and Paleogene Torsk formations are used for the sonic and interval velocity methods. The Jurassic Tubåen and Stø formations, used for the sandstone diagenesis method are also shown.

sediments deposited along the western margin is likely towards the east and south, i.e. the Loppa High, Stappen High and mainland Norway.

3.3.2. Miocene

3.3.2.1. Major tectonic event(s). The Miocene marked the opening of the Fram Strait (Fig. 4d), allowing for deep-water exchange between the Arctic and Atlantic oceans (Kristoffersen, 1990; Jakobsson et al., 2007; Engen et al., 2008), although pre-strait seaways have been suggested (Poirier and Hillaire-Marcel, 2011). Neogene volcanic activity is indicated on Svalbard (Prestvik, 1977; Vågnes and Amundsen, 1993; Treiman, 2012), possibly causing the episode of uplift as identified by Harland (1969). Miocene uplift has also been reported on NE Greenland (Døssing et al., 2016). Although this period is inferred to be relatively tectonically quiet along the western Barents Shelf margin (Ryseth et al., 2003), inversion structures are observed in the Vestbakken volcanic province and may be related to far-field ridge-push from the Knipovich Ridge (Gabrielsen et al., 1997; Gac et al., 2016; Giannenas, 2018). In addition, global sea level fluctuations (Haq et al., 1987) and the pattern of regional ocean circulation as established from this time onwards (e.g. Rydningen et al., 2020) might have played a role in controlling sedimentation and erosion in the western and northern Barents Sea area.

3.3.2.2. Paleoenvironment. Contourites have been reported from the western Barents Sea continental margin (e.g. Fig. 5d; Eiken and Hinz, 1993; Rebesco et al., 2013; Gebhardt et al., 2014; Elger et al., 2017; Rydningen et al., 2020), and offshore mainland Norway (e.g. Laberg et al., 1999, 2001, 2005). Contourites in the Fram Strait area continue towards the northern margin of the Barents Shelf (Lasabuda et al., 2018a). These observations show that the western and northern margin were highly influenced by along-slope, ocean current processes from the Miocene and onwards, probably until the present (Fig. 8). The deposition of contourites suggests a slope morphology along the margin. The source area in the Neogene was likely similar to that of the Oligocene.

3.3.3. Pliocene-Quaternary

3.3.3.1. Major event(s). During the Plio-Pleistocene, the glaciations of the northern hemisphere intensified, with ice sheets repeatedly growing to continental sizes over North America, Greenland and Eurasia (Fig. 4e). Earlier periods of glaciation might have existed in the Svalbard area and the northern Barents Shelf (Knies and Gaina, 2008; Knies et al., 2009) and even earlier in the Oligocene–Miocene in East Greenland (Larsen et al., 1994; Eldrett et al., 2007; Tripati and Darby, 2018). Glacial landforms found on, and buried beneath, the present seafloor reflect the dynamic behaviour of the ice sheet during the last glacial (e.g. Andreassen et al., 2008; Patton et al., 2015; Piasecka et al., 2016). Ice sheets repeatedly reached the Barents Shelf edge during full glacial conditions (e.g. Vorren et al., 1989; Laberg and Vorren, 1995, 1996b; Dowdeswell and Cofaigh, 2002). A series of trough mouth fans (TMFs) are located on the Barents Shelf continental margin, comprising sediments eroded from the shelf and transported to the shelf break by fast-flowing ice streams (Vorren and Laberg, 1997). The Bjørnøyrenna (Bear Island) TMF (Vorren et al., 1991; Faleide et al., 1996) and Storfjordrenna TMF (Hjelstuen et al., 1996; Laberg and Vorren, 1996a) are the two largest along the western margin of the Barents Shelf, comprising a total volume of c. 5 x 10^5 km^3.

Uplift during this period is related to glacial isostatic rebound due to the northern hemisphere glaciations and the dynamics of the ice with variable thicknesses and extents. During the glaciations, the crust isostatically adjusted to the changing ice sheet load, responding rapidly over millennial timescales. Furthermore, erosion of the ice sheet led to

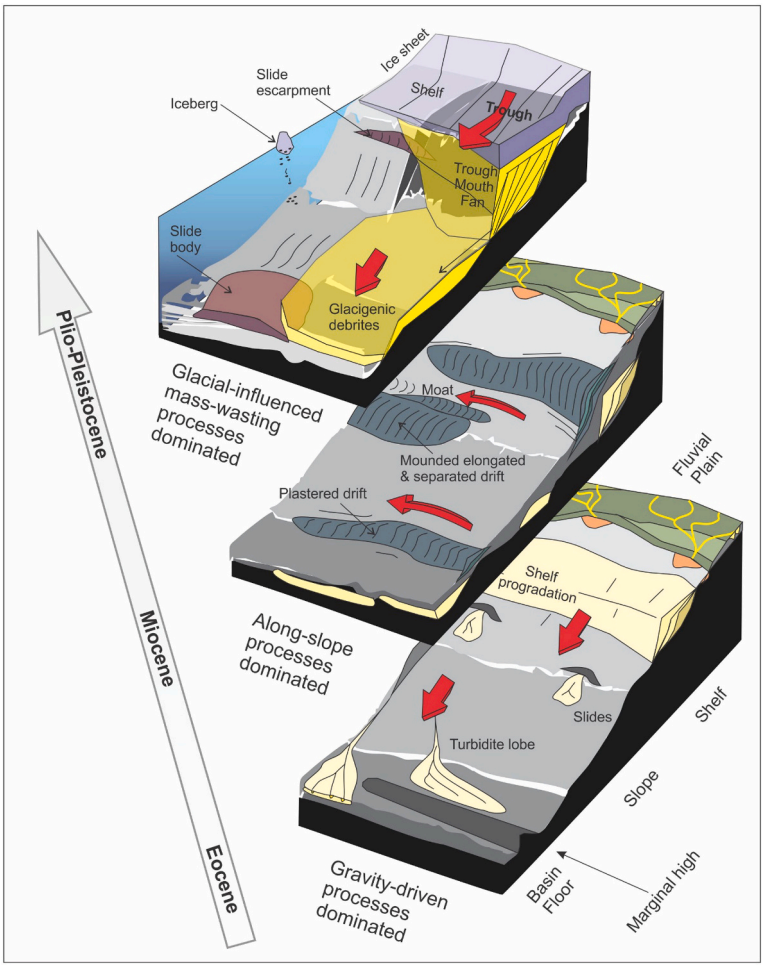

Fig. 8. Three key periods of erosion and sedimentation in the Cenozoic with the dominant sedimentary processes represented by red arrows, and major events along the Barents Sea continental margin.

removal of large amounts of sediments from the shelf that were deposited in TMFs along the slope. From these processes the crust experienced isostatic rebound (uplift) and tilting (e.g. Zieba and Grøver, 2016; Medvedev et al., 2018; Løtveit et al., 2019). However, the heterogeneous rheology of the crust and mantle, i.e. largely thinning from west to east, may have imparted a more complex pattern of uplift on the Barents Shelf (e.g. Klitzke et al., 2015; Auriac et al., 2016; Faleide et al., 2018). On Svalbard, AFT data show a cooling due to exhumation during the past 5 Ma (Blythe and Kleinspehn, 1998; Dörr et al., 2019).

3.3.3.2. Paleoenvironment. During full-glacial conditions, ice streams (the fast-flowing corridors of the ice sheet) and the subglacial hydrological system transported sediments to the shelf break (Fig. 8). These glacigenic sediments are prone to instability due to oversteepening and the build-up of excess pore pressure, eventually causing slope failures (Dimakis et al., 2000; Laberg and Vorren, 2000), which subsequently evolve into debris flows. Glacigenic debris flows are the predominant sediment transport process of the TMFs, which lead to the deposition of glacigenic debrites (e.g. Vorren et al., 1989; King et al., 1996; Laberg and Vorren, 1996b; Dahlgren et al., 2002; Lucchi et al., 2013; Dowdeswell et al., 2016; Laberg et al., 2017). Such debris flows can transfer sediments downslope for 10's to 100's of kms, with individual debris lobes up to a few km in width and up to 50 m thick (e.g. King et al., 1996; Batchelor et al., 2013), and may transform into turbidity currents. Furthermore, meltwater sediment discharges from the ice margin may be responsible for the development of turbidite channel systems within TMFs (e.g. Laberg et al., 2010; Bellwald et al., 2020; Harishidayat et al., 2020).

4. Overview of methods for estimating Barents Shelf uplift and erosion

Reviews of methods for measuring the amount and timing of exhumation, each with their advantages and limitations, have been presented elsewhere (Doré et al., 2002; Corcoran and Doré, 2005; Anell et al., 2009). Here we summarize the methods that have been applied on the Barents Shelf with emphasis on their uncertainties, together with the key references (Table 1). This synthesis categorizes the methods based on stratigraphy, physical properties and numerical modelling.

4.1. Methods based on stratigraphy

Methods based on stratigraphy include the mass balance method, the offshore-onshore correlation of paleosurfaces, and seismic stratigraphic interpretations. These methods generally use seismic data and include a quantification of the eroded intervals/volumes. They may also include a direct correlation of erosion and sedimentation, which can be applied for large areas (regional studies), sometimes in combination with other methods (see below).

4.1.1. Mass balance

The mass balance method is a holistic approach considering erosional, transport and depositional processes of sediments within a source-to-sink framework (Fig. 9a). The amount of erosion in the

Table 1
Methods for quantifying net uplift and erosion applied on the Norwegian Barents Shelf and their main uncertainties.

Methods	Main uncertainties when applied on the Norwegian Barents Shelf	Key references
Mass balance	i) it may be difficult to define the boundary of the source area(s); ii) reworking/redeposition by ocean contour currents may complicate the sediment budgeting, particularly in the basins along the continental margin; iii) it may be complicated to quantify the volume of biogenic input (ooze sediments) in the basin; and iv) compaction-decompaction correction should be applied	Vorren et al. (1991); Fiedler and Faleide et al. (1996); Hjelstuen et al. (1996); Laberg et al. (2012); Lasabuda et al. (2018a, b, c); **this study**
Offshore extrapolation to onshore geomorphic features	i) it requires a long-distance extrapolation; and ii) assumption of thickness may be problematic for areas/depth of limited well control	Riis and Fjeldskaar (1992); Riis (1996)
Seismic stratigraphic interpretation	i) it may be difficult to separate between unconformity from glacial or pre-glacial succession; ii) erosion and redeposition from the last glaciation may complicate the dating of the stratigraphy; iii) it may be challenging in a basin with salt/evaporites (e.g. Nordkapp Basin); iv) it may rely on long-distance extrapolation; and v) the quality of velocity model may influence the time-depth conversion accuracy	Løseth et al. (1993); Corcoran and Doré (2005)
Sonic velocity	i) it requires a consistent reference trend, ideally from a basin with no uplift (presently using the North Sea basin); ii) Paleogene Torsk shales are inconsistent in terms of thickness and quality, therefore relies also on Cretaceous Kolmule Formation; and iii) reburial by glacial sediments may mask the true magnitude of erosion	Vassmyr (1989); Henriksen et al. (2011); Baig et al. (2016); Ktenas et al. (2017, 2019); **this study**
Interval velocity	It may need a combination of two stratigraphic references (e.g. adding BCU or URU horizon) around structural highs as there is a high uncertainty related to the presence of shale interval (e.g. missing Kolmule Formation on the Loppa High)	Løseth et al., 1993; Richardsen et al. (1993); Johansen (2016); Ktenas et al. (2019); **this study**
Shot gathers	i) it may give higher net erosion estimates due to the velocity from shot gathers; ii) it may include higher velocities from deeper strata; and iii) overpressure in the Paleogene strata may complicate the results	Baig et al. (2016)
Resistivity	i) it can be very sensitive to pore fluid content as the presence of conductive brine influences the resistivity more than change in the lithology; ii) resistivity of pore fluid changes with temperature; iii) it requires additional pre-conditioning preparation and further consideration including picking clean shale intervals, and avoiding carbonates and volcanics; and iv) it is relatively a new approach, and may require a calibration from a velocity-based method to estimate the cooling effect	Johansen (2016); Senger et al. (2020)
Porosity	i) it requires corrections if the pore fluid is not salty water; and ii) high pore pressure may complicate the results	Licciardi et al. (2019)
Sandstone diagenesis	i) it requires a number of assumptions in rock mineralogy (e.g. clay content, matrix, quartz cementation); ii) different temperature gradients may influence the erosion estimates; iii) overpressures and differential compaction may affect the net erosion estimates; and iv) it may not be practical for a regional study as it may requires readjustment to different sandstones (Stø and Tubåen formations)	Henriksen et al. (2011); Avseth et al. (2014); Johansen (2016); **this study**
Vitrinite reflectance (VR)	i) it may be difficult to constrain paleotemperature, e.g. Svalbard may have a different geothermal gradient then the rest of the Barents Shelf; ii) in area with igneous intrusion such as Vestbakken volcanic province, VR may be problematic; and iii) reworked glacial sediment may lower the confidence of VR measurement	Manum and Throndsen (1978); Nyland et al. (1992); Løseth et al. (1993); Henriksen et al. (2011a, b); Baig et al. (2016)
Apatite fission track (AFT)	i) it may be problematic in capturing the recent glacial exhumation; ii) it may be sensitive to local temperature change such as igneous intrusion; and iii) it may be difficult to estimate paleo-heat flow and paleotemperature in a recently exhumed (and hence disequilibrium) situation	Løseth et al. (1993); Blythe and Kleinspehn (1998); Green and Duddy (2010); Henriksen et al. (2011a); Hokstad et al. (2017); Dörr et al. (2019)
Numerical modelling (to include isostasy, flexural rigidity and ice sheet erosion)	i) it is often an oversimplification of complex scenarios, in particular deeper tectonic process; ii) it contains uncertainty in the ice-sheet extent, thickness and timing of detailed glacial cycle; and iii) It requires sufficient calibration based on empirical data (i.e. not from another model)	Riis and Fjeldskaar (1992); Rasmussen and Fjeldskaar (1996); Amantov and Fjeldskaar (2018); Fjeldskaar and Amantov (2018); Patton et al. (in review).

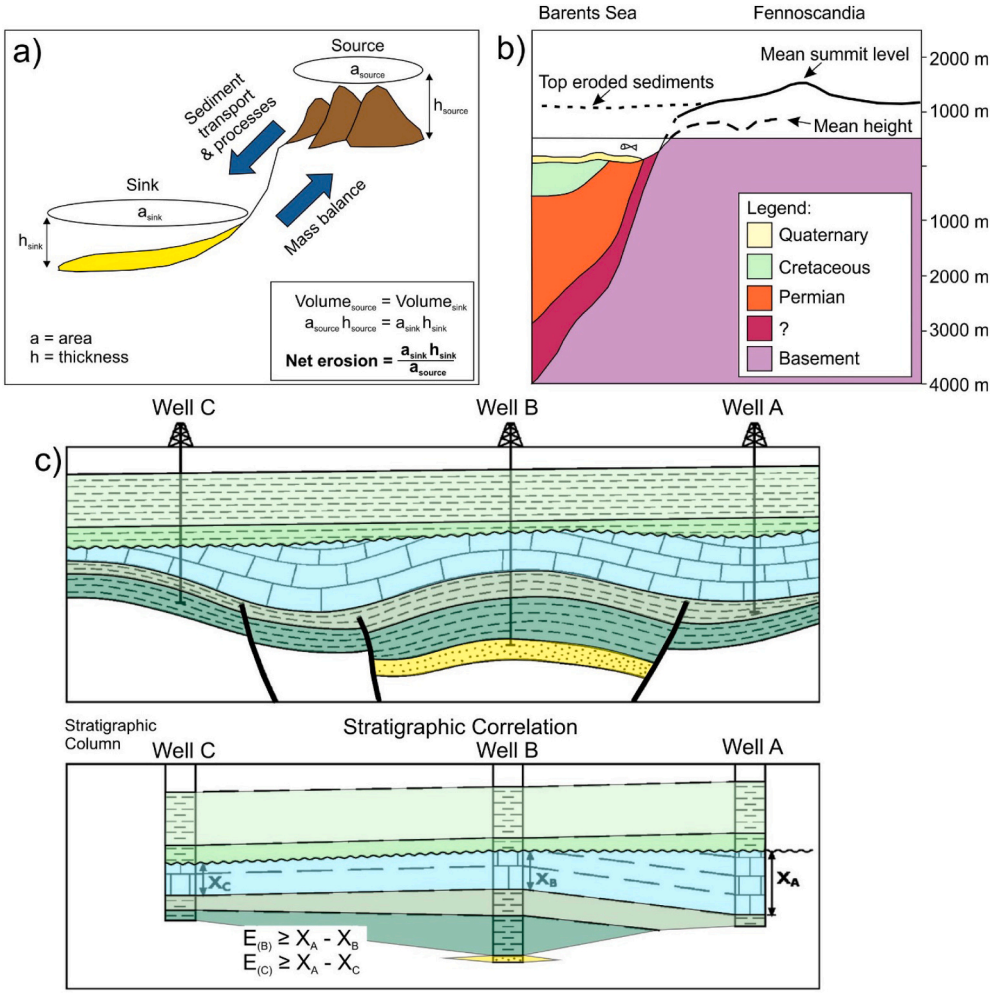

Fig. 9. Methods based on stratigraphy. a) Mass balance method for quantifying net erosion. b) Offshore extrapolation to onshore geomorphic features (modified from Riis and Fjeldskaar, 1992). c) Seismic stratigraphic interpretation method (modified from Corcoran and Doré, 2005). E: Erosion; X: Thickness

inferred source area can be estimated through volume calculations of individual seismic units in the sink area, i.e. individual periods of erosion as well as the net erosion can be estimated. The net erosion can be estimated as follows:

$$\text{Net erosion} = (a_{sink} \cdot h_{sink}) / a_{source} \quad (2)$$

The a_{source} and a_{sink} in Eq. (2) are the area of the source and the sink, respectively, and h_{sink} is the thickness of the sink. The mass balance method gives mean values of sedimentation in the sink area and from this, mean values of erosion from the source area, i.e. it gives limited information on spatial and temporal variations of erosion. It is also worth noting that the mass balance in this context is a volumetric mass balance that compares volumes and their overall lithological compositions (thus densities) as a proxy for mass.

Some of the key uncertainties are listed in Table 1: i) it may be difficult to outline the source area(s); ii) reworking/redeposition by ocean contour currents may complicate the sediment budgeting, particularly in the basins along the continental margin; iii) it may be complicated to quantify the volume of biogenic input (ooze sediments) in the basin; and iv) compaction-decompaction correction should be applied. We discuss these uncertainties in Subsection 6.2.1. The mass balance method has previously been applied for a number of high-latitude continental margins for both glacial (e.g. Vorren et al., 1991; Fiedler and Faleide, 1996; Hjelstuen et al., 1996; Laberg et al., 2009; Dowdeswell et al., 2010b; Laberg et al., 2012; Rydningen et al., 2016) and pre-glacial sedimentary successions (e.g. Sømme et al., 2009b, 2013; Eide et al., 2017; Lasabuda et al., 2018a, c).

4.1.2. *Offshore extrapolation to onshore geomorphic features*

The main principle of this technique is the correlation from an offshore stratigraphic marker horizon to an onshore paleosurface in order to estimate the missing onshore section from erosion (Fig. 9b). A limitation of this method is that a long-distance correlation may be problematic as this technique may be prone to miss-ties when attempting to connect to the 'correct' onshore surface (Doré et al., 2002; Anell et al., 2009), due to seismic time-to-depth conversion in areas/depths of limited well control (Table 1).

Riis and Fjeldskaar (1992) applied this technique for extrapolating the seismic sequences on the Barents Shelf to paleosurfaces of mainland Norway, which are additional sources of information on the Cenozoic uplift (Lidmar-Bergström et al., 2007). Calibration of the results from this technique by dating onshore paleosurfaces may increase the level of confidence of the erosion estimates.

4.1.3. *Seismic stratigraphic interpretation*

This technique includes a detailed seismic stratigraphic analysis of the area of erosion including the identification of unconformities (Fig. 9c). The chronology of the remaining succession can give reliable timing estimates on the removal of sediments from the source area. However, it is often not straightforward to identify an "erosional event" and separate this from a period of non-deposition (resulting in a condensed section) (Table 1). It requires a comprehensive

understanding of the geological history of the area for the pre-glacial and glacial succession, as both an erosion and non-depositional episode may appear similar in a predominantly horizontal succession in a seismic profile. Erosion and redeposition from the last glaciation may complicate the dating of the stratigraphy.

It may be challenging to apply this method in a basin with salt/evaporites (e.g. Nordkapp Basin) due to complex stratigraphy and imaging issues (see Fig. 2b for location). In an area where there is limited well-control, this technique relies on long-distance seismic correlation, which will lower the level of confidence in the chronology. The quality of the velocity model will also influence the time-depth conversion accuracy. These uncertainties may influence the erosion estimates (Doré et al., 2002; Anell et al., 2009).

At present, this method is probably less applicable on the northern and eastern Norwegian Barents Shelf due to the limited chronology from wells and sparse 2D seismic coverage. In contrast, in an area where there is wide coverage of 2D/3D seismic data such as the North Sea, this method is valid for estimating the net erosion (e.g. Huuse, 2002).

4.2. Methods based on physical properties

Methods based on physical properties include sonic velocity, interval velocity, shot gather, resistivity, porosity, sandstone diagenesis, vitrinite reflectance and apatite fission track analyses. Interpolation between wells and extrapolation away from wells are needed for regional studies which then introduces various levels of confidence. Frontier provinces such as the northern Barents Sea, are particularly hampered by lack of significant well-control.

4.2.1. Sonic velocity analysis

The shale compaction technique involves a compaction analysis of shale from well data and then a comparison of the results to an 'ideal' compaction trend from areas of no or little erosion (Fig. 10a). Any compaction anomalies (i.e. an overcompacted shale interval at a shallower depth) will be regarded as a proxy for either erosion/exhumation or overpressure. Establishing a standard compaction trend may be the main source of uncertainty due to the typical non-uniqueness character of a basin, and there are often more than one proposed baseline in a single basin/region (e.g. Japsen, 2000; Storvoll et al., 2005).

This method often requires a shale interval from more than one formation for a regional study. For example, in some areas on the Barents Shelf, the Paleogene Torsk shales are inconsistent in terms of thickness and quality. Therefore, one has to rely also on the Cretaceous Kolmule Formation (Fig. 7). Another major uncertainty of this method lies in the mechanical compaction and reburial of strata after exhumation (Table 1). Baig et al. (2016) and Ktenas et al. (2019) among others applied this method to the southwestern Barents Shelf and concluded that this method works well in areas where abundant well data are available, for example in the Hammerfest Basin.

4.2.2. Interval velocity analysis

Interval velocity analysis utilizes stacking velocities by sequentially considering the velocity from the layer above and below to generate an interval velocity. Interval velocities are derived from seismic stacking velocities using the Dix (1955) formula:

$$V_{n,layer} = \frac{V_n^2 t_n - V_{n-1}^2 t_{n-1}}{t_n - t_{n-1}}^{1/2} \quad (3)$$

The interval velocity, *Vn,layer*, for each layer can be derived from stacking velocities. Here, *Vn-1* and *Vn* are the stacking velocities for the reflectors above and below the layer respectively, and t_{n-1} and t_n are the corresponding reflected-ray travel times. The Eq. (3) assumes small offsets, and flat and parallel layers.

The method requires a non-uplifted basin such as the North Sea as reference. However, they have to be calibrated first from a local well that has experienced minimal uplift (e.g. in the Tromsø Basin). The interval velocities from the Barents Sea and the North Sea can then be used to create two velocity cubes. The net erosion is estimated by subtracting the depth generated from the Barents Sea average velocity cube from the North Sea reference cube (Fig. 10b).

This method may need a combination of two stratigraphic references around structural highs as there is a high uncertainty related to the presence of shale intervals (Table 1). For example, the Kolmule Formation is missing on the Loppa High, therefore the Base Cretaceous Unconformity (BCU) or the Upper Regional Unconformity (URU) horizon may be added. Few studies have used this method on the Barents Shelf (e.g. Løseth et al., 1993; Richardsen et al., 1993; Johansen, 2016; Ktenas et al., 2019), but they are considered reliable with some geological calibrations (see Subsection 6.2.2).

4.2.3. Shot gather analysis

Shot gather analysis utilizes first arrivals, both direct and refracted waves, to calculate P-wave velocities. The calculation incorporates Herglotz-Wiechert inversion techniques (Baig et al., 2016). To estimate net erosion, velocity-depth gradient curves derived from individual shot gathers are compared with the normal compaction trend from non- or little uplifted basin (see Fig. 10a). Some of the key uncertainties are listed in Table 1: i) it may give higher net erosion estimates due to the velocity from shot gathers; ii) it may include higher velocities from deeper strata; and iii) overpressure in the Paleogene strata may complicate the results. The direct and refracted waves used for this method sample the subsurface more laterally/horizontally than the near-vertical sonic velocities from wells and interval velocities derived from seismic reflection data. Refraction velocities have a tendency of being slightly larger, and therefore give higher net erosion estimates. However, overall, this method has produced reliable results on the Barents Shelf (Baig et al., 2016).

4.2.4. Resistivity analysis

Resistivity analysis compares resistivity logs from an uplifted basin with 'normal' resistivity-depth trends derived from a basin where no or little uplift occurred. This method is very sensitive to pore fluid content as the presence of conductive brine influences the resistivity more than change in the lithology (Johansen and Gabrielsen, 2015). Moreover, the resistivity of pore fluid changes with temperature (Table 1). Thus, this method requires additional pre-conditioning preparation and further consideration including picking clean shale intervals, and avoiding carbonates and volcanics, as these may influence the measured resistivity. The location, depth and maturation stage of the selected shale intervals should also be considered (Senger et al., 2020), and calibration from a velocity-based method to estimate the cooling effect may be required. This technique has not been much applied to the Barents Shelf (e.g. Johansen, 2016).

4.2.5. Porosity analysis

The porosity curve is not directly measured, but derived from different logs such as neutron, density and sonic. Porosity curves may come with uncertainties depending on which log they have been derived from. To estimate net erosion, the porosity curves are compared with reference trend lines from a basin where no or little uplift has occurred, for example the North Sea (Fig. 10c). A common reference trend line is presented by Sclater and Christie (1980). Some uncertainties in this method are listed in Table 1: i) this method requires corrections if the pore fluid is not salty water; and ii) high pore pressure may complicate the results. Licciardi et al. (2019) have tested this method on the Barents Shelf. Their results show that this is a promising method to estimate net erosion.

4.2.6. Sandstone diagenesis analysis

Using suitable shale units in estimating net erosion is common in most of the methods based on well data. However, on the western

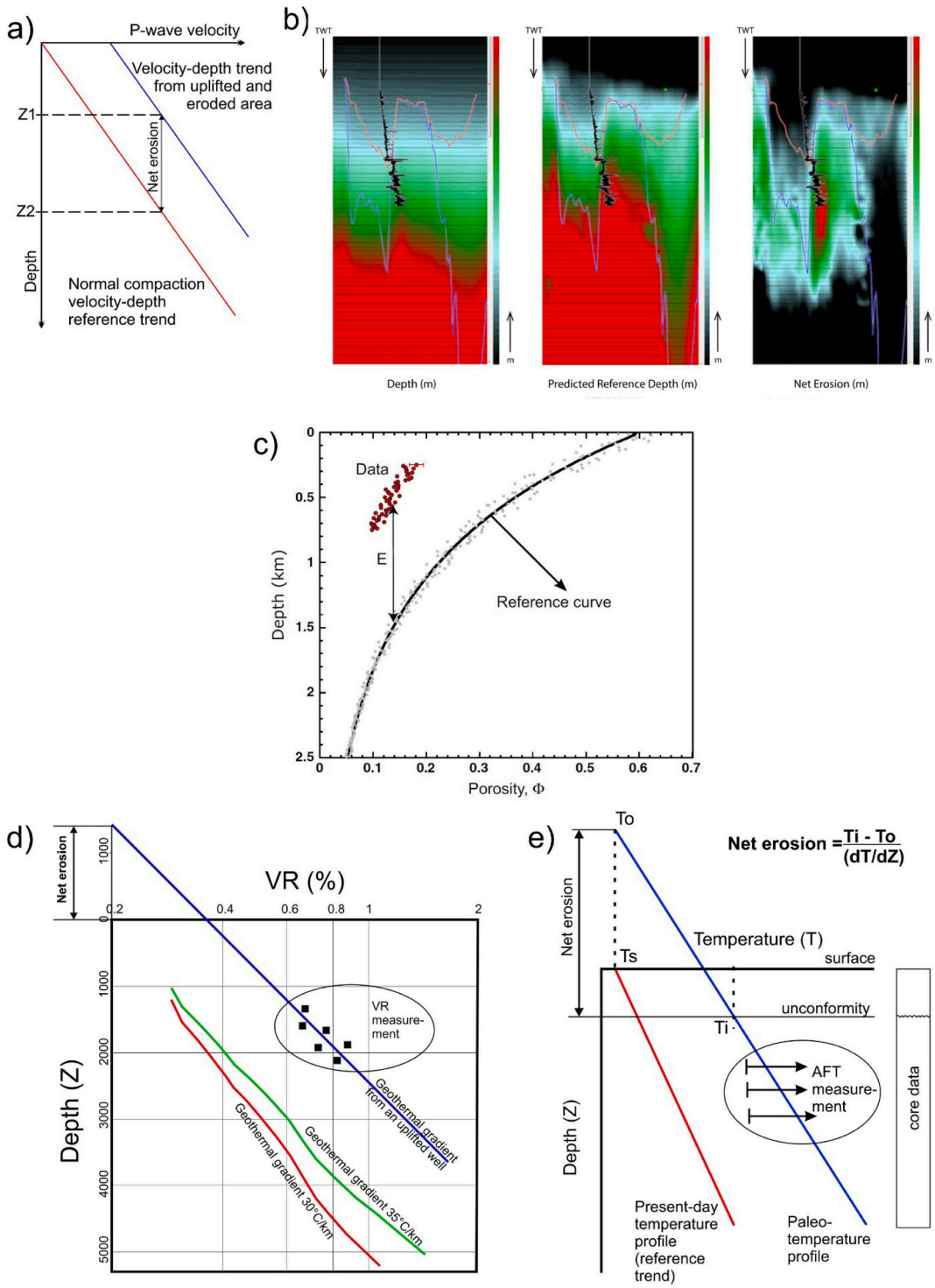

Fig. 10. Methods based on physical properties. a) Quantification of net erosion from compaction techniques using sonic velocity vs. depth trend for shales. The difference between the reference trend (red) and the blue trend line which has undergone uplift and erosion will give the net erosion estimate. The net erosion is the difference between present day burial depth for the formation (Z1) and maximum burial depth (Z2). b) A depth-converted cube derived from an interval velocity from the Barents Shelf (left), a depth-converted cube using an interval velocity from the North Sea as a reference (middle), and net erosion calculated by subtracting the middle from left. The Kolmule- (red line) and BCU horizons (blue line) are shown. Figure is modified from Johansen (2016). c) Porosity as a tool to estimate net erosion (Licciardi et al., 2019). d) Vitrinite reflectance method (Dow, 1977), Reference geothermal gradients at 30 and 35 degrees per km follow Sweeney and Burnham (1990). Figure is modified from Baig et al. (2016). e) Net erosion estimates using apatite fission track method. Note that temperature and paleotemperature measurements should be referred to the seabed as a datum. Ts: Present-day surface temperature; To: paleosurface temperature; Ti: paleotemperature; (dT/dZ): paleogeothermal gradient. Figure is modified from Green et al. (2002).

Barents Shelf, the shale interval is not always present, e.g. on the Loppa High the shale-rich Cretaceous Kolmule Formation is lacking (Fig. 7). When this is the case, using sandstones for estimating net erosion may be an alternative approach. Sandstone diagenesis analysis is based on the chemical compaction of sandstone which occurs after the burial temperature has reached a certain point, commonly around 70°C (Bjørlykke and Jahren, 2015). The chemical compaction process (i.e. growth of quartz minerals resulting in quartz cementation and therefore reduced porosity) is considered irreversible, meaning that a net uplift history will be recorded in the sandstone (e.g. Avseth and Lehocki, 2016; Bredesen et al., 2019). The porosity loss due to mechanical compaction is calculated using the formula for inter-granular volume (IGV) (Lander and Walderhaug, 1999) assuming perfectly sorted sandstones. For chemical compaction, the amount of quartz cement is given by the formula from Walderhaug (1996).

Some sources of uncertainties are listed in Table 1: i) it requires a number of assumptions in rock mineralogy (e.g. clay content, matrix, quartz cementation); ii) different temperature gradients may influence the net erosion estimates; iii) overpressures and differential compaction may affect the net erosion estimates; and iv) it may not be practical for a regional study as it may require readjustment to different sandstones (e.g. the Stø and Tubåen formations). We discuss these uncertainties in Subsection 6.2.2. Although rarely used, this method shows a good agreement with other techniques on the Barents Shelf (e.g. Avseth et al., 2014; Johansen, 2016).

4.2.7. Vitrinite reflectance (VR) analysis

Vitrinite reflectance analysis utilizes the amount of reflection of vitrinite, which rises proportionally to the temperature level and duration of heating. To estimate net erosion, the geothermal gradient from VR measurements needs to be compared with a normal geothermal gradient trend of 30–35°C/km following Sweeney and Burnham (1990) (Fig. 10d). However, such knowledge about (paleo) temperature gradients are often difficult to constrain (Table 1). Limitations may also rise from reworked and oxidized vitrinite and from the rareness of these data in siliciclastic sediments and basement rocks. Studies from Svalbard have used this method to constrain exhumation (e.g. Manum and Throndsen, 1978). In areas with high igneous activity such as the Vestbakken volcanic province of the western Barents Shelf, transient heat flow may be problematic for this method.

4.2.8. Apatite fission track (AFT) analysis

Apatite fission track analysis is based on damages due to spontaneous nuclear fission of uranium in apatite crystals. The linear damage features are referred to as fission tracks in detrital grains of rocks, and they are highly temperature dependent (e.g. Donelick et al., 2005) (Fig. 10e). The net erosion estimate is given as the following:

$$\text{Net erosion} = (T_i - T_o)/(\mathrm{d}T/\mathrm{d}Z) \quad (4)$$

In Eq. (4), T_i is the paleotemperature intercept at the unconformity, T_o is the paleosurface temperature, and $\mathrm{d}T/\mathrm{d}Z$ is the paleogeothermal gradient (Green et al., 2002). Uncertainties include the partitioning of basal and transient heat flow, as well as quantifying the annealing temperature (see Green et al., 1986). Annealing is a process where fission tracks shorten and finally disappear at a high temperature. The AFT method has shown less confidence in addressing recent cooling events (Corcoran and Doré, 2005; Anell et al., 2009). This method may be sensitive to local temperature changes such as from igneous intrusion (Table 1). Moreover, it may be difficult to estimate paleo heat flow and paleotemperature in a recently exhumed (and hence disequilibrium) setting (Hokstad et al., 2017). This method has been applied to constrain the Cenozoic cooling episodes from uplift on Svalbard (e.g. Blythe and Kleinspehn, 1998; Dörr et al., 2013; Barnes and Schneider, 2019; Dörr et al., 2019) and on the Barents Shelf (e.g. Green and Duddy, 2010).

4.3. Numerical modelling

Numerical models can be used to reconstruct the cumulative effects of surface uplift and net erosion that may have led to the present-day basin configuration (Wangen, 2010). Primary inputs include results from seismic and well data (i.e. thickness, volume and aerial distribution of targeted intervals), with inputs dependent on the type of model. On the Barents Shelf, models have been applied to simulate the uplift and erosion processes and the influence and sensitivity from various parameters including sediment densities, decompaction, isostasy, the β factor (i.e. the crustal stretching factor), crustal flexural rigidities, and effective elastic thickness of the lithosphere (EET) (e.g. Dimakis et al., 1998; Butt et al., 2002; Duran et al., 2013; Clark et al., 2014; Ostanin et al., 2017; Zieba et al., 2017; Gac et al., 2018; Medvedev et al., 2018). Furthermore, forward stratigraphic modelling may potentially be used to simulate erosion-deposition relationships (i.e. basin infilling and the draining processes of the sediment source area) on the Barents Shelf.

A model is often an oversimplification of complex scenarios, in particular deeper tectonic process (Table 1). There are also uncertainties in the ice-sheet extent, thickness and timing of detailed glacial cycle. It is worth noting that complex models can produce infinite scenarios that are internally consistent, but the majority will be geologically unrealistic/improbable. A modelled solution is only useful if reliable data constraints exist that can be used to calibrate the model or validate model outputs.

5. Net erosion estimates

5.1. Net erosion estimates using the mass balance method

In the following subsection, the depositional volumes and net eroded thickness for both Cenozoic pre-glacial and glacial strata are combined to estimate the total Cenozoic net erosion. In the southwestern Barents Shelf and adjacent deep-sea basins, between 162,000 – 280,000 km^3 of sediments have been deposited during the Paleocene to Neogene (Vorren et al., 1991; Fiedler and Faleide, 1996; Lasabuda et al., 2018b; Table 2). Around 115,000 km^3 of Cenozoic pre-glacial sediments were deposited in basins of the northwestern Barents Shelf (Hjelstuen et al., 1996; Lasabuda et al., 2018c). However, this does not include the western Svalbard and northern Barents Shelf continental margins, as there are presently no published results quantifying the volume of Cenozoic pre-glacial sediments there.

The pre-glacial, net eroded thicknesses consist of the Paleocene (150 – 190 m), Eocene (320 – 490 m), Oligocene (120 – 220 m) and Miocene (260 – 470 m), according to Lasabuda et al. (2018b). The corresponding source areas cover 191,500 – 334,000 km^2, for instance, the Stappen High, Loppa High, Bjarmeland Platform (Lasabuda et al., 2018b). The source areas may vary for each time period and therefore, the net erosion would be different for each structural element. For example, the Hammerfest Basin may have only been eroded during the Oligocene and Miocene, so that the pre-glacial net erosion may have been 380 – 690 m for this area (see Fig. 15 in Lasabuda et al., 2018b). Meanwhile, the highs (e.g. the Loppa High and Stappen High) are likely to experience higher net erosion.

The Cenozoic glacial volume is generally higher than the pre-glacial volume along the western Barents Shelf margin (Fig. 11). The volume of glacigenic sediments is about 395,000 km^3 – 464,000 km^3 in the Bjørnøyrenna TMF (Table 2; Vorren et al., 1991; Fiedler and Faleide, 1996; Laberg et al., 2012), and 116,000 km^3 in the Storfjordrenna TMF (Hjelstuen et al., 1996). Several smaller fans along the western Svalbard margin have contributed to c. 43 km^3 of sediments (Elverhøi et al., 1998, their Table 1). The total Cenozoic glacial volume for the western and northern Barents Shelf continental margin is inferred to be 1,280,000 – 1,350,000 km^3 (Rasmussen and Fjeldskaar, 1996; Hjelstuen and Sejrup, 2020). From mass balance estimates, the Cenozoic pre-glacial to glacial sediment volume ratio varies from 40%, 50% and 70% along the

Table 2
Average deposition (m) derived from the volume of sediment divided by depositional area. Note that the depositional area for glacial strata is adapted from Fiedler and Faleide et al. (1996). In this table, the depocenters for Paleocene–Eocene are assumed to be located in the Sørvestsnaget Basin and Vestbakken volcanic province, while depocenter for Oligocene–Neogene is considered to be located in the Lofoten Basin. The pre-glacial depositional volume from Lasabuda et al. (2018b) is the maximum estimate comprising c. 280,000 km^3.

			Depositional volume (10^3 km^3)	Depositional area (10^3 km^2)	Average deposition (m)		
					Sørvestsnaget Basin and Vestbakken volcanic province	Lofoten Basin	
Glacial	Vorren et al. (1991); Laberg et al. (2012)	Pleistocene	464	542	–	2041	–
	Fiedler and Faleide et al. (1996); Laberg et al. (2012)	Pleistocene	395		1638	–	1638
Pre-glacial	Lasabuda et al. (2018b)	Neogene	96	171.6	–	559	
		Oligocene	45.3	130.9	–	346	
		Eocene	99.6	119.6	833	–	–
		Paleocene	39.3	55.7	706	–	–
Total					3177	2946	2543

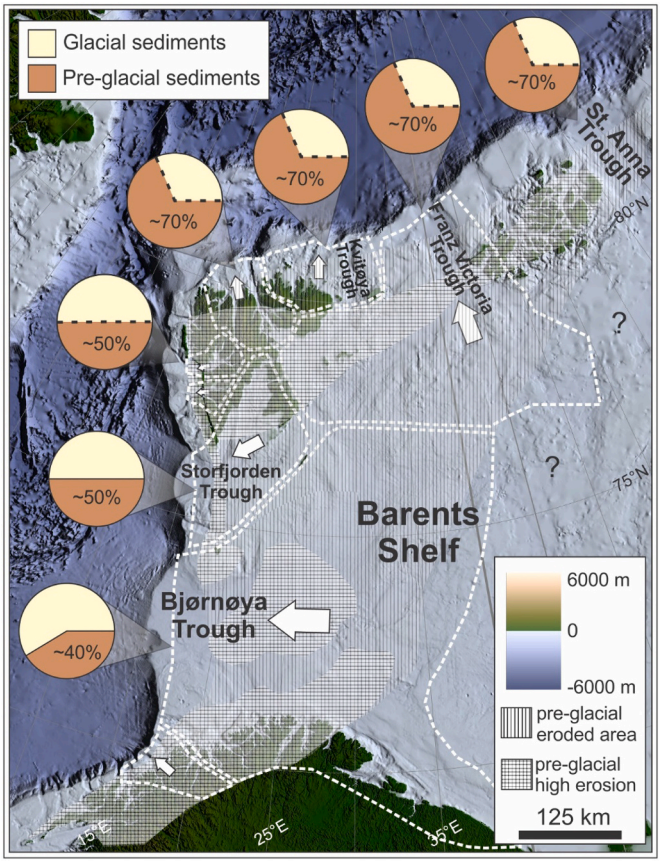

Fig. 11. Pie charts representing the ratio between the Cenozoic glacial and pre-glacial erosional sediment deposited in the basins off the Norwegian Barents Sea continental margin are based on volumetric quantification. Ratio estimates for the margin west of Svalbard (Eiken, 1994; Solheim et al., 1998; Butt et al., 2000), Yermak Plateau (Geissler et al., 2011), Kvitøya Trough (Lasabuda et al., 2018a), Franz Victoria Trough (Berglar et al., 2016) and St. Anna Trough (Nikishin et al., 2019) are based on qualitative inspection of seismic profile and therefore shown using thin dashed lines. Note the similarities in size does not correspond to similar volumes. The pre-glacial eroded areas are based on Rasmussen and Fjeldskaar (1996) and Lasabuda et al. (2018b, c). The thick dashed lines represent the drainage areas for the glacial period following Vorren et al. (1991), Hjelstuen et al. (1996), Fiedler and Faleide et al. (1996), Elverhøi et al. (1998), Ottesen et al. (2005), Laberg et al. (2012) and Rydningen et al. (2016). Arrows show the relative draining direction of ice during glaciations. Bathymetry is adapted from IBCAO v. 4.0 (Jakobsson et al., 2020).

southwestern, northwestern and northern Barents Shelf continental margins, respectively (Fig. 11).

The changing intensity of glaciations through the late Cenozoic demarcate the net eroded thicknesses into three major intervals: i) from 2.7 Ma to 1.5 Ma (170 – 230 m of net erosion); ii) from 1.5 Ma to 0.7 Ma (330 – 420 m of net erosion); and iii) from 0.7 Ma to present (440 – 530 m of net erosion) (Laberg et al., 2012). The net missing overburden for the entire glacial period in the southwestern Barents Sea is estimated to be 1000 – 1100 m over an area of ~575,000 km^2 (Laberg et al., 2012).

The combined Cenozoic pre-glacial net erosion estimates from Lasabuda et al. (2018b) and the glacial net erosion estimates from Laberg et al. (2012) indicate that the area of the Sørvestnaget Basin, the Vestbakken volcanic province and Lofoten Basin acted as depocenters, whereas the Stappen High, the Loppa High, the Bjarmeland Platform, the Finnmark Platform and the Nordkapp Basin experienced relatively high erosion during the Cenozoic (Table 3; see Fig. 2b for location). The total net erosion shows variation depending on the location of different structural elements. For example, the Hammerfest Basin is predicted to have experienced 1380 – 1480 m of net erosion, while net erosion of the Bjarmeland Platform is estimated to be more severe at 1860 to 2220 m (Table 3). A compilation of mass balance results from the southwestern Barents Sea area shows a significant N-S and E-W trending increase of net erosion (Fig. 12).

5.2. Net erosion estimates using sonic velocity

We apply this method to the studied wells (Table 4). We use only the cleanest shales in the Cretaceous Kolmule and Paleogene Torsk formations for comparison with the reference trend. Examples of the net erosion estimates from two wells show net erosion of 1380 – 1480 m (well 7224/6-1) and 1220 – 1340 m (well 7223/5-1) (Fig. 13a and b). The regression line derived from shale interval of the Kolmule Formation is compared with the normal shale trend line. A reliable net erosion estimate is derived from a parallel regression line to the trend line. The thickness of the shale interval is also influenced by the reliability of the regression line. In this case, well 7224/6-1 (Fig. 13a) gives a higher confidence than well 7223/5-1 (Fig. 13b) in terms of orientation of the regression line to the reference line and also the shale thickness. An overall trend of increasing net erosion (up to 2200 m) from this technique is observed towards the east and northeast (Fig. 13c).

5.3. Net erosion estimates using interval velocity

One of the key advantages of using the interval velocity method is that the lateral variation of net erosion can be shown and directly related to the geological development. We examine two transects with an E-W and overall NW-SE orientation, respectively (Table 4; see Fig. 2b for location). The actual net erosion value should be read at the top Kolmule

Table 3
Comparison of net erosion estimates (m) from published results.

Structural elements	Average net erosion (m) from different methods								
	Mass balance Cenozoic pre-glacial	Mass balance Cenozoic glacial	Mass balance total Cenozoic	Shale compaction, thermal maturity and shot gathers	Shale compaction	Vitrinite reflectance	Vitrinite reflectance	Compilation including vitrinite reflectance, sandstone diagenesis, apatite fission track and shale compaction	Modelling
	Lasabuda et al. (2018b)	Laberg et al. (2012)	Lasabuda et al. (2018b) + Laberg et al. (2012)	Baig et al. (2016)	Ktenas et al. (2019)	Riis and Fjeldskaar (1992)	Ohm et al. (2008)	Henriksen et al. (2011a)	Amantov and Fjeldskaar (2018)
Hammerfest Basin	380	1000–1100	1380–1480	800–1400	1800–2000	1000–1500	700–1200	1000–1200	500–2000
Finnmark Platform (banks area)	700–1180	500–650	1200–1830	1200–1400	2000–2200	800–1400	800–1400	800–1400	500–1000
Finnmark Platform (trough area)	700–1360	1000–1100	1700–2460	1700	1800–2000	1500	750	1400	1500–2500
Sørvestsnaget Basin	0	0	0	0	800–1200	0	250	0	0
Vestbakken volcanic province	0	0	0	0	1200–1400	500–1000	1500	350	0
Loppa High	760–1360	1000–1100	1760–2460	1150–1950	1800–2200	1500–2000	1500–2200	1200–2000	2000–2500
Bjarmeland Platform	860–1180	1000–1100	1860–2280	1250–2400	2200–2600	1400–2500	1400–2500	1400–2500	1000–1500
Stappen High	760–1360	500–650	1260–2000	2100	3200	2500–3000	2000–2500	2200	2000–2500
Nordkapp Basin	700	500–650	1200–1350	1400	2600–2800	1100	900	1400–1600	500–1500

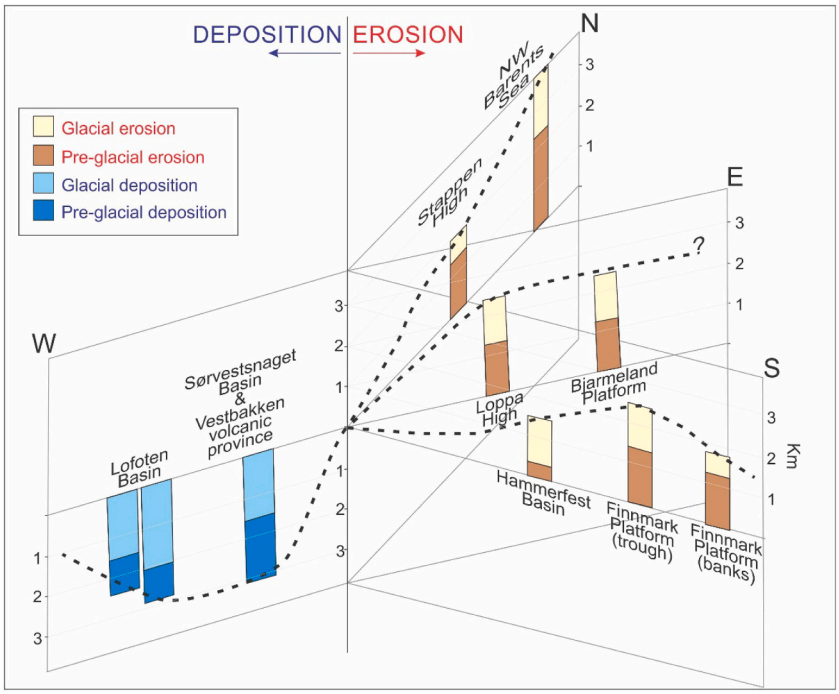

Fig. 12. Diagram summarizing the mass balance approach for the Cenozoic interval in the southwestern Barents Sea. This diagram shows the significance of N-S and E-W trending erosion and deposition. The deposition values are taken from Table 2. The net erosion estimates from the mass balance method are taken from Table 3.

Formation, except on the Loppa High, where it appears to merge with the Base Cretaceous Unconformity (BCU) or the Upper Regional Unconformity (URU) horizon (Figs. 14 and 15).

From transect 1, the net erosion estimate shows high values of up to 2500 m at the deeper Permian/Carboniferous level on the Loppa High (Fig. 14). This estimate appears unlikely and is mainly caused by lithological effects from Permian/Carboniferous carbonate succession (primarily dolomites) with very high velocities (> 6 km/s). Therefore, we exclude wells from our average net erosion map that are inconsistent with geological observations (e.g. lithological effects as in well 7220/6-1). From transect 1, an overall trend of increasing net erosion eastwards is observed (Fig. 14).

From transect 2, the Hammerfest Basin shows net erosion of c. 750 m and displays lower net erosion compared to the flanking highs (the

Table 4
Results of net erosion estimates from three methods based on physical properties (sonic velocity, interval velocity and sandstone diagenesis) and their average using the studied wells.

Wells	Sonic velocity (m)	Interval velocity (m)	Sandstone diagenesis (m)	Average (m)	Structural elements
7117/9-1	287	250		269	Tromsø Basin
7319/12-1	758	750		754	Bjørnøya Basin
7219/9-1	1152	1200	1230	1194	Bjørnøya Basin
7219/8-1 S	876	800		838	Bjørnøya Basin
7219/8-2	1545	1450		1498	Bjørnøya Basin
7220/8-1	1223	1300	1330	1284	Bjørnøya Basin
7220/4-1	1323	1350	1270	1314	Bjørnøya Basin
7122/7-3	904	1000	1380	1095	Hammerfest Basin
7120/9-1	1044	1100	1100	1081	Hammerfest Basin
7120/6-3 S	1047	1150	875	1024	Hammerfest Basin
7120/2-2	1468	1450	1170	1363	Hammerfest Basin
7121/4-1	1149	1200	750	1033	Hammerfest Basin
7120/2-3 S	1338	1400	1240	1326	Loppa High
7120/1-2	1330	1450	1140	1307	Loppa High
7120/1-3	1098	1150		1124	Loppa High
7220/10-1	1271	1250	1310	1277	Loppa High
7222/6-1 S	1500	1450	1420	1457	Loppa High
7222/11-1	1657	1600	1585	1614	Loppa High
7223/5-1	1291	1300	1295	1295	Bjarmeland Platform South
7224/6-1	1434	1400	1485	1440	Bjarmeland Platform South
7225/3-1			1600	1600	Bjarmeland Platform South
7226/2-1	1581	1550	1670	1600	Bjarmeland Platform South
7324/10-1	1647	1700	1660	1669	Bjarmeland Platform South
7324/8-1	1277	1300	1760	1289	Bjarmeland Platform North
7324/7-1 S	1603	1600	1810	1671	Bjarmeland Platform North
7324/7-2			1735	1735	Bjarmeland Platform North
7324/2-1	1858	1850	1835	1848	Bjarmeland Platform North
7324/8-2	1579	1650	1750	1660	Bjarmeland Platform North
7324/9-1			1510	1510	Bjarmeland Platform North
7325/1-1			2035	2035	Bjarmeland Platform North
7321/7-1	1981	1950	1800	1910	Fingerdjupet Subbasin
7321/8-1	1718	1800	1805	1774	Fingerdjupet Subbasin
7321/9-1	1907	1850		1879	Fingerdjupet Subbasin

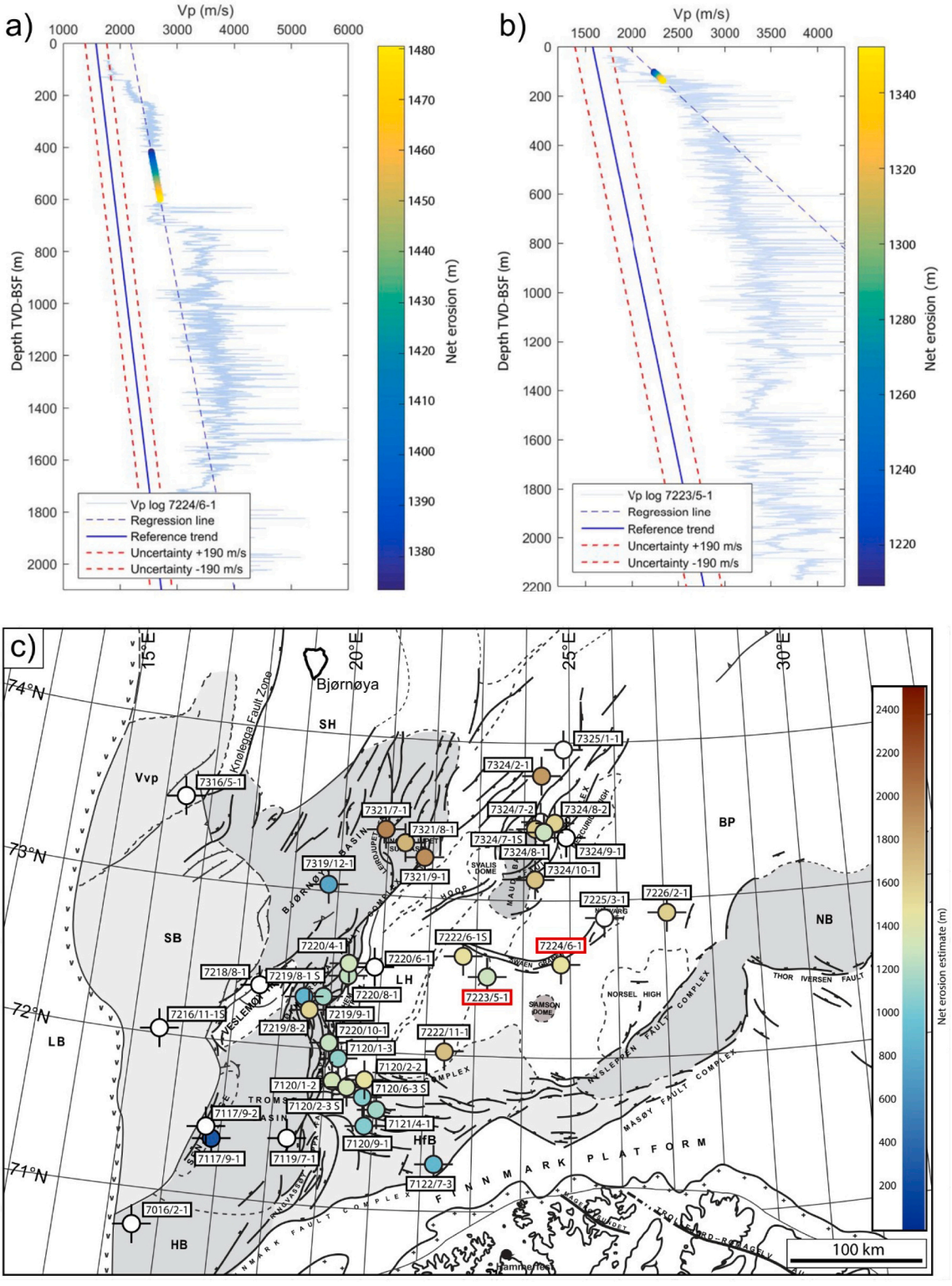

Fig. 13. Example of net erosion estimates using sonic velocity analysis from well a) 7224/6-1 and b) 7223/5-1. Net erosion is defined by the difference between the reference trend and the uplifted formation of interest (represented by the velocity well log curve). Shales in the Kolmule Formation are chosen for comparison with the reference trend in these two wells (note that shales from the Torsk Formation are also used in other wells). The uncertainty related to the reference trend line is shown with stippled red lines. c) A net erosion map based on sonic velocity analysis, showing an increasing trend to the east and northeast. Wells in (a) and (b) are highlighted in red boxes. Grey areas are major basins. Abbreviations used: BP: Bjarmeland Platform; HfB: Hammerfest Basin; HB: Harstad Basin; LH: Loppa High; NB: Nordkapp Basin; SH: Stappen High; SB: Sørvestsnaget Basin; Vvp: Vestbakken volcanic province.

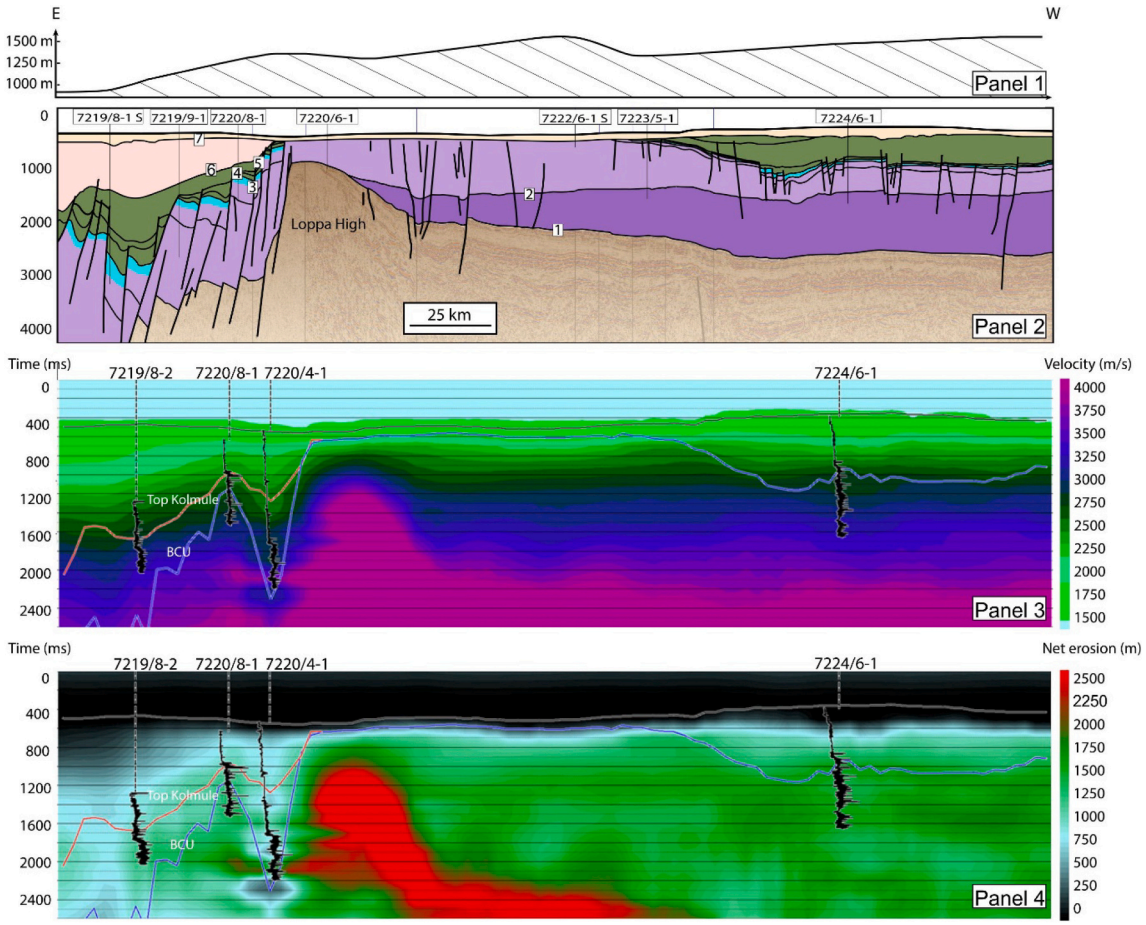

Fig. 14. Transect 1 shows the amount of net erosion illustrated by the shaded area below the smoothed line (Panel 1), regional geo-seismic profile (Panel 2), seismic interval velocitites (Panel 3) and net erosion estimates (Panel 4). In Panel 3 and 4, velocity logs are included in the well positions together with the top Kolmule and BCU (red and blue horizons). The net erosion estimates (Panel 4) are derived from the difference between seismic interval velocities (Panel 3) and the reference velocity cube. The actual net erosion value (Panel 4) should be read at the targeted seismic horizon (see Subsection 5.3). Note that the unrealistic high values of net erosion in, for example, the Loppa High are caused by lithological effects. 1: Base Triassic; 2: Base Upper Triassic; 3: Base Mid-Upper Jurassic; 4: BCU/Base Cretaceous Unconformity; 5: Base Upper Cretaceous; 6: Base Cenozoic; 7: URU/Upper Regional Unconformity. See Fig. 2b for location of transect and wells.

Loppa High and Finnmark Platform) (Fig. 15). This area was at its maximum burial sometime in the Paleogene, so our net erosion estimate should reflect younger Cenozoic uplift/erosion. The net erosion map from this method shows an overall increasing trend to the east and northeast (Fig. 16).

5.4. Net erosion estimates using sandstone diagenesis

We choose the Jurassic Stø and Tubåen formations for our sandstone diagenesis technique, which are generally observed as clean reservoirs on the Barents Shelf (Fig. 7). In the sandstone model, we apply the Lander and Walderhaug (1999) formula. The clay content (m_0) is assumed to be 5%, since completely clean sands are very rare in reality. The initial depositional porosity (ϕ_0) is set to 40%, and as suggested by Lander and Walderhaug (1999) the IGV_f and β constants are set to 28% and 0.06, respectively. There will normally appear some coating on the grain surface, and the volume of the material covering the sandstone grain surfaces is therefore assumed to be 10% in all cases. For the shales in the Barents Sea, a lower depositional porosity of 30% was used. Cretaceous shales in the Barents Sea were generally deposited in open to shallower marine environments (NPD, 2016) and occasionally have a higher content of silt and marl than the marine shales in the North Sea (Avseth and Lehocki, 2016). In shales, the transition from smectite to illite can cause the rocks to stiffen as quartz is a byproduct of the transition (Thyberg et al., 2009). However, only the effect of mineralogy is taken into account in the modelling since this stiffening process is very complex and poorly understood.

In the chemical compaction domain, the amount of quartz cement is given by the equation presented by Walderhaug (1996). An average default temperature gradient was estimated for each subbasin, ranging between 35° and 42°C/km. These gradients were used in the calculation for the Barents Sea wells. The gradients are rough estimates based on data from NPD (2016) and a seabed temperature of 4°C. The estimated average temperature gradients for the different basins are: Hammerfest Basin (35°C/km), Bjørnøya Basin/Loppa High West (38°C/km), Bjarmeland Platform South (38°C/km), Bjarmeland Platform North/Hoop (42°C/km), Fingerdjupet subbasin (36°C/km) and Loppa High (36°C/km).

Our results from the studied wells are shown in Table 4 and examples of net erosion estimates using sandstone diagenesis from selected wells are shown in Fig. 17a and b. Well 7120/9-1 in the Hammerfest Basin includes the Stø Formation, which is proven to have a high porosity and low clay content (Fig. 17a). The input burial history curve for the Stø Formation was set starting from 175 Ma with maximum burial depth at 40 Ma. The net erosion estimates show that 1100 m of sediment has been removed.

Another example is from well 7224/6-1 on the Bjarmeland Platform, which utilized the sand interval from the Tubåen Formation (Fig. 17b). The net erosion estimate from this well is 1500 m. The overall trend of net erosion estimates using sandstone diagenesis analysis is similar to

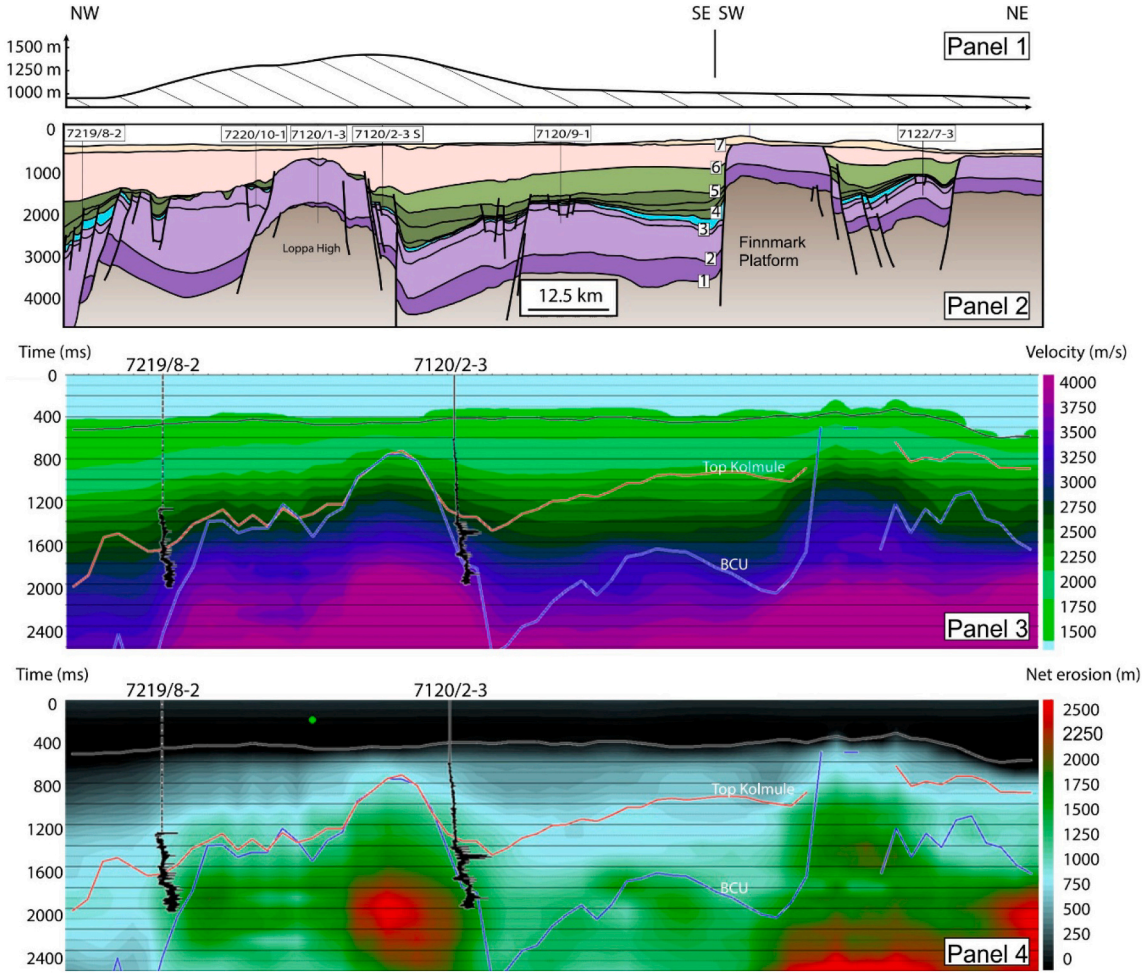

Fig. 15. Transect 2 shows the amount of net erosion illustrated by the shaded area below the smoothed line (Panel 1), regional geo-seismic profile (Panel 2), seismic interval velocitites (Panel 3) and net erosion estimates (Panel 4). In Panel 3 and 4, velocity logs are included in the well positions together with the top Kolmule and BCU (red and blue horizons). The net erosion estimates (Panel 4) are derived from the difference between seismic interval velocities (Panel 3) and the reference velocity cube. The actual net erosion value (Panel 4) should be read at the targeted depth/seismic horizon (see Subsection 5.3). Note that the unrealistic high values of net erosion in, for example, the Loppa High are caused by lithological effects. See Fig. 14 for horizon's number. See Fig. 2b for location of transect and wells.

other methods, with increasing net erosion to the east and northeast (Fig. 17c). These two wells are chosen as examples that represent two different sandstones, where both sandstones from the Stø and Tubåen formations show consistent estimates.

6. Discussion

In this section, we directly compare our results with other published net erosion maps and discuss the variation in the magnitude of net erosion derived from different methods, and their associated uncertainties. Moreover, erosion rates, predicted drainage areas and future research directions are discussed.

6.1. Compilation of net erosion maps

Results from this study are compiled together with recently published net erosion maps (Henriksen et al., 2011a; Baig et al., 2016; Amantov and Fjeldskaar, 2018; Ktenas et al., 2019). All maps are presented using the same colour scale for easier comparison of the spatial differences in erosion patterns (Fig. 18).

Net erosion estimates using stratigraphy-based method, represented by the mass balance method, show that erosion was concentrated in the areas of the Loppa High, the Bjarmeland Platform and the Hammerfest Basin, coinciding with the deepest part of the Bjørnøyrenna Trough on the present-day seabed (Fig. 18a). This pattern captures the amplification of pre-glacial erosion along structural highs along the western margin of the Barents Shelf (Lasabuda et al., 2018c) coupled with glacial erosion in the trough area (Laberg et al., 2012). Average values from methods based on physical properties and performed in this study (sonic velocity, interval velocity and sandstone diagenesis) show a trend of increasing erosion towards the north and northeast of the southwestern Barents Shelf (Fig. 18b). The Loppa High, the Bjarmeland Platform and parts of the Hammerfest Basin show high net erosion values which are consistent with results from the mass balance method.

The previous compilation map by Henriksen et al. (2011a) already considered estimates from older erosion maps (e.g. Vassmyr, 1989; Nyland et al., 1992; Riis and Fjeldskaar, 1992; Ohm et al., 2008), and shows prominent high net erosion of the Stappen High (Fig. 18c). The two studies focusing on methods based on physical properties show similar trends (Fig. 18d and f), although the net erosion map by Ktenas et al. (2019) shows higher erosion estimates than Baig et al. (2016). This is likely due to variations in the reference model for the shale compaction trend and an assumption of zero net erosion in the two westernmost wells (7216/11-1S and 7316/5-1) used by Baig et al. (2016) as opposed to Ktenas et al. (2019) who suggested glacial erosion has affected these wells.

The modelling results as shown in the net erosion map by Amantov and Fjeldskaar (2018) displays greater net erosion in the Stappen High,

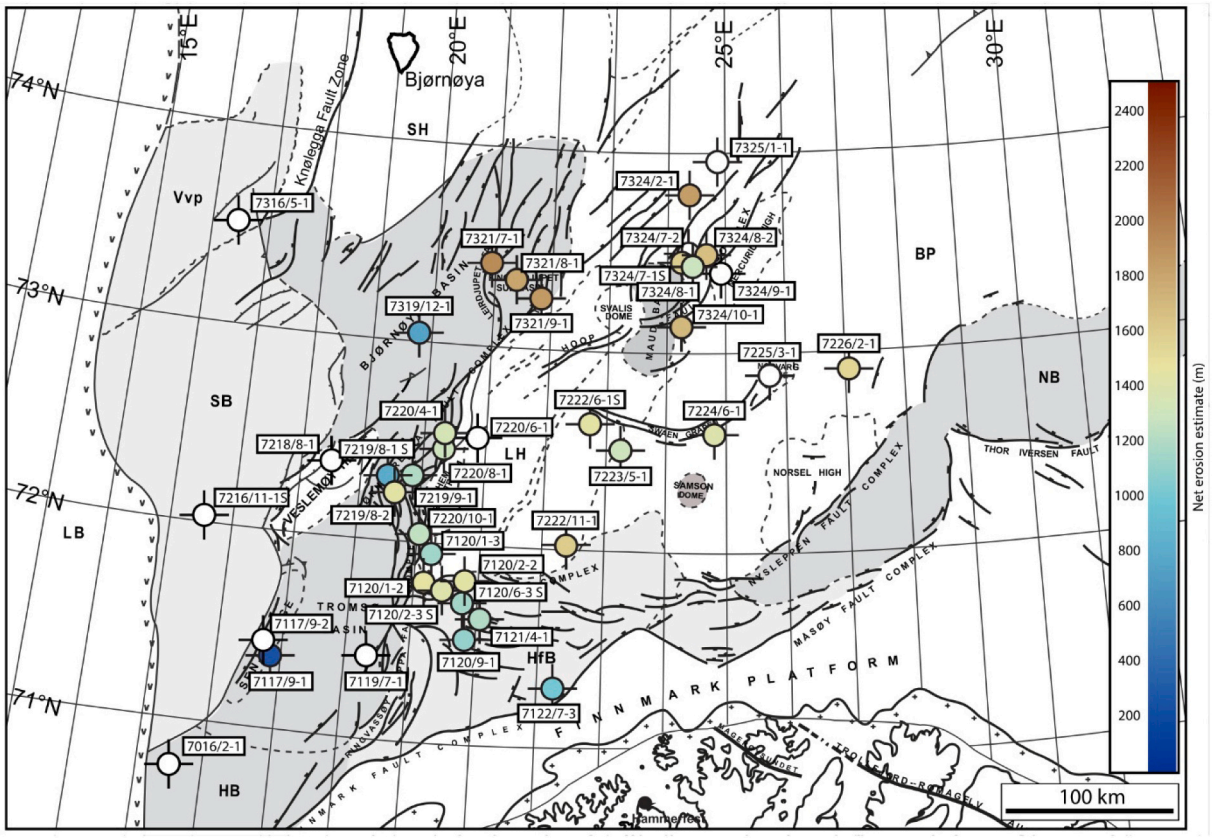

Fig. 16. Net erosion map from an interval velocity analysis showing an increasing trend to the north and northeast. Grey areas are major basins. Abbreviations used: BP: Bjarmeland Platform; HfB: Hammerfest Basin; HB: Harstad Basin; LH: Loppa High; NB: Nordkapp Basin; SH: Stappen High; SB: Sørvestsnaget Basin; Vvp: Vestbakken volcanic province.

the Loppa High and in the area of the Finnmark Platform and mainland northern Norway (Fig. 18e). This high erosion in the south may be related to rift flank uplift associated with the contemporaneous opening of the Norwegian-Greenland Sea (e.g. Weissel and Karner, 1989). Other possible mechanisms include the fact that mainland northern Norway, as an elevated, passive continental margin, has undergone episodic, post-rifts burial and exhumation (Japsen et al., 2012; Green et al., 2018).

Despite varying degrees of confidence between different areas and different studies (based on different methods), there is a comparable trend from all maps where the net erosion is generally higher towards the north (Fig. 18a–f). Therefore, we calculated an arithmetic mean of the recently published estimates above and present a new compilation map of net erosion (Fig. 19a and b). Our new net erosion map for the southwestern Barents Sea shows consistency with the overall pattern of net erosion, displaying high values on the Stappen High, the Loppa High and the Bjarmeland Platform (Fig. 19a). This is likely due to tectonic uplift affecting the northwestern margin of the Barents Shelf including Svalbard during the early Cenozoic. This uplift event was later amplified by isostatic uplift associated with glacial erosion.

For the greater Barents-Kara Sea area (Fig. 19b), we compiled the net erosion maps from Henriksen et al. (2011a) and Amantov and Fjeldskaar (2018), and used the new net erosion map for the southwestern Barents Sea. The regional net erosion map shows erosion concentrated along the western margin of the Barents Shelf with a general northward increase towards Svalbard as well as high net erosion values in the south following Amantov and Fjeldskaar (2018) (Fig. 19b). However, the high net erosion on Svalbard (>3.2 km) in the Henriksen et al. (2011a) map follows VR results from Manum and Throndsen (1978), who assumed a normal temperature gradient (c. 30°C/km) on Svalbard. This net erosion estimate may be overestimated due to the fact that Svalbard likely has a larger temperature gradient (e.g. Blythe and Kleinspehn, 1998; Marshall et al., 2015; Dörr et al., 2018, 2019; Ohm et al., 2019; Olaussen et al., 2019).

6.2. *Magnitude of net erosion – a comparison from various methods*

Our new compilation map presented here are compared to results from published work on the Barents Shelf (Fig. 20).

Results from Riis and Fjeldskaar (1992), Ohm et al. (2008), Henriksen et al. (2011a), Baig et al. (2016), Amantov and Fjeldskaar (2018) and Ktenas et al. (2019), which used different methods including shale compaction, thermal maturity, shot gather, vitrinite reflectance and AFT analyses, have been incorporated into our quantification of the net erosion of the southwestern Barents Shelf structural elements (Table 3 and Fig. 20). The majority of these studies quantifying net erosion estimates show discrepancies of c. 500 m in the Hammerfest Basin (from 1000 – 1500 m of net erosion) (Fig. 20). A discrepancy of 1000 m (from 1500 – 2500 m of net erosion) is observed on the Bjarmeland Platform (Fig. 20). This reflects the uncertainties in the methods applied and spatial variability among structural elements.

Results using the stratigraphy-based methods, as represented by the mass balance technique (shown in blue in Fig. 20), show good agreement with other net erosion estimation techniques for the Hammerfest Basin, the Sørvestsnaget Basin and the Bjarmeland Platform. However, the mass balance technique has a large uncertainty range (e.g. the Finnmark Platform area) and does not capture spatial variations (see below).

A comparison among methods based on physical properties from this study is plotted in Fig. 21 (note that some wells only provide net erosion estimates from one or two methods). The comparison of results using sonic velocity, interval velocity and sandstone diagenesis methods show overall similar trends, with increasing net erosion estimates eastwards.

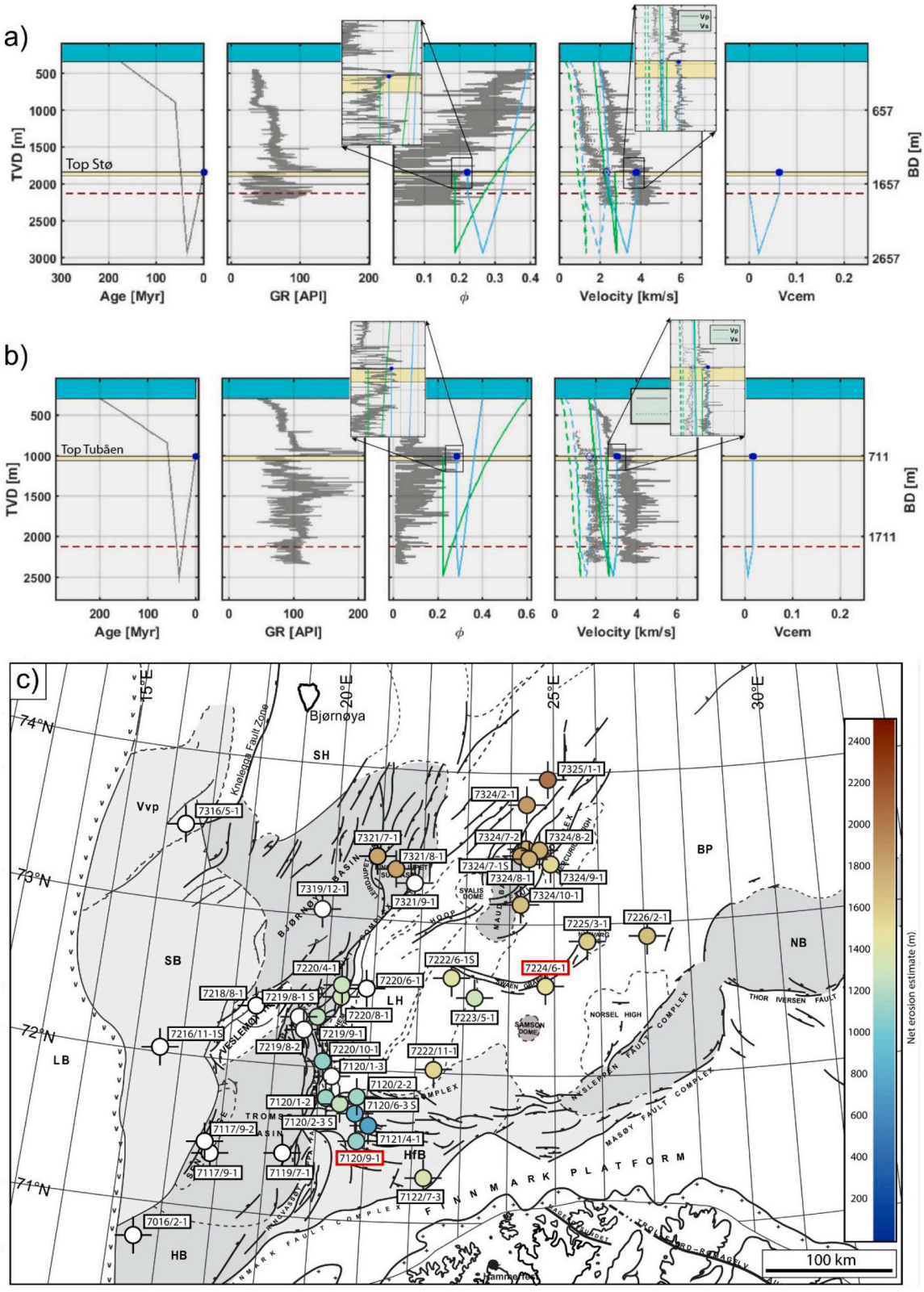

Fig. 17. Example of a sandstone diagenesis analysis from wells a) 7120/9-1 and b) 7224/6-1. The well 7120/9-1 uses the Stø Formation meanwhile 7224/6-1 utilizes the Tubåen Formation. For both a) and b), from left to right: input burial history curve (maximum burial at 40 Ma); Gamma Ray log (GR); well log porosity and modelled sandstone porosity; P-wave and S-wave velocity with modelled velocities; calculated cement volume. The red dashed line represents the 70°C threshold. The green line represents the shale line and the blue line represents the brine sand. c) Net erosion estimates from sandstone diagenesis also show an increasing trend to the east and northeast. Wells in (a) and (b) are highlighted in red boxes. Grey areas are major basins. Abbreviations used: SB: Sørvestsnaget Basin; Vvp: Vestbakken volcanic province; SH: Stappen High; LH: Loppa High; BP: Bjarmeland Platform; HB: Harstad Basin; HfB: Hammerfest Basin; NB: Nordkapp Basin.

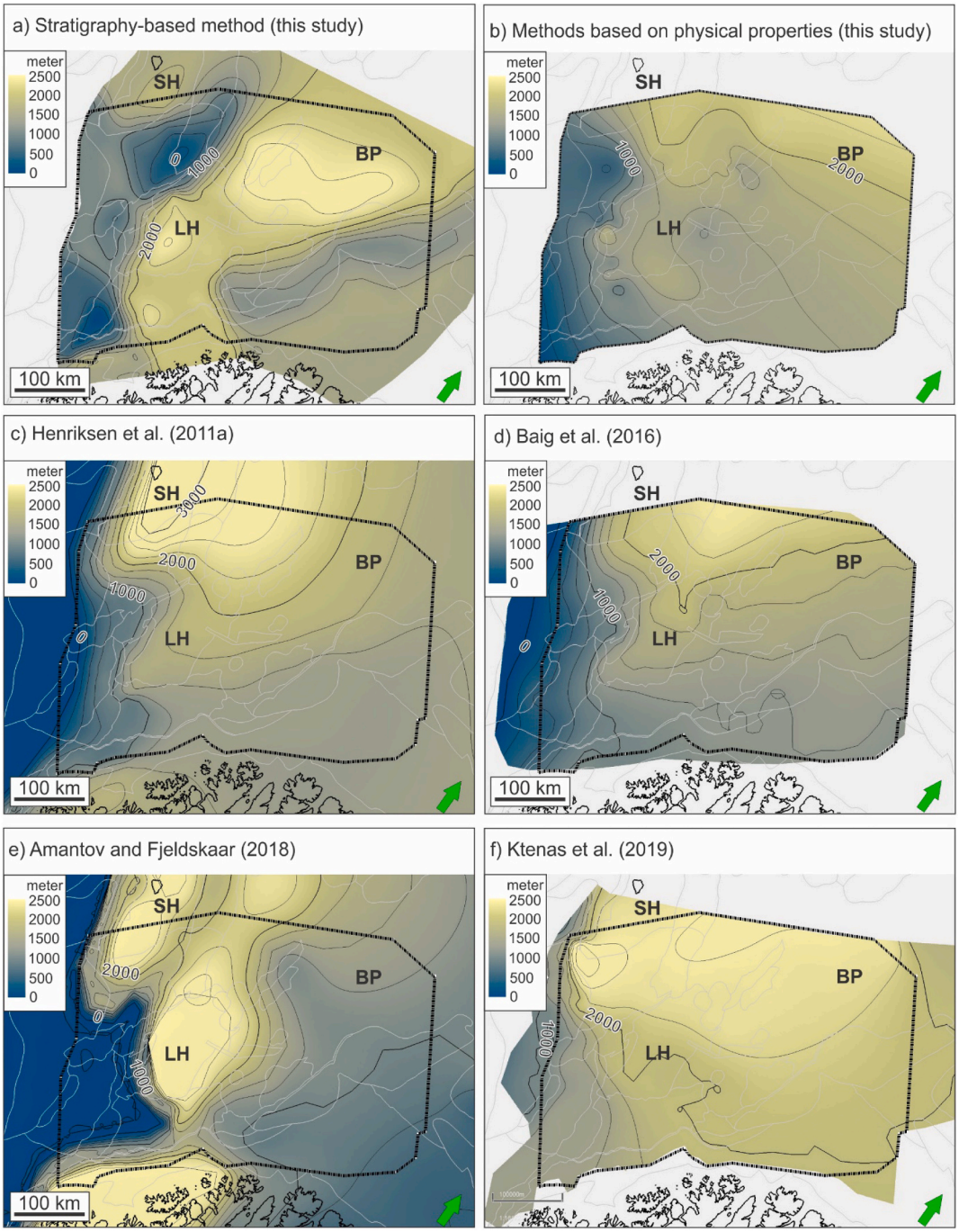

Fig. 18. Net erosion maps of the southwestern Barents Sea scaled to the same colour ramp. a) Stratigraphy-based method, represented by the mass balance method. The sum of net erosion estimates in this study based on results from the Cenozoic pre-glacial (Lasabuda et al., 2018b) and glacial strata (Laberg et al., 2012). b) Methods based on physical properties in this study, i.e. the average of net erosion estimates from sonic velocity, interval velocity and sandstone diagenesis methods based on Johansen (2016) and this study. c) Henriksen et al. (2011a). d) Baig et al. (2016). e) Amantov and Fjeldskaar (2018). f) Ktenas et al. (2019). Abbreviations used: BP: Bjarmeland Platform; LH: Loppa High; SH: Stappen High.

However, results from sandstone diagenesis show discrepancies of more than 300 m compared to the other two methods (e.g. well 7120/2-2, 7121/4-1 and 7324/8-1).

This variation may indicate a spatial variability of net erosion in each structural element, probably linked to the complex tectonic history involving semi-localized pre-glacial tectonic uplift (e.g. Faleide et al., 1993; Lasabuda et al., 2018b, c), strain partitioning along the sheared margin (e.g. Kristensen et al., 2018, 2020), and a differential erosion by ice-sheets in the late Cenozoic (e.g. Laberg et al., 2012; Patton et al., 2016).

There are varying degrees of confidence in the different methods, which are difficult to quantify. Each method has its own range of uncertainty which has to be narrowed in order to increase the precision of the uplift and erosion estimates. There is no direct way to determine the most reliable methods for addressing uplift and erosion. For example, methods which show low uncertainty in some areas can show higher uncertainty in others (Fig. 20). Overall, the accuracy in estimating uplift and erosion is proportional to the amount of data (seismic and well data). We argue that the optimal way to better capture the erosion pattern is to choose a method depending on the geographical target and

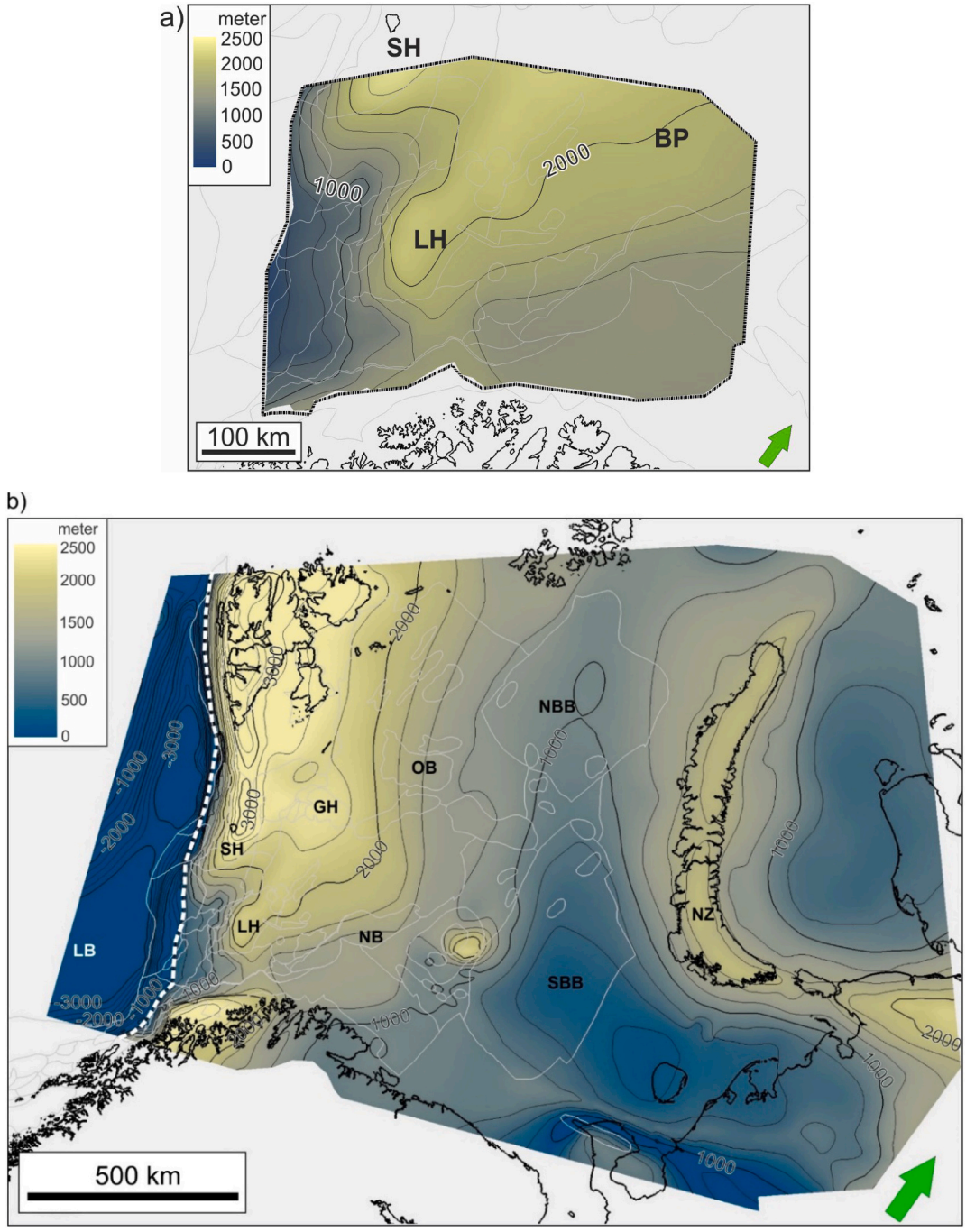

Fig. 19. a) Net erosion map based on the average of different net erosion maps shown in Fig. 18a–f. b) Compiled net erosion map for the greater Barents Shelf. To the west, the contours within the map also show sedimentary thicknesses in the depositional areas. Note also that the contours may show higher net erosion than 2500 m (more than the optimum value shown in the colour scale). Abbreviations used: BP: Bjarmeland Platform; GH: Gardarbanken High; LB: Lofoten Basin; LH: Loppa High; NB: Nordkapp Basin; NBB: North Barents Basin; NZ: Novaya Zemlya; OB: Olga Basin; SBB: South Barents Basin; SH: Stappen High.

data availability.

6.2.1. Uncertainties related to the mass balance method

Each stratigraphic layer deposited offshore is assumed to represent the corresponding erosion in the source area. The pre-glacial and glacial net erosion can thus be separated when using the mass balance method. It is also assumed that the overall Norwegian Barents Shelf was a major depocenter during the Cretaceous (e.g. Grundvåg et al., 2017; Corseri et al., 2018; Midtkandal et al., 2019a), Jurassic (e.g. Smelror et al., 2009; Klausen et al., 2019; Marín et al., 2020) and Triassic (e.g. Klausen et al., 2015; Eide et al., 2017; Gilmullina et al., 2021). Therefore, the Cenozoic is considered a key period for uplift and erosion, with the Barents Shelf interpreted to be the primary source area.

As part of the mass balance analysis, a series of assumptions needs to be addressed in order to capture the sensitivity of the method. As the method relies on the direct measurement of the deposited sediment volume, seismic data coverage and time-depth conversion are crucial for the sediment volume estimates. For the western Barents Shelf continental margin, depth conversion relies on check-shot data from sparsely distributed wells and velocities from seismic reflection and refraction data. Farther north, this is even more challenging as these offshore areas are not open for hydrocarbon exploration, no commercial wells have

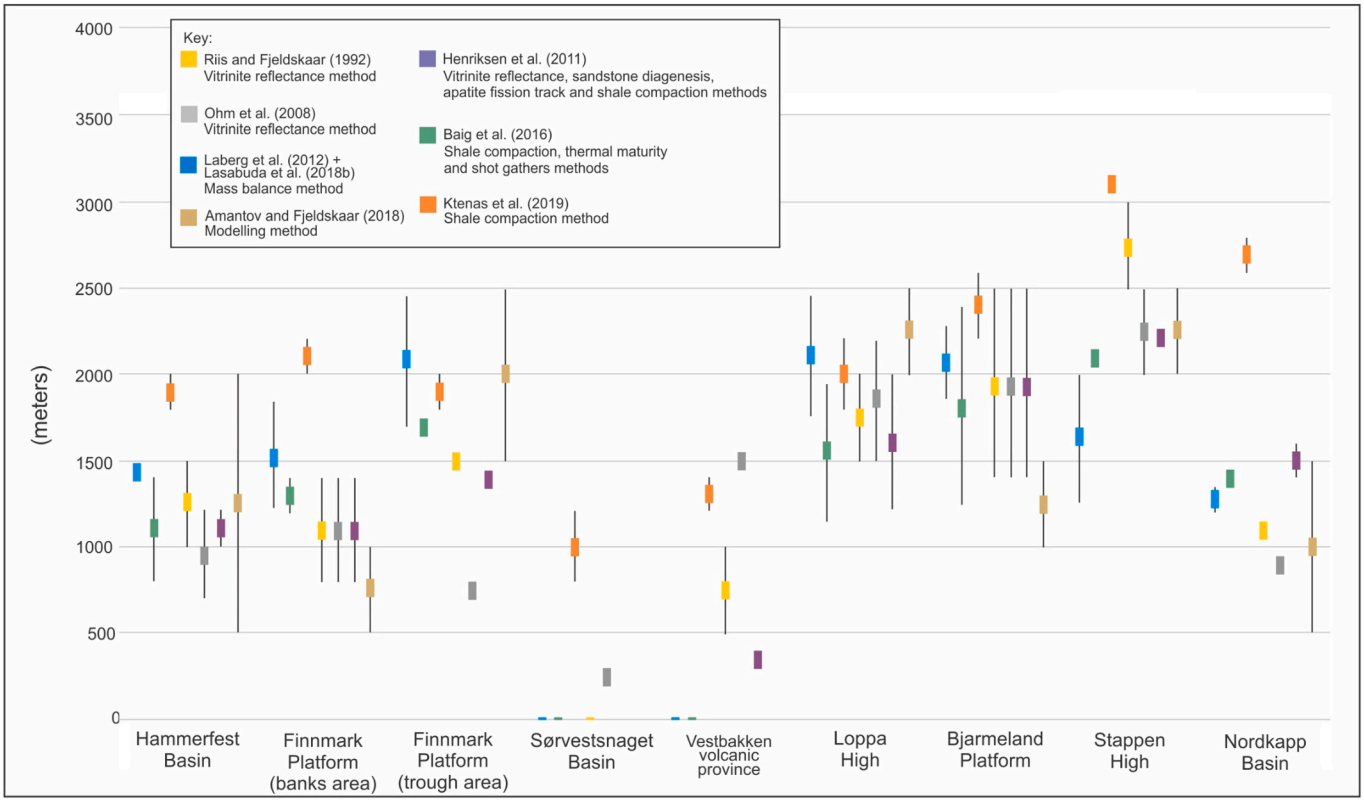

Fig. 20. Cenozoic net erosion in the southwestern Barents Sea compiled from various references in Table 3, showing the estimated range of net erosion. Note that they are not box-whisker plots. See Fig. 2b for location.

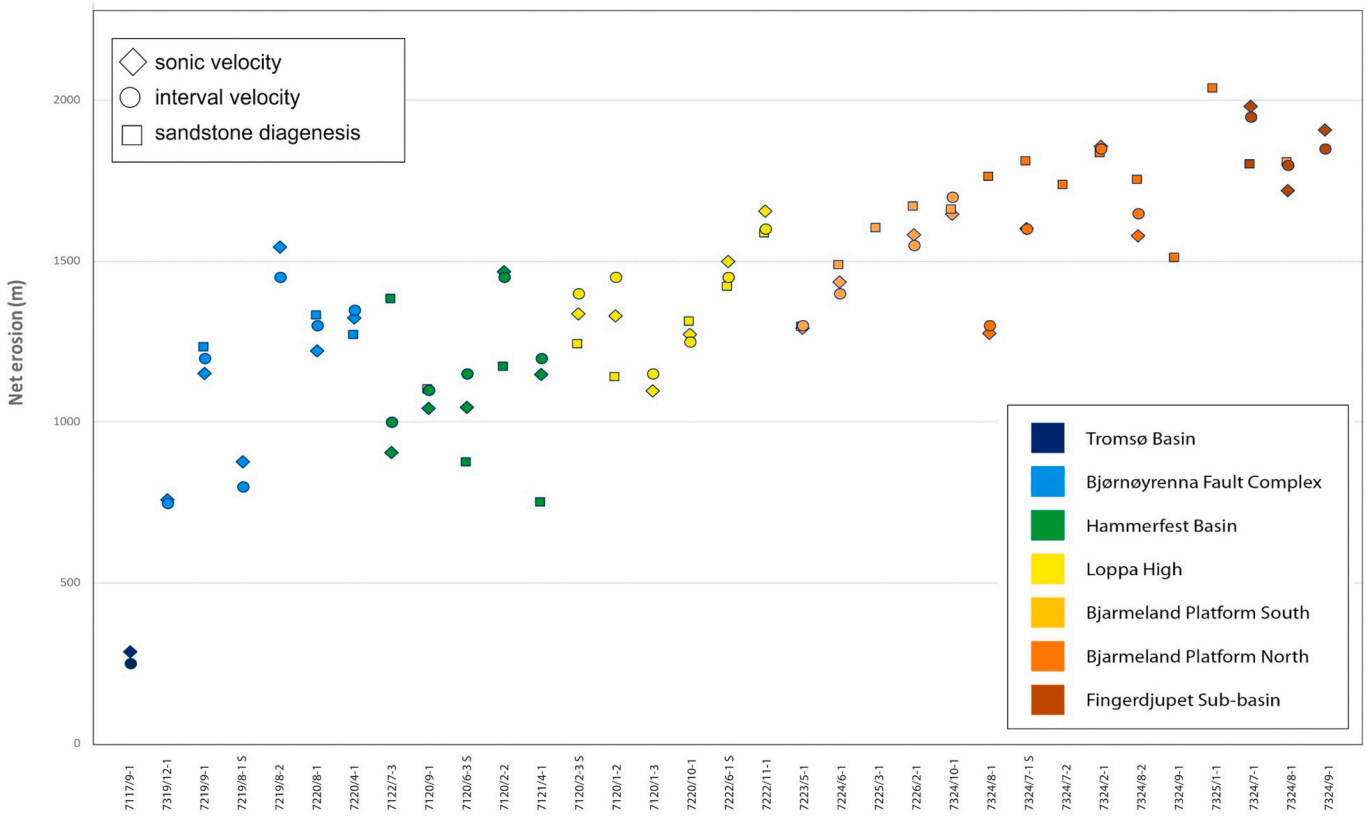

Fig. 21. Comparison of net erosion estimates showing variation of results from this study using sonic, interval velocity and sandstone diagenesis in different structural elements based on Table 4. For some of the wells, only one or two net erosion estimates are available.

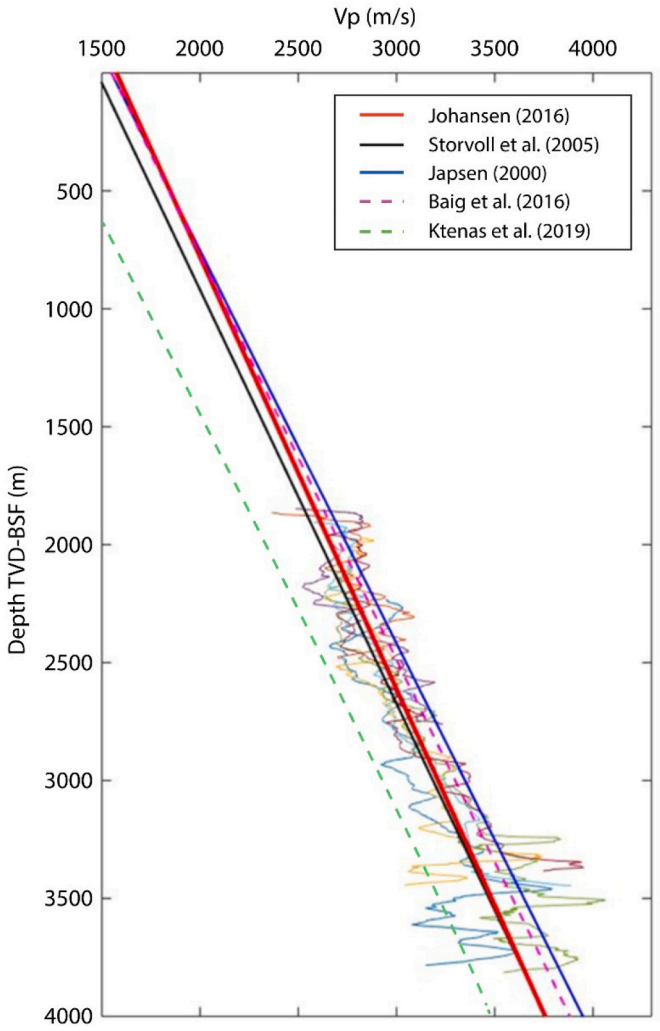

Fig. 22. Comparison of the North Sea reference trend line from this study and Johansen (2016) with previously established trend lines. Velocity well logs used for estimation of the reference trend line are shown in various colours.

been drilled except onshore Svalbard (Senger et al., 2019), and few seismic lines are available.

There are uncertainties that may affect the sediment budget, which are often difficult to quantify. For example, it is important to separate the amount of sediments that were derived from within the basin or outside the source area (e.g. biogenic ooze/silica or sediment derived from ocean contour currents). These sediments should not be included in the volume of sediments derived from the adjacent onshore area and shelf, so a correction factor must be applied. Sediment compaction due to overburden also needs to be calibrated. Sediments may have been compacted due to thick overburden including the glacigenic TMFs in the western margin of the Barents Shelf. Finally, a correction is required due to differences in the lithological composition between the source area and the basin area. This is because the erodability of crystalline bedrock is lower compared to sedimentary bedrock. This correction is determined by assessing the lithology of the source area (e.g. Dowdeswell et al., 2010b; Laberg et al., 2012).

6.2.2. *Uncertainties related to the velocity analysis and sandstone diagenesis method*

For the velocity analysis, it is crucial to have a reliable compaction trend from a basin where no or little uplift occurred, for example the North Sea (Japsen, 2000; Storvoll et al., 2005; Johansen, 2016; Baig et al., 2016; Ktenas et al., 2019). Normal compaction trend lines from this study and previously published work are plotted in Fig. 22. All trend lines show an overall similar trend and gradient, meaning that they are consistent as a reference and will give a rather low variation in net erosion estimates (200 – 300 m). At larger burial depths, effects of chemical compaction occur, and the use of corresponding velocities for net erosion estimate should be done with caution. Lithological effects (e.g. deposition of dolomites) may give anomalously high velocities and thus, unrealistic net erosion estimates (see example in Fig. 14). We suggest that the best net erosion estimates based on compaction trends come from comparing similar mudstone within the mechanical compaction window.

Several factors can influence the estimates derived from the sandstone diagenesis method. Firstly, different burial histories can result in the same net erosion results. However, different burial histories may produce different amount of cement. The amount of cement is dependent on the time the formation has been subjected to temperatures higher than approximately 70°C (Bjørlykke and Jahren, 2015). More cement will lead to a smaller net erosion estimate. Secondly, the calculated volume of cement will also change due to change in temperature gradient. The temperature gradients for each subbasin in the western Barents Shelf area vary from approximately 35°C in the Hammerfest Basin to 42°C in the Hoop area and the northern Bjarmeland Platform (NPD, 2016). Decreases in the temperature gradient will increase the net erosion estimates. Thirdly, actual properties of the sandstone may show different results. This method assumes a well-sorted and homogenous quartz as well as brine as the pore fluid. Grain size and coating will also affect the generated cement volumes. Finally, overpressure and differential compaction may affect the results, factors which are not taken into account in this study. Overpressure may slow down the compaction processes, which will result in an underestimation of the net erosion.

6.3. *Comparison of erosion rates*

The pre-glacial erosion rates are comparable to fluvial systems, and are generally lower than rates for the glacial period (e.g. Lasabuda, 2018). Cenozoic pre-glacial erosion rates for the southwestern and northwestern Barents Sea area are presented in Fig. 23. There is slight decreasing trend from Paleocene (0.052 m/ky) to Neogene (0.032 m/ky) in the northwestern Barents Sea. For the southwestern Barents Sea, the erosion rates are relatively constant (0.18 – 0.23 m/ky). The average values are in agreement with results from Hjelstuen et al. (1996) and Fiedler and Faleide et al. (1996).

The amount and rate of erosion for the non-glacial period depends largely on the size of the source area and the type of bedrock. For the pre-glacial strata on the western Barents Shelf, the paleocatchment analysis and delineation of source areas are more uncertain as most of the source areas have been subsequently altered by profound glacial erosion. The spatial extent of the source areas is also likely to vary through time owing to the dynamics of plate configuration along the western Barents Sea margin. A complete understanding of the regional tectonics, detailed structural and stratigraphic mapping, and analysis of the sedimentary patterns (e.g. direction of progradation into sedimentary basin) from seismic data are thus crucial.

Differences in the rate of erosion across different parts of the Barents Shelf for the glacial period may reflect broad-scale differences in bedrock composition (e.g. Dowdeswell et al., 2010b; Hjelstuen et al., 2012; Laberg et al., 2012; Rydningen et al., 2016). However, transient simulations of landscape denudation suggest rates of glacial erosion are influenced by an amalgam of factors, including climate, ice-sheet basal thermo-mechanics, topographic relief, and the evolving configuration of the ice cover (e.g. Patton et al., 2015, (in review)). The intensity by which glaciers selectively erode their substrate is thus highly variable, both through space and time.

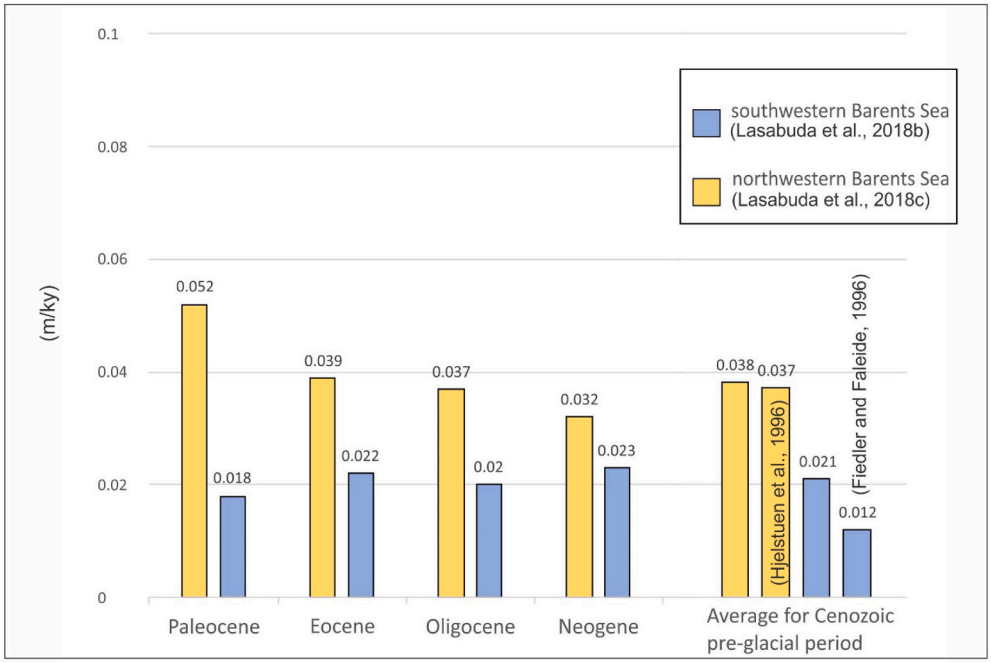

Fig. 23. Cenozoic pre-glacial erosion rates (m/ky) estimates. There is a slight decreasing trend from the Paleocene to Neogene in the northwestern Barents Sea. For the southwestern Barents Sea the erosion rates are relatively constant. These values are comparable with results from Hjelstuen et al. (1996) and Fiedler and Faleide et al. (1996).

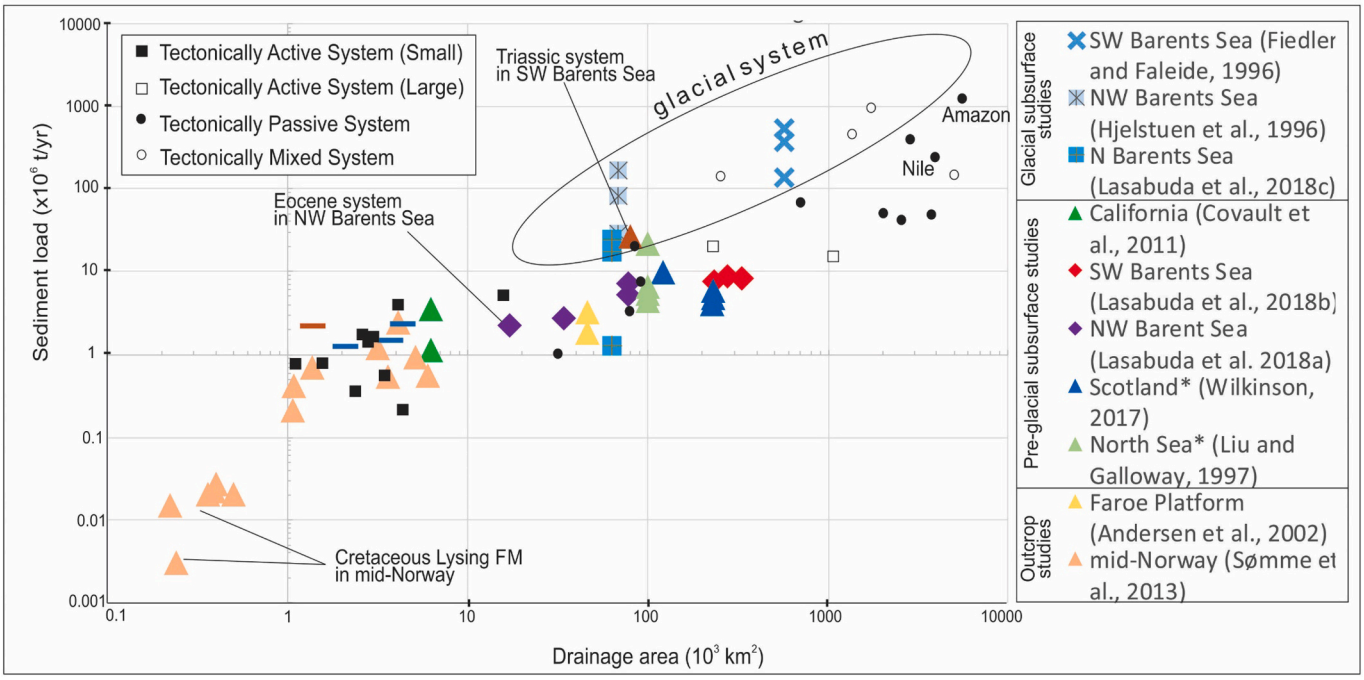

Fig. 24. Cross-plot diagram showing sediment load versus drainage area of glacial systems, non-glacial systems, and outcrop studies. The black and white rectangles and circles are modern systems from different tectonic settings (Sømme et al., 2009a). The coloured points are compiled from various areas based on Table 5.

6.4. Relief prediction of the source area

Sediment load reflects the amount of sediments discharged over a certain time period from the drainage area. We attempt to predict the catchment relief of pre-glacial and glacial systems on the Barents Shelf by plotting the sediment load against the catchment size following a diagram from Sømme et al. (2009a). Although an expanded database of source-to-sink systems has been presented by Nyberg et al. (2018), sediment load (Qs) in both databases of Sømme et al. (2009a) and Nyberg et al. (2018) shows r^2=0.97, meaning that the diagram is still reliable (Fig. 24). Note that the correlation between the relief of a catchment in the source area and the morphology of deposits may be more complex due to the non-uniqueness of a source-to-sink system, which is associated with its tectonic history, climate variation and the relative maturity of a system (Nyberg et al., 2018).

Sømme et al. (2009a) plotted sediment load against the catchment

Table 5
Comparison of sediment load and drainage area for the pre-glacial, glacial and outcrop studies from various areas. The studies marked with (*) indicate density of 2.2 g/cm^3 is applied.

	Area (references)	Period	Sediment load (10^6 t/y)	Max. drainage area (10^3 km^2)
Glacial subsurface studies	Southwestern Barents Sea (Fiedler and Faleide, 1996)	Pleistocene (GIII)	373	576
		Pleistocene (GII)	543	576
		Pleistocene (GI)	137	576
	Northwestern Barents Sea (Hjelstuen et al., 1996)	Pleistocene (GIII)	29	69
		Pleistocene (GII)	167	69
		Pleistocene (GI)	82.4	69
	Northern Barents Sea (Lasabuda et al., 2018a)	Plesitocene (NB-3C)	1.3	63.2
		Pleistocene (NB-3B)	24.1	63.2
		Late Pliocene?–Pleistocene (NB-3A)	17.4	63.2
Pre-glacial subsurface studies	California (Covault et al., 2011)	Holocene	3.5	6.2
		Holocene	1.12	6.2
	Southwestern Barents Sea (Lasabuda et al., 2018b)	Neogene	9.3	334
		Oligocene	8.3	334
		Eocene	8.8	275.8
		Paleocene	7.7	232.6
	Northwestern Barent Sea (Lasabuda et al., 2018c)	Neogene	5.3	78.2
		Oligocene	7.1	78.2
		Eocene	2.7	34
		Paleocene	2.2	17
	Scotland* (Wilkinson, 2017)	Miocene	4.9	231
		Oligocene	4	227
		Eocene	6.0	230
		Paleocene	9.9	122
	North Sea* (Liu and Galloway, 1997)	Miocene	4.4	100
		Oligocene	6.6	100
		Eocene	5.5	100
		Paleocene	22	100
	Faroe Platform (Andersen et al., 2002)	Miocene	1.84	46
		Eocene–Oligocene	3.22	46
	mid-Norway (Sømme et al., 2013)	Paleocene	0.7	1.36
		Paleocene	0.42	1.08
		Paleocene	1.19	3.15
		Paleocene	0.92	5.11
		Cretaceous	0.003	0.24
		Cretaceous	0.022	0.39
		Cretaceous	0.211	1.06
		Cretaceous	0.02	0.5
		Cretaceous	0.02	0.36
		Cretaceous	0.015	0.22
		Cretaceous	0.027	0.4
		Cretaceous	0.538	3.59
		Jurassic	0.56	5.95
		Jurassic	2.46	4.08
	SW Barents Sea (Eide et al., 2017)	Triassic	27	80
Outcrop studies	Pyrenees (Michael et al., 2014)	Eocene	1.2	2.1
		Eocene	1.5	3.7
		Eocene	2.3	4.4
	Greece* (Pechlivanidou et al., 2018)	Holocene	2.2	1.4

size of different systems worldwide based on their tectonic regime (tectonically active, small or large, passive, or a mixed system). From this, we can predict the likely relief of the paleocatchment of different periods, whether they resemble paleocatchment from tectonically active (small or large), passive or a mixed system (Fig. 24). In order to test the diagram of Sømme et al. (2009a), we can compare results from relatively well-known geographical settings to the background information of the tectonic regime (Table 5). The source-to-sink system in the Pyrenees (Michael et al., 2014), Greece (Pechlivanidou et al., 2018), California (Covault et al., 2011) and mid-Norway (Sømme et al., 2013) fall into the smaller tectonically active system part of the diagram. Similarly, data from the North Sea (Liu and Galloway, 1997) are in agreement with data from a tectonically passive system. As such, these examples reflect the consistency of this diagram (Fig. 24).

The comparison of sediment load and drainage area for pre-glacial systems of the western Barents Sea area shows a good fit with similar Cenozoic studies from the Faroe Islands (Andersen et al., 2002), the North Sea (Liu and Galloway, 1997) and Scotland (Wilkinson, 2017) (Fig. 24). The drainage areas for pre-glacial sediments in the western Barents Sea include uplifted areas such as the Stappen High, the Loppa High and the Bjarmeland Platform. In the northwestern Barents Sea, the Stappen High, NE Greenland and Edgeøya platform are considered as key source areas during the pre-glacial period. These structural elements are thought to have been affected by the early Cenozoic tectonism involving transform movements between Greenland and the western Barents Shelf (Faleide et al., 2008, 2015). The results on the western Barents Shelf show a positive match with present-day systems in large tectonically active or passive systems.

The glacial systems, including the northern Barents Shelf, show a generally high sediment load (Fig. 24). However, the younger strata shows low sediment load (Lasabuda et al., 2018a), probably due to most of the ice on the northern Barents Shelf draining towards the Franz Victoria Trough during the LGM (Dowdeswell et al., 2010a; see Fig. 11 for location). Results from the glacial systems are of the same order of magnitude as results reported from source-to-sink systems in tectonically mixed areas (Sømme et al., 2009a). The relatively high value from systems in tectonically mixed settings is likely due to a combination of high sediment flux resulting from active tectonics, and a relatively wide drainage area, typical of a passive tectonic setting (e.g. the Bengal Fan system). This may also explain the high sediment load from the Triassic system of the southwestern Barents Shelf in Fig. 24 (Eide et al., 2017). The mixed system probably fits with the wide and deep system of the foreland setting of Nyberg et al. (2018).

6.5. Comparison with other Cenozoic-uplifted basins

Here we highlight examples of other basins that have undergone similar Cenozoic uplift with regard to the magnitude and the nature of uplift and timing, according to Dore and Jensen (1996), Henriksen et al. (2011a) and references therein. In terms of magnitude, the km-scale uplift and erosion of the Barents Shelf has also been observed in the Sverdrup Basin (up to 1 km) and in the Western Canada Basin (up to 4 km). In terms of the nature of uplift, a number of basins have an orogenic cause (e.g. the Maracaibo Basin in Venezuela, Zagros Foreland Basin in Iran and Junggar Basin in China). Other basins have been affected by an epeirogenic event, i.e. regional vertical movements of continental crust, for example the Permian and San Juan basins in the USA. Some basins, particularly in the circum-Arctic region (e.g. the Western Canada, Sverdrup, Barents Sea and Timan-Pechora basins), have been heavily glaciated by major continental ice sheets during past glaciations, implying an isostatic uplift mechanism for the latter stage of their development. These basins also hold considerable petroleum resources, which has drawn particular interest towards the topic of the Cenozoic uplift and erosion. In terms of timing, some basins, including the Barents Sea basins, were initially uplifted in the early Cenozoic (e.g. the San Juan and Maracaibo basins) while other basins started their uplift more recently (e.g. the Zagros Foreland and Junggar basins experienced Miocene uplift).

6.6. Future research directions

The Barents Shelf is predicted to hold much of the remaining petroleum resources (c. 2500 million standard cubic meters of oil equivalent) of the Norwegian Continental Shelf (NPD, 2018, 2019). Today, the southwestern Barents Sea sector remains the core location for petroleum exploration activities in the Norwegian Arctic, where two fields are currently producing; the Snøhvit gas field and the Goliat oil field. Extensive studies in the Barents Sea offer a well-constrained analogue for other basins, as large parts of the Norwegian Continental Shelf are affected by uplift and erosion, for example the flanks of the North Sea basin (e.g. Baig et al., 2019; Medvedev et al., 2019).

Understanding the spatial variations in uplift and erosion rates is crucial for basin and petroleum system modelling during the early exploration phase since the actual timing of maximum depth of burial remains uncertain. This has resulted in diverging basin modelling results in a single basin, for instance in the Hammerfest Basin, where a maximum depth of burial could have occurred during the Paleogene or the Neogene (e.g. Ben-Awuah et al., 2013; Duran et al., 2013; Baig et al., 2016; Mohammedyasin, 2017; Ostanin et al., 2017). Uplift and erosion may influence the exploration strategy of the Barents Shelf, following the re-migration of hydrocarbons to a shallower level, which may be the case for the Wisting oil discovery at just c. 250 m below the seabed (Veire et al., 2016). Assessing further effects on other petroleum system elements, for instance, sealing capacity, will contribute to a better assessment of potential sites for CO_2 storage on the Barents Shelf.

The precise timing of different uplift episodes also needs more detailed quantification. How uplift and erosion relates to each other will also be crucial in determining their relative importance as controlling factors. Both deeper processes (e.g. mantle dynamics/processes) and surface processes (e.g. ice-sheet thickness and spatial variability through time) play a crucial role in vertical motions. These processes affect the sediment routing from source to sink areas, and thus the spatial preference of erosion and deposition. They will also lead to a better understanding of the spatiotemporal distribution of methane and gas hydrates occurrences on seafloor (e.g. Andreassen et al., 2017; Waghorn et al., 2020), a possible proxy for future climate predictions.

By increasing the number of wells used in future analyses, we expect to produce higher resolution paleoenvironmental maps. Higher resolution numerical models with more detailed parameterisations of physical processes are being developed. Modelling on the deformation of the crust by considering the anisotropy condition will also enhance the confidence level. Machine learning will likely play a role in quantitative studies utilizing the current >120 wells on the Barents Shelf. Other geophysical methods such as using electromagnetic data from controlled source electromagnetic (CSEM) and magnetotelluric (MT), which are currently underexplored (e.g. Senger et al., 2020), have potential for estimating uplift and erosion.

7. Conclusions

We present a new compilation map of net erosion estimates for the Barents Shelf based on our results integrated with previous work. The map shows an increasing trend of net erosion to the north and northeast on the southwestern Barents Shelf, as well as around Svalbard. We highlight a range of key mechanisms for the Cenozoic uplift and erosion, from tectonic, including compression, rift-flank uplift, thermo-mechanical coupling and flexural/isostatic response, to magmatic and glacial-related processes. These mechanisms are discussed in light of three main episodes of uplift on the Barents Shelf, during the early, middle and late Cenozoic.

From the mass balance method, we combine the two major periods of erosion (pre-glacial and glacial) to estimate the Cenozoic net erosion.

The ratio between the Cenozoic pre-glacial and glacial sediment volume is estimated to be 40%, 50% and 70%, for the southwestern, northwestern and northern Barents Shelf, respectively.

By testing sonic velocity, interval velocity and sandstone diagenesis methods, we find that these methods are reliable, given some geological calibrations. Estimates from sonic and interval velocities show similar values, while the estimates from the sandstone diagenesis method differ by up to c. 300 m.

The current discrepancies of net erosion estimates in different structural elements vary up to 500 m in areas with dense seismic and well data (e.g. 1000 – 1500 m of net erosion estimate in the Hammerfest Basin) and around 1000 m on the Bjarmeland Platform (i.e. having been eroded 1500 – 2500 m). These numbers thereby contribute to varying levels of confidence in published net erosion maps. Generally, higher uncertainties in estimates are related to areas where data are lacking, requiring long distance correlation and interpolation.

Future directions of this research on the Barents Shelf should focus on: (1) lowering the uncertainties of net erosion estimates by reducing sources of error in each method, (2) constraining the precise timing of uplift/erosion for better validation of basin modelling results, and (3) investigating the detailed effects of uplift and erosion on petroleum systems to reduce exploration uncertainties.

Declaration of Competing Interest

The authors declare that they have no known competing financial interests or personal relationships that could have appeared to influence the work reported in this paper.

Acknowledgements

This research was funded by the Research Centre for Arctic Petroleum Exploration (ARCEx) partners and the Research Council of Norway (grant 228107). APEL and HP are supported with a grant from the Equinor–UiT *Akademia* agreement. JIF and HP acknowledge the Centre for Earth Evolution and Dynamics (CEED) and Centre for Arctic Gas Hydrate, Environment and Climate (CAGE), funded by the Research Council of Norway through its Centres of Excellence funding scheme (grant 223272 and 223259), respectively. Some of the results presented in this paper were part of the doctoral thesis of APEL and master thesis of NSJ. The perceptually uniform colour maps of Crameri et al. (2020) were used to avoid visual distortion. We thank Edward L. King, Alvar Braathen, Matthias Forwick and Rowan Romeyn for commenting an earlier version of the manuscript. The Reviewers Tony Doré, Jolante van Wijk and an anonymous reviewer, and the Editor Carlo Doglioni are acknowledged for their thorough reviews which improved the quality of the paper.

References

Amantov, A., Fjeldskaar, W., 2018. Meso-Cenozoic exhumation and relevant isostatic process: the Barents and Kara shelves. J. Geodyn. 118, 118–139. https://doi.org/10.1016/j.jog.2017.12.001.

Andersen, M.S., Sørensen, A.B., Boldreel, L.O., Nielsen, T., 2002. Cenozoic evolution of the Faroe Platform: comparing denudation and deposition. Geol. Soc. London Spec. Publ. 196 (1), 291–311. https://doi.org/10.1144/GSL.SP.2002.196.01.16.

Andreassen, K., Laberg, J.S., Vorren, T.O., 2008. Seafloor geomorphology of the SW Barents Sea and its glaci-dynamic implications. Geomorphology 97 (1), 157–177. https://doi.org/10.1016/j.geomorph.2007.02.050.

Andreassen, K., Hubbard, A., Winsborrow, M., Patton, H., Vadakkepuliyambatta, S., Plaza-Faverola, A., Gudlaugsson, E., Serov, P., Deryabin, A., Mattingsdal, R., 2017. Massive blow-out craters formed by hydrate-controlled methane expulsion from the Arctic seafloor. Science 356 (6341), 948–953. https://doi.org/10.1126/science.aal4500.

Anell, I., Thybo, H., Artemieva, I., 2009. Cenozoic uplift and subsidence in the North Atlantic region: Geological evidence revisited. Tectonophysics 474 (1), 78–105. https://doi.org/10.1016/j.tecto.2009.04.006.

Auriac, A., Whitehouse, P., Bentley, M., Patton, H., Lloyd, J., Hubbard, A., 2016. Glacial isostatic adjustment associated with the Barents Sea ice sheet: a modelling inter-comparison. Quat. Sci. Rev. 147, 122–135. https://doi.org/10.1016/j.quascirev.2016.02.011.

Avseth, P., Lehocki, I., 2016. Combining burial history and rock-physics modeling to constrain AVO analysis during exploration. Lead. Edge 35 (6), 528–534. https://doi.org/10.1190/tle35060528.1.

Avseth, P., Veggeland, T., Lehocki, I., 2014. Combined burial history and rock physics modeling of quartz-rich sandstones–Norwegian shelf demonstrations. SEG Technical Program Expanded Abstracts 2014, 2809–2813. https://doi.org/10.1190/segam2014-1676.1.

Baig, I., Faleide, J.I., Jahren, J., Mondol, N.H., 2016. Cenozoic exhumation on the southwestern Barents Shelf: Estimates and uncertainties constrained from compaction and thermal maturity analyses. Mar. Pet. Geol. 73, 105–130. https://doi.org/10.1016/j.marpetgeo.2016.02.024.

Baig, I., Faleide, J.I., Mondol, N.H., Jahren, J., 2019. Burial and exhumation history controls on shale compaction and thermal maturity along the Norwegian North Sea basin margin areas. Mar. Pet. Geol. 104, 61–85. https://doi.org/10.1016/j.marpetgeo.2019.03.010.

Barnes, C.J., Schneider, D.A., 2019. Late Cretaceous – Paleogene burial and exhumation history of the Southwestern Basement Province, Svalbard, revealed by zircon (U-Th)/He thermochronology. In: Circum-Arctic Structural Events: Tectonic Evolution of the Arctic Margins and Trans-Arctic Links with Adjacent Orogens, 541, p. 131.

Batchelor, C., Dowdeswell, J., Pietras, J., 2013. Seismic stratigraphy, sedimentary architecture and palaeo-glaciology of the Mackenzie Trough: evidence for two Quaternary ice advances and limited fan development on the western Canadian Beaufort Sea margin. Quat. Sci. Rev. 65, 73–87. https://doi.org/10.1016/j.quascirev.2013.01.021.

Bellwald, B., Planke, S., Becker, L.W., Myklebust, R., 2020. Meltwater sediment transport as the dominating process in mid-latitude trough mouth fan formation. Nat. Commun. 11 (1), 1–10. https://doi.org/10.1038/s41467-020-18337-4.

Ben-Awuah, J., Adda, G., Mijinyawa, A., Andriamihaja, S., Siddiqui, N., 2013. 2D Basin modelling and petroleum system analysis of the triassic play in the hammerfest basin of the norwegian barents sea. Res. J. Appl. Sci. Eng. Technol. 6 (17), 3137–3150. https://doi.org/10.19026/rjaset.6.3615.

Bergh, S.G., Grogan, P., 2003. Tertiary structure of the Sørkapp-Hornsund Region, South Spitsbergen, and implications for the offshore southern extension of the fold-thrust Belt. Norw. J. Geol./Norsk Geologisk Forening 83 (1).

Bergh, S.G., Braathen, A., Andresen, A., 1997. Interaction of basement-involved and thin-skinned tectonism in the Tertiary fold-thrust belt of central Spitsbergen, Svalbard. AAPG Bull. 81 (4), 637–661. https://doi.org/10.1306/522B43F7-1727-11D7-8645000102C1865D.

Berglar, K., Franke, D., Lutz, R., Schreckenberger, B., Damm, V., 2016. Initial opening of the Eurasian Basin, Arctic Ocean. Front. Earth Sci. 4, 91. https://doi.org/10.3389/feart.2016.00091.

Bird, K.J., Charpentier, R.R., Gautier, D.L., Houseknecht, D.W., Klett, T.R., Pitman, J.K., Moore, T.E., Schenk, C.J., Tennyson, M.E., Wandrey, C.R., 2008. Circum-Arctic Resource Appraisal: Estimates of Undiscovered Oil and Gas North of the Arctic Circle, 2327-6932, US Geological Survey. https://doi.org/10.3133/fs20083049.

Bjørlykke, K., Jahren, J., 2015. Sandstones and sandstone reservoirs. In: Pet. Geosci. Springer, pp. 119–149. https://doi.org/10.1007/978-3-642-34132-8_4.

Blaich, O., Tsikalas, F., Faleide, J., 2017. New insights into the tectono-stratigraphic evolution of the southern Stappen High and its transition to Bjørnøya Basin, SW Barents Sea. Mar. Pet. Geol. 85, 89–105. https://doi.org/10.1016/j.marpetgeo.2017.04.015.

Blinova, M., Thorsen, R., Mjelde, R., Faleide, J.I., 2009. Structure and evolution of the Bellsund Graben between Forlandsundet and Bellsund (Spitsbergen) based on marine seismic data. Nor. J. Geol. 89, 215–228.

Blinova, M., Inge Faleide, J., Gabrielsen, R.H., Mjelde, R., 2012. Seafloor expression and shallow structure of a fold-and-thrust system, Isfjorden, west Spitsbergen. Polar Res. 31 (1), 11209 https://doi.org/10.3402/polar.v31i0.11209.

Blinova, M., Faleide, J.I., Gabrielsen, R.H., Mjelde, R., 2013. Analysis of structural trends of sub-sea-floor strata in the Isfjorden area of the West Spitsbergen Fold-and-Thrust Belt based on multichannel seismic data. J. Geol. Soc. 170 (4), 657–668. https://doi.org/10.1144/jgs2012-109.

Blythe, A.E., Kleinspehn, K.L., 1998. Tectonically versus climatically driven Cenozoic exhumation of the Eurasian plate margin, Svalbard: Fission track analyses. Tectonics 17 (4), 621–639. https://doi.org/10.1029/98TC01890.

Braathen, A., Bergh, S., Maher, H., 1995. Structural outline of a Tertiary Basement-cored uplift/inversion structure in western Spitsbergen, Svalbard: Kinematics and controlling factors. Tectonics 14 (1), 95–119. https://doi.org/10.1029/94TC01677.

Bredesen, K., Avseth, P., Johansen, T.A., Olstad, R., 2019. Rock physics modelling based on depositional and burial history of Barents Sea sandstones. Geophys. Prospect. 67 (4), 825–842. https://doi.org/10.1111/1365-2478.12683.

Breivik, A.J., Mjelde, R., Grogan, P., Shimamura, H., Murai, Y., Nishimura, Y., 2003. Crustal structure and transform margin development south of Svalbard based on ocean bottom seismometer data. Tectonophysics 369 (1), 37–70. https://doi.org/10.1016/S0040-1951(03)00131-8.

Brozena, J., Childers, V., Lawver, L., Gahagan, L., Forsberg, R., Faleide, J., Eldholm, O., 2003. New aerogeophysical study of the Eurasia Basin and Lomonosov Ridge: implications for basin development. Geology 31 (9), 825–828. https://doi.org/10.1130/G19528.1.

Butt, F., Elverhøi, A., Solheim, A., Forsberg, C., 2000. Deciphering Late Cenozoic development of the western Svalbard Margin from ODP Site 986 results. Mar. Geol. 169 (3-4), 373–390. https://doi.org/10.1016/S0025-3227(00)00088-8.

Butt, F.A., Drange, H., Elverhøi, A., Otterå, O.H., Solheim, A., 2002. Modelling Late Cenozoic isostatic elevation changes in the Barents Sea and their implications for oceanic and climatic regimes: preliminary results. Quat. Sci. Rev. 21 (14), 1643–1660. https://doi.org/10.1016/S0277-3791(02)00018-5.

Carminati, E., Doglioni, C., 2010. North Atlantic geoid high, volcanism and glaciations. Geophys. Res. Lett. 37 (3) https://doi.org/10.1029/2009GL041663.
Carminati, E., Cuffaro, M., Doglioni, C., 2009. Cenozoic uplift of Europe. Tectonics 28 (4). https://doi.org/10.1029/2009TC002472.
Cavanagh, A.J., Di Primio, R., Scheck-Wenderoth, M., Horsfield, B., 2006. Severity and timing of Cenozoic exhumation in the southwestern Barents Sea. J. Geol. Soc. 163 (5), 761–774. https://doi.org/10.1144/0016-76492005-146.
Clark, S., Glorstad-Clark, E., Faleide, J., Schmid, D., Hartz, E., Fjeldskaar, W., 2014. Southwest Barents Sea rift basin evolution: comparing results from backstripping and time-forward modelling. Basin Res. 26 (4), 550–566. https://doi.org/10.1111/bre.12039.
Cook, S.J., Swift, D.A., Kirkbride, M.P., Knight, P.G., Waller, R.I., 2020. The empirical basis for modelling glacial erosion rates. Nat. Commun. 11 (1), 1–7. https://doi.org/10.1038/s41467-020-14583-8.
Corcoran, D., Doré, A., 2005. A review of techniques for the estimation of magnitude and timing of exhumation in offshore basins. Earth-Sci. Rev. 72 (3-4), 129–168. https://doi.org/10.1016/j.earscirev.2005.05.003.
Corseri, R., Faleide, T.S., Faleide, J.I., Midtkandal, I., Serck, C.S., Trulsvik, M., Planke, S., 2018. A diverted submarine channel of Early Cretaceous age revealed by high-resolution seismic data, SW Barents Sea. Mar. Pet. Geol. 98, 462–476. https://doi.org/10.1016/j.marpetgeo.2018.08.037.
Covault, J.A., Romans, B.W., Graham, S.A., Fildani, A., Hilley, G.E., 2011. Terrestrial source to deep-sea sink sediment budgets at high and low sea levels: Insights from tectonically active Southern California. Geology 39 (7), 619–622. https://doi.org/10.1130/G31801.1.
Crameri, F., Shephard, G.E., Heron, P.J., 2020. The misuse of colour in science communication. Nat. Commun. 11 (1), 1–10. https://doi.org/10.1038/s41467-020-19160-7.
Dahlgren, K.T., Vorren, T.O., Laberg, J.S., 2002. Late Quaternary glacial development of the mid-Norwegian margin—65 to 68 N. Mar. Pet. Geol. 19 (9), 1089–1113. https://doi.org/10.1016/S0264-8172(03)00004-7.
Dallmann, W.K.E., 2015. Geoscience Atlas of Svalbard. Norsk Polarinstitutt Rapportserie 148. http://hdl.handle.net/11250/2580810.
De Paor, D.G., Bradley, D.C., Eisenstadt, G., Phillips, S.M., 1989. The Arctic Eurekan orogen: A most unusual fold-and-thrust belt. Geol. Soc. Am. Bull. 101 (7), 952–967. https://doi.org/10.1130/0016-7606(1989)101<0952:TAEOAM>2.3.CO;2.
Dimakis, P., Braathen, B.I., Faleide, J.I., Elverhøi, A., Gudlaugsson, S.T., 1998. Cenozoic erosion and the preglacial uplift of the Svalbard–Barents Sea region. Tectonophysics 300 (1), 311–327. https://doi.org/10.1016/S0040-1951(98)00245-5.
Dimakis, P., Elverhøi, A., Høeg, K., Solheim, A., Harbitz, C., Laberg, J.S., Vorren, T.O., Marr, J., 2000. Submarine slope stability on high-latitude glaciated Svalbard–Barents Sea margin. Mar. Geol. 162 (2-4), 303–316. https://doi.org/10.1016/S0025-3227(99)00076-6.
Dix, C.H., 1955. Seismic velocities from surface measurements. Geophysics 20 (1), 68–86. https://doi.org/10.1190/1.1438126.
Donelick, R.A., O'Sullivan, P.B., Ketcham, R.A., 2005. Apatite fission-track analysis. Rev. Mineral. Geochem. 58 (1), 49–94. https://doi.org/10.2138/rmg.2005.58.3.
Doré, A., Jensen, L., 1996. The impact of late Cenozoic uplift and erosion on hydrocarbon exploration: offshore Norway and some other uplifted basins. Glob. Planet. Chang. 12 (1), 415–436. https://doi.org/10.1016/0921-8181(95)00031-3.
Doré, A., Cartwright, J., Stoker, M., Turner, J., White, N., 2002. Exhumation of the North Atlantic margin: introduction and background. Geol. Soc. Lond. Spec. Publ. 196 (1), 1–12. https://doi.org/10.1144/GSL.SP.2002.196.01.01.
Doré, A., Lundin, E., Gibbons, A., Sømme, T., Tørudbakken, B., 2016. Transform margins of the Arctic: a synthesis and re-evaluation. Geol. Soc. Lond. Spec. Publ. 43 (1), 63–94. https://doi.org/10.1144/SP431.8.
Dörr, N., Clift, P., Lisker, F., Spiegel, C., 2013. Why is Svalbard an island? Evidence for two-stage uplift, magmatic underplating, and mantle thermal anomalies. Tectonics 32 (3), 473–486. https://doi.org/10.1002/tect.20039.
Dörr, N., Lisker, F., Jochmann, M., Rainer, T., Schlegel, A., Schubert, K., Spiegel, C., 2018. Subsidence, rapid inversion, and slow erosion of the Central Tertiary Basin of Svalbard: evidence from the thermal evolution and basin modeling. In: Circum-Arctic Structural Events: Tectonic Evolution of the Arctic Margins and Trans-Arctic Links with Adjacent Orogens, 541. https://doi.org/10.1130/2018.2541(09).
Dörr, N., Lisker, F., Piepjohn, K., Spiegel, C., 2019. Cenozoic development of northern Svalbard based on thermochronological data. Terra Nova 31 (3), 306–315. https://doi.org/10.1111/ter.12402.
Døssing, A., Japsen, P., Watts, A.B., Nielsen, T., Jokat, W., Thybo, H., Dahl-Jensen, T., 2016. Miocene uplift of the NE Greenland margin linked to plate tectonics: Seismic evidence from the Greenland Fracture Zone, NE Atlantic. Tectonics 35 (2), 257–282. https://doi.org/10.1002/2015TC004079.
Døssing, A., Gaina, C., Brozena, J.M., 2017. Building and breaking a large igneous province: An example from the High Arctic. Geophys. Res. Lett. 44 (12), 6011–6019. https://doi.org/10.1002/2016GL072420.
Dow, W.G., 1977. Kerogen studies and geological interpretations. J. Geochem. Explor. 7, 79–99. https://doi.org/10.1016/0375-6742(77)90078-4.
Dowdeswell, J.A., Cofaigh, C.Ó., 2002. Glacier-influenced sedimentation on high-latitude continental margins: introduction and overview. Geol. Soc. Lond. Spec. Publ. 203 (1), 1–9. https://doi.org/10.1144/GSL.SP.2002.203.01.01.
Dowdeswell, J.A., Hogan, K., Evans, J., Noormets, R., Cofaigh, Ó., C. and Ottesen, D., 2010. Past ice-sheet flow east of Svalbard inferred from streamlined subglacial landforms. Geology 38 (2), 163–166. https://doi.org/10.1130/G30621.1.
Dowdeswell, J.A., Ottesen, D., Rise, L., 2010. Rates of sediment delivery from the Fennoscandian Ice Sheet through an ice age. Geology 38 (1), 3–6. https://doi.org/10.1130/G25523.1.
Dowdeswell, J.A., Canals, M., Jakobsson, M., Todd, B., Dowdeswell, E.K., Hogan, K., 2016. The variety and distribution of submarine glacial landforms and implications for ice-sheet reconstruction. Geol. Soc. Lond. Mem. 46 (1), 519–552. https://doi.org/10.1144/M46.183.
Duran, E.R., di Primio, R., Anka, Z., Stoddart, D., Horsfield, B., 2013. 3D-basin modelling of the Hammerfest Basin (southwestern Barents Sea): A quantitative assessment of petroleum generation, migration and leakage. Mar. Pet. Geol. 45, 281–303. https://doi.org/10.1016/j.marpetgeo.2013.04.023.
Eide, C.H., Klausen, T.G., Katkov, D., Suslova, A.A., Helland-Hansen, W., 2017. Linking an Early Triassic delta to antecedent topography: Source-to-sink study of the southwestern Barents Sea margin. Geol. Soc. Am. Bull. https://doi.org/10.1130/B31639.1.
Eidvin, T., Jansen, E., Riis, F., 1993. Chronology of Tertiary fan deposits off the western Barents Sea: implications for the uplift and erosion history of the Barents Shelf. Mar. Geol. 112 (1), 109–131. https://doi.org/10.1016/0025-3227(93)90164-Q.
Eidvin, T., Goll, R.M., Grogan, P., Smelror, M., Ulleberg, K., 1998. The Pleistocene to Middle Eocene stratigraphy and geological evolution of the western Barents Sea continental margin at well site 7316/5-1 (Bjørnøya West area). Nor. Geol. Tidsskr. 78, 99–124.
Eikelmann, I.E.S., 2017. Shallow stratigraphic cores NW of Bjørnøya, results and implications. UiT Norges Arktiske Univ.. M.Sc. Thesis. https://hdl.handle.net/10037/11069
Eiken, O., 1994. Seismic Atlas of Western Svalbard: A Selection of Regional Seismic Transects. Norsk Polarinstitutt Årbok. http://hdl.handle.net/11250/2396881.
Eiken, O., Hinz, K., 1993. Contourites in the Fram Strait. Sediment. Geol. 82 (1-4), 15–32. https://doi.org/10.1016/0037-0738(93)90110-Q.
Eldholm, O., Faleide, J.I., Myhre, A.M., 1987. Continent-ocean transition at the western Barents Sea/Svalbard continental margin. Geology 15 (12), 1118–1122. https://doi.org/10.1130/0091-7613(1987)15<1118:CTATWB>2.0.CO;2.
Eldrett, J.S., Harding, I.C., Wilson, P.A., Butler, E., Roberts, A.P., 2007. Continental ice in Greenland during the Eocene and Oligocene. Nature 446 (7132), 176–179. https://doi.org/10.1038/nature05591.
Elger, J., Berndt, C., Krastel, S., Piper, D.J., Gross, F., Geissler, W.H., 2017. Chronology of the Fram Slide Complex offshore NW Svalbard and its implications for local and regional slope stability. Mar. Geol. 393, 141–155. https://doi.org/10.1016/j.margeo.2016.11.003.
Elverhøi, A., Hooke, R.L., Solheim, A., 1998. Late Cenozoic erosion and sediment yield from the Svalbard–Barents Sea region: Implications for understanding erosion of glacierized basins. Quat. Sci. Rev. 17 (1), 209–241. https://doi.org/10.1016/S0277-3791(97)00070-X.
Engen, Ø., Faleide, J.I., Dyreng, T.K., 2008. Opening of the Fram Strait gateway: a review of plate tectonic constraints. Tectonophysics 450 (1), 51–69. https://doi.org/10.1016/j.tecto.2008.01.002.
England, P., Molnar, P., 1990. Surface uplift, uplift of rocks, and exhumation of rocks. Geology 18 (12), 1173–1177. https://doi.org/10.1130/0091-7613(1990)018<1173:SUUORA>2.3.CO;2.
Estrada, S., Damaske, D., Henjes-Kunst, F., Schreckenberger, B., Oakey, G.N., Piepjohn, K., Eckelmann, K., Linnemann, U., 2016. Multistage Cretaceous magmatism in the northern coastal region of Ellesmere Island and its relation to the formation of Alpha Ridge–evidence from aeromagnetic, geochemical and geochronological data. Nor. J. Geol. 96 (2), 65–95. https://doi.org/10.17850/njg96-2-03.
Faleide, J., Myhre, A., Eldholm, O., 1988. Early Tertiary volcanism at the western Barents Sea margin. Geol. Soc. Lond. Spec. Publ. 39 (1), 135–146. https://doi.org/10.1144/GSL.SP.1988.039.01.13.
Faleide, J.I., Vågnes, E., Gudlaugsson, S.T., 1993. Late Mesozoic-Cenozoic evolution of the south-western Barents Sea in a regional rift-shear tectonic setting. Mar. Pet. Geol. 10 (3), 186–214. https://doi.org/10.1016/0264-8172(93)90104-Z.
Faleide, J.I., Solheim, A., Fiedler, A., Hjelstuen, B.O., Andersen, E.S., Vanneste, K., 1996. Late Cenozoic evolution of the western Barents Sea-Svalbard continental margin. Glob. Planet. Chang. 12 (1), 53–74. https://doi.org/10.1016/0921-8181(95)00012-7.
Faleide, J.I., Tsikalas, F., Breivik, A.J., Mjelde, R., Ritzmann, O., Engen, O., Wilson, J., Eldholm, O., 2008. Structure and evolution of the continental margin off Norway and the Barents Sea. Episodes 31 (1), 82–91. https://doi.org/10.18814/epiiugs/2008/v31i1/012.
Faleide, J.I., Bjørlykke, K., Gabrielsen, R.H., 2015. Geology of the Norwegian continental shelf. In: Petroleum Geoscience. Springer, pp. 603–637.
Faleide, J.I., Pease, V., Curtis, M., Klitzke, P., Minakov, A., Scheck-Wenderoth, M., Kostyuchenko, S., Zayonchek, A., 2018. Tectonic implications of the lithospheric structure across the Barents and Kara shelves. Geol. Soc. Lond. Spec. Publ. 460 (1), 285–314. https://doi.org/10.1144/SP460.18.
Faleide, T.S., Midtkandal, I., Planke, S., Corseri, R., Faleide, J.I., Serck, C.S., Nystuen, J. P., 2019. Characterisation and development of Early Cretaceous shelf platform deposition and faulting in the Hoop area, southwestern Barents Sea-constrained by high-resolution seismic data. Nor. J. Geol. 99 https://doi.org/10.17850/njg99-3-7.
Fiedler, A., Faleide, J.I., 1996. Cenozoic sedimentation along the southwestern Barents Sea margin in relation to uplift and erosion of the shelf. Glob. Planet. Chang. 12 (1), 75–93. https://doi.org/10.1016/0921-8181(95)00013-5.
Fjeldskaar, W., Amantov, A., 2018. Effects of glaciations on sedimentary basins. J. Geodyn. 118, 66–81. https://doi.org/10.1016/j.jog.2017.10.005.
Gabrielsen, R.H., Faerseth, R.B., Jensen, L.N., 1990. Structural Elements of the Norwegian Continental Shelf. Pt. 1. The Barents Sea Region. NPD Bull., p. 6
Gabrielsen, R., Kløvjan, O.S., Haugsbø, H., Midbøe, P.S., Nøttvedt, A., Rasmussen, E., Skott, P., 1992. A structural outline of Forlandsundet Graben, Prins Karls Forland, Svalbard. Nor. Geol. Tidsskr. 72, 105–120.

Gabrielsen, R.H., Grunnaleite, I., Rasmussen, E., 1997. Cretaceous and tertiary inversion in the Bjørnøyrenna Fault Complex, south-western Barents Sea. Mar. Pet. Geol. 14 (2), 165–178. https://doi.org/10.1016/S0264-8172(96)00064-5.
Gac, S., Klitzke, P., Minakov, A., Faleide, J.I., Scheck-Wenderoth, M., 2016. Lithospheric strength and elastic thickness of the Barents Sea and Kara Sea region. Tectonophysics 691, 120–132. https://doi.org/10.1016/j.tecto.2016.04.028.
Gac, S., Hansford, P.A., Faleide, J.I., 2018. Basin modelling of the SW Barents Sea. Mar. Pet. Geol. 95, 167–187. https://doi.org/10.1016/j.marpetgeo.2018.04.022.
Gac, S., Minakov, A., Shephard, G.E., Faleide, J.I., Planke, S., 2020. Deformation Analysis in the Barents Sea in Relation to Paleogene Transpression Along the Greenland-Eurasia Plate Boundary. Tectonics 39 (10), e2020TC006172. https://doi.org/10.1029/2020TC006172.
Gebhardt, A.C., Geissler, W.H., Matthiessen, J., Jokat, W., 2014. Changes in current patterns in the Fram Strait at the Pliocene/Pleistocene boundary. Quat. Sci. Rev. 92, 179–189. https://doi.org/10.1016/j.quascirev.2013.07.015.
Geissler, W., Jokat, W., Brekke, H., 2011. The Yermak Plateau in the Arctic Ocean in the light of reflection seismic data-implication for its tectonic and sedimentary evolution. Geophys. J. Int. 187 (3), 1334–1362. https://doi.org/10.1111/j.1365-246X.2011.05197.x.
Giannenas, P.A., 2018. The Structural Development of the Vestbakken Volcanic Province, Western Barents Sea. Relation Between Faults and Folds. University of Oslo. http://urn.nb.no/URN:NBN:no-66933.
Gilmullina, A., Klausen, T.G., Paterson, N.W., Suslova, A., Haug Eide, C., 2021. Regional correlation and seismic stratigraphy of Triassic Strata in the Greater Barents Sea: implications for sediment transport in Arctic basins. Basin Res. https://doi.org/10.1111/bre.12526 in press.
Green, P., Duddy, I., 2010. Synchronous exhumation events around the Arctic including examples from Barents Sea and Alaska North Slope. Geol. Soc. Lond. Pet. Geol. Conf. Ser. 7, 633–644. https://doi.org/10.1144/0070633.
Green, P., Duddy, I., Gleadow, A., Tingate, P., Laslett, G., 1986. Thermal annealing of fission tracks in apatite: 1. A qualitative description. Chem. Geol. Isotope Geosci. Sect. 59, 237–253. https://doi.org/10.1016/0168-9622(86)90074-6.
Green, P.F., Duddy, I.R., Hegarty, K.A., 2002. Quantifying exhumation from apatite fission-track analysis and vitrinite reflectance data: precision, accuracy and latest results from the Atlantic margin of NW Europe. Geol. Soc. Lond. Spec. Publ. 196 (1), 331–354. https://doi.org/10.1144/GSL.SP.2002.196.01.18.
Green, P.F., Japsen, P., Chalmers, J.A., Bonow, J.M., Duddy, I.R., 2018. Post-breakup burial and exhumation of passive continental margins: Seven propositions to inform geodynamic models. Gondwana Res. 53, 58–81. https://doi.org/10.1016/j.gr.2017.03.007.
Grundvåg, S.-A., Olaussen, S., 2017. Sedimentology of the Lower Cretaceous at Kikutodden and Keilhaufjellet, southern Spitsbergen: implications for an onshore–offshore link. Polar Res. 36, 1. https://doi.org/10.1080/17518369.2017.1302124.
Grundvåg, S.-A., Marin, D., Kairanov, B., Śliwińska, K., Nøhr-Hansen, H., Jelby, M.E., Escalona, A., Olaussen, S., 2017. The Lower Cretaceous succession of the northwestern Barents Shelf: onshore and offshore correlations. Mar. Pet. Geol. 86, 834–857. https://doi.org/10.1016/j.marpetgeo.2017.06.036.
Grundvåg, S.-A., Jelby, M.E., Śliwińska, K.K., Nøhr-Hansen, H., Aadland, T., Sandvik, S. E., Tennvassås, I., Engen, T., Olaussen, S., 2019. Sedimentology and palynology of the Lower Cretaceous succession of central Spitsbergen: integration of subsurface and outcrop data. Nor. J. Geol. 99 (2) https://doi.org/10.17850/njg006.
Guarnieri, P., 2015. Pre-break-up palaeostress state along the East Greenland margin. J. Geol. Soc. 172 (6), 727–739. https://doi.org/10.1144/jgs2015-053.
Haq, B.U., Hardenbol, J., Vail, P.R., 1987. Chronology of fluctuating sea levels since the Triassic. Science 235 (4793), 1156–1167. https://doi.org/10.1126/science.235.4793.1156.
Harishidayat, D., Omosanya, K.O., Johansen, S.E., Eruteya, O.E., Niyazi, Y., 2018. Morphometric analysis of sediment conduits on a bathymetric high: Implications for palaeoenvironment and hydrocarbon prospectivity. Basin Res. 30 (5), 1015–1041. https://doi.org/10.1111/bre.12291.
Harishidayat, D., Johansen, S.E., Batchelor, C., Omosanya, K.O., Ottaviani, L., 2020. Pliocene-Pleistocene glacimarine shelf to slope processes in the southwestern Barents Sea. Basin Res. https://doi.org/10.1111/bre.12516.
Harland, W.B., 1969. Contribution of Spitsbergen to Understanding of Tectonic Evolution of North Atlantic Region: Chapter 58: Arctic Regions.
Helland-Hansen, W., 2010. Facies and stacking patterns of shelf-deltas within the Palaeogene Battfjellet Formation, Nordenskiöld Land, Svalbard: implications for subsurface reservoir prediction. Sedimentology 57 (1), 190–208. https://doi.org/10.1111/j.1365-3091.2009.01102.x.
Helland-Hansen, W., Grundvåg, S.A., 2020. The Svalbard Eocene-Oligocene (?) Central Basin succession: Sedimentation patterns and controls. Basin Res. https://doi.org/10.1111/bre.12492.
Hendriks, B.W., Andriessen, P.A., 2002. Pattern and timing of the post-Caledonian denudation of northern Scandinavia constrained by apatite fission-track thermochronology. Geol. Soc. Lond. Spec. Publ. 196 (1), 117–137. https://doi.org/10.1144/GSL.SP.2002.196.01.08.
Henriksen, E., Bjørnseth, H., Hals, T., Heide, T., Kiryukhina, T., Kløvjan, O., Larssen, G., Ryseth, A., Rønning, K., Sollid, K., 2011. Uplift and erosion of the greater Barents Sea: impact on prospectivity and petroleum systems. Geol. Soc. Lond. Mem. 35 (1), 271–281. https://doi.org/10.1144/M35.17.
Henriksen, E., Ryseth, A., Larssen, G., Heide, T., Rønning, K., Sollid, K., Stoupakova, A., 2011. Tectonostratigraphy of the greater Barents Sea: implications for petroleum systems. Geol. Soc. Lond. Mem. 35 (1), 163–195. https://doi.org/10.1144/M35.10.
Hjelstuen, B.O., Sejrup, H.P., 2020. Latitudinal variability in the Quaternary development of the Eurasian ice sheets—Evidence from the marine domain. Geology. https://doi.org/10.1130/G48106.1.
Hjelstuen, B.O., Elverhøi, A., Faleide, J.I., 1996. Cenozoic erosion and sediment yield in the drainage area of the Storfjorden Fan. Glob. Planet. Chang. 12 (1), 95–117. https://doi.org/10.1016/0921-8181(95)00014-3.
Hjelstuen, B.O., Nygård, A., Sejrup, H.P., Haflidason, H., 2012. Q uaternary denudation of southern F ennoscandia–evidence from the marine realm. Boreas 41 (3), 379–390. https://doi.org/10.1111/j.1502-3885.2011.00239.x.
Hokstad, K., Tašárová, Z.A., Clark, S.A., Kyrkjebø, R., Duffaut, K., Fichler, C., Wiik, T., 2017. Radiogenic heat production in the crust from inversion of gravity and magnetic data. Nor. J. Geol. 97 (3), 241–254. https://doi.org/10.17850/njg97-3-04.
Huuse, M., 2002. Cenozoic uplift and denudation of southern Norway: insights from the North Sea Basin. Geol. Soc. Lond. Spec. Publ. 196 (1), 209–233. https://doi.org/10.1144/GSL.SP.2002.196.01.13.
Indrevær, K., Gabrielsen, R.H., Faleide, J.I., 2017. Early Cretaceous synrift uplift and tectonic inversion in the Loppa High area, southwestern Barents Sea, Norwegian shelf. J. Geol. Soc. 174 (2), 242–254. https://doi.org/10.1144/jgs2016-066.
Indrevær, K., Gac, S., Gabrielsen, R.H., Faleide, J.I., 2018. Crustal-scale subsidence and uplift caused by metamorphic phase changes in the lower crust: a model for the evolution of the Loppa High area, SW Barents Sea from late Paleozoic to Present. J. Geol. Soc. 175 (3), 497–508. https://doi.org/10.1144/jgs2017-063.
Jackson, H.R., Johnson, G.L., Sundvor, E., Myhre, A.M., 1984. The Yermak Plateau: formed at a triple junction. J. Geoph. Res. Solid Earth 89 (B5), 3223–3232. https://doi.org/10.1029/JB089iB05p03223.
Jakobsson, M., Backman, J., Rudels, B., Nycander, J., Frank, M., Mayer, L., Jokat, W., Sangiorgi, F., O'Regan, M., Brinkhuis, H., 2007. The early Miocene onset of a ventilated circulation regime in the Arctic Ocean. Nature 447 (7147), 986–990. https://doi.org/10.1038/nature05924.
Jakobsson, M., Mayer, L.A., Bringensparr, C., Castro, C.F., Mohammad, R., Johnson, P., Ketter, T., Accettella, D., Amblas, D., An, L., 2020. The international bathymetric chart of the Arctic Ocean version 4.0. Scientific Data 7 (1), 1–14. https://doi.org/10.1038/s41597-020-0520-9.
Japsen, P., 2000. Investigation of multi-phase erosion using reconstructed shale trends based on sonic data. Sole Pit axis, North Sea. Glob. Planet. Chang. 24 (3-4), 189–210. https://doi.org/10.1016/S0921-8181(00)00008-4.
Japsen, P., Chalmers, J.A., 2000. Neogene uplift and tectonics around the North Atlantic: overview. Glob. Planet. Chang. 24 (3-4), 165–173. https://doi.org/10.1016/S0921-8181(00)00006-0.
Japsen, P., Green, P., Bonow, J., Rasmussen, E., Chalmers, J., Kjennerud, T., 2010. Episodic uplift and exhumation along North Atlantic passive margins: implications for hydrocarbon prospectivity. Geol. Soc. Lond. Pet. Geol. Conf. Seri. 7 (1), 979–1004. https://doi.org/10.1144/0070979.
Japsen, P., Chalmers, J.A., Green, P.F., Bonow, J.M., 2012. Elevated, passive continental margins: Not rift shoulders, but expressions of episodic, post-rift burial and exhumation. Glob. Planet. Chang. 90, 73–86. https://doi.org/10.1016/j.gloplacha.2011.05.004.
Johansen, N.J., 2016. Regional Net Erosion Estimations and Implications for Seismic AVO Signatures in the Western Barents Sea. NTNU. http://hdl.handle.net/11250/2433690.
Johansen, S.E., Gabrielsen, P.T., 2015. Interpretation of marine CSEM and marine MT data for hydrocarbon prospecting. In: Pet. Geosci. Springer, pp. 515–544. https://doi.org/10.1007/978-3-642-34132-8_20.
Jokat, W., Uenzelmann-Neben, G., Kristoffersen, Y., Rasmussen, T., 1992. Lomonosov Ridge—A double-sided continental margin. Geology 20 (10), 887–890. https://doi.org/10.1130/0091-7613(1992)020<0887:LRADSC>2.3.CO;2.
Kairanov, B., Escalona, A., Mordasova, A., Śliwińska, K., Suslova, A., 2018. Early Cretaceous tectonostratigraphic evolution of the north central Barents Sea. J. Geodyn. 119, 183–198. https://doi.org/10.1016/j.jog.2018.02.009.
Karasik, A., 1968. Magnetic anomalies of the Gakkel Ridge and origin of the Eurasia Subbasin of the Arctic Ocean. Geophys. Methods Prospect. Arctic 5, 8–19.
King, E.L., Sejrup, H.P., Haflidason, H., Elverhøi, A., Aarseth, I., 1996. Quaternary seismic stratigraphy of the North Sea Fan: glacially-fed gravity flow aprons, hemipelagic sediments, and large submarine slides. Mar. Geol. 130 (3-4), 293–315. https://doi.org/10.1016/0025-3227(95)00168-9.
Klausen, T.G., Ryseth, A.E., Helland-Hansen, W., Gawthorpe, R., Laursen, I., 2015. Regional development and sequence stratigraphy of the Middle to Late Triassic Snadd formation, Norwegian Barents Sea. Mar. Pet. Geol. 62, 102–122. https://doi.org/10.1016/j.marpetgeo.2015.02.004.
Klausen, T.G., Müller, R., Poyatos-Moré, M., Olaussen, S., Stueland, E., 2019. Tectonic, provenance and sedimentological controls on reservoir characteristics in the Upper Triassic to Middle Jurassic Realgrunnen Subgroup–Southwest Barents Sea. Geol. Soc. Lond. Spec. Publ. 495. SP495-2018-165.
Kleman, J., Stroeven, A.P., 1997. Preglacial surface remnants and Quaternary glacial regimes in northwestern Sweden. Geomorphology 19 (1-2), 35–54. https://doi.org/10.1016/S0169-555X(96)00046-3.
Klitzke, P., Faleide, J., Scheck-Wenderoth, M., Sippel, J., 2015. A lithosphere-scale structural model of the Barents Sea and Kara Sea region. Solid Earth 6 (1), 153–172. https://doi.org/10.5194/se-6-153-2015.
Knies, J., Gaina, C., 2008. Middle Miocene ice sheet expansion in the Arctic: Views from the Barents Sea. Geochem. Geophys. Geosyst. 9 (2) https://doi.org/10.1029/2007GC001824.
Knies, J., Matthiessen, J., Vogt, C., Laberg, J.S., Hjelstuen, B.O., Smelror, M., Larsen, E., Andreassen, K., Eidvin, T., Vorren, T.O., 2009. The Plio-Pleistocene glaciation of the Barents Sea–Svalbard region: a new model based on revised chronostratigraphy. Quat. Sci. Rev. 28 (9), 812–829. https://doi.org/10.1016/j.quascirev.2008.12.002.

Knutsen, S.-M., Vorren, T.O., 1991. Early cenozoic sedimentation in the Hammerfest Basin. Mar. Geol. 101 (1-4), 31–48.
Kristensen, T.B., Rotevatn, A., Marvik, M., Henstra, G.A., Gawthorpe, R.L., Ravnås, R., 2018. Structural evolution of sheared margin basins: the role of strain partitioning. Sørvestsnaget Basin, Norwegian Barents Sea. Basin Res. 30 (2), 279–301. https://doi.org/10.1111/bre.12253.
Kristensen, T.B., Rotevatn, A., Marvik, M., Henstra, G.A., Gawthorpe, R.L., Ravnås, R., 2020. Quantitative analysis of fault and fold growth in a salt-bearing transtensional basins: the Sørvestsnaget Basin, Western Barents Sea. Geol. Soc. Lond. Spec. Publ. 495 https://doi.org/10.1144/SP495-2020-123.
Kristoffersen, Y., 1990. On the Tectonic Evolution and Paleoceanographic Significance of the Fram Strait gateway, Geological History of the Polar Oceans: Arctic Versus Antarctic. Springer, pp. 63–76. https://doi.org/10.1007/978-94-009-2029-3_4.
Kristoffersen, Y., Ohta, Y., Hall, J., 2020. On the the origin of the Yermak Plateau north of Svalbard, Arctic Ocean. Nor. J. Geol. https://doi.org/10.17850/njg100-1-5.
Ktenas, D., Henriksen, E., Meisingset, I., Nielsen, J.K., Andreassen, K., 2017. Quantification of the magnitude of net erosion in the southwest Barents Sea using sonic velocities and compaction trends in shales and sandstones. Mar. Pet. Geol. https://doi.org/10.1016/j.marpetgeo.2017.09.019.
Ktenas, D., Meisingset, I., Henriksen, E., Nielsen, J.K., 2019. Estimation of net apparent erosion in the SW Barents Sea by applying velocity inversion analysis. Pet. Geosci. 25 (2), 169–187. https://doi.org/10.1144/petgeo2018-002.
Laberg, J., Vorren, T., 1995. Late Weichselian submarine debris flow deposits on the Bear Island Trough mouth fan. Mar. Geol. 127 (1), 45–72. https://doi.org/10.1016/0025-3227(95)00055-4.
Laberg, J., Vorren, T., 1996. The glacier-fed fan at the mouth of Storfjorden trough, western Barents Sea: a comparative study. Geol. Rundsch. 85 (2), 338–349. https://doi.org/10.1007/BF02422239.
Laberg, J., Vorren, T., 1996. The Middle and Late Pleistocence evolution and the Bear Island Trough Mouth Fan. Glob. Planet. Chang. 12 (1), 309–330. https://doi.org/10.1016/0921-8181(95)00026-7.
Laberg, J.S., Vorren, T.O., 2000. Flow behaviour of the submarine glacigenic debris flows on the Bear Island Trough Mouth Fan, western Barents Sea. Sedimentology 47 (6), 1105–1117. https://doi.org/10.1046/j.1365-3091.2000.00343.x.
Laberg, J., Vorren, T., Knutsen, S.-M., 1999. The Lofoten contourite drift off Norway. Mar. Geol. 159 (1), 1–6. https://doi.org/10.1016/S0025-3227(98)00198-4.
Laberg, J.S., Dahlgren, T., Vorren, T.O., Haflidason, H., Bryn, P., 2001. Seismic analyses of Cenozoic contourite drift development in the Northern Norwegian Sea. Mar. Geophys. Res. 22 (5), 401–416. https://doi.org/10.1023/A:1016347632294.
Laberg, J.S., Stoker, M.S., Dahlgren, K.T., de Haas, H., Haflidason, H., Hjelstuen, B.O., Nielsen, T., Shannon, P.M., Vorren, T.O., van Weering, T.C., 2005. Cenozoic alongslope processes and sedimentation on the NW European Atlantic margin. Mar. Pet. Geol. 22 (9), 1069–1088. https://doi.org/10.1016/j.marpetgeo.2005.01.008.
Laberg, J., Eilertsen, R., Vorren, T., 2009. The paleo–ice stream in Vestfjorden, north Norway, over the last 35 ky: Glacial erosion and sediment yield. Geol. Soc. Am. Bull. 121 (3-4), 434–447. https://doi.org/10.1130/B26277.1.
Laberg, J.S., Andreassen, K., Knies, J., Vorren, T.O., Winsborrow, M., 2010. Late Pliocene–Pleistocene development of the Barents Sea ice sheet. Geology 38 (2), 107–110. https://doi.org/10.1130/G30193.1.
Laberg, J.S., Andreassen, K., Vorren, T.O., 2012. Late Cenozoic erosion of the high-latitude southwestern Barents Sea shelf revisited. Geol. Soc. Am. Bull. 124 (1-2), 77–88. https://doi.org/10.1130/B30340.1.
Laberg, J.S., Forwick, M., Husum, K., 2017. New geophysical evidence for a revised maximum position of part of the NE sector of the Greenland ice sheet during the last glacial maximum. Arktos 3 (1), 3. https://doi.org/10.1007/s41063-017-0029-4.
Lander, R.H., Walderhaug, O., 1999. Predicting porosity through simulating sandstone compaction and quartz cementation. AAPG Bull. 83 (3), 433–449. https://doi.org/10.1306/00AA9BC4-1730-11D7-8645000102C1865D.
Larsen, H., Saunders, A., Clift, P., Beget, J., Wei, W., Spezzaferri, S., 1994. Seven million years of glaciation in Greenland. Science 264 (5161), 952–955. https://doi.org/10.1126/science.264.5161.952.
Lasabuda, A., 2018. Cenozoic tectonosedimentary development and erosion estimates for the Barents Sea continental margin. In: Norwegian Arctic. UiT - The Arctic University of Norway, Tromsø. Doctoral dissertation Thesis. http://hdl.handle.net/10037/12800.
Lasabuda, A., Geissler, W.H., Laberg, J.S., Knutsen, S.-M., Rydningen, T.A., Berglar, K., 2018. Late Cenozoic erosion estimates for the northern Barents Sea: Quantifying glacial sediment input to the Arctic Ocean. Geochemistry, Geophysics, Geosystems 19. https://doi.org/10.1029/2018GC007882.
Lasabuda, A., Laberg, J.S., Knutsen, S.-M., Høgseth, G., 2018. Early to middle Cenozoic paleoenvironment and erosion estimates of the southwestern Barents Sea: Insights from a regional mass-balance approach. Mar. Pet. Geol. 96, 501–521. https://doi.org/10.1016/j.marpetgeo.2018.05.039.
Lasabuda, A., Laberg, J.S., Knutsen, S.-M., Safronova, P.A., 2018. Cenozoic tectonostratigraphy and pre-glacial erosion: a mass-balance study of the northwestern Barents Sea margin, Norwegian Arctic. J. Geodyn. https://doi.org/10.1016/j.jog.2018.03.004.
Leever, K.A., Gabrielsen, R.H., Faleide, J.I., Braathen, A., 2011. A transpressional origin for the West Spitsbergen fold-and-thrust belt: Insight from analog modeling. Tectonics 30 (2). https://doi.org/10.1029/2010TC002753.
Licciardi, A., Gallagher, K., Clark, S., 2019. Estimating uncertainties on net erosion from well-log porosity data. Basin Res. 32 (1), 51–67. https://doi.org/10.1111/bre.12366.
Lidmar-Bergström, K., Näslund, J.-O., Ebert, K., Neubeck, T., Bonow, J.M., 2007. Cenozoic landscape development on the passive margin of northern Scandinavia. Norw. J. Geol./Norsk Geologisk Forening 87.
Liu, X., Galloway, W.E., 1997. Quantitative determination of Tertiary sediment supply to the North Sea Basin. AAPG Bull. 81 (9), 1482–1509. https://doi.org/10.1306/3B05BB28-172A-11D7-8645000102C1865D.
Løseth, H., Lippard, S., Sættem, J., Fanavoll, S., Fjerdingstad, V., Leith, T., Ritter, U., Smelror, M., 1993. Cenozoic uplift and erosion of the Barents Sea—Evidence from the Svalis Dome area. In: Norwegian Petroleum Society Special Publications. Elsevier, pp. 643–664. https://doi.org/10.1016/B978-0-444-88943-0.50042-3.
Løtveit, I.F., Fjeldskaar, W., Sydnes, M., 2019. Tilting and flexural stresses in basins due to glaciations—An example from the Barents Sea. Geosciences 9 (11), 474. https://doi.org/10.3390/geosciences9110474.
Lucchi, R., Camerlenghi, A., Rebesco, M., Colmenero-Hidalgo, E., Sierro, F., Sagnotti, L., Urgeles, R., Melis, R., Morigi, C., Bárcena, M.-A., 2013. Postglacial sedimentary processes on the Storfjorden and Kveithola trough mouth fans: Significance of extreme glacimarine sedimentation. Glob. Planet. Chang. 111, 309–326. https://doi.org/10.1016/j.gloplacha.2013.10.008.
Lundin, E.R., Doré, A.G., 2018. Non-Wilsonian break-up predisposed by transforms: examples from the North Atlantic and Arctic. Geol. Soc. Lond. Spec. Publ. 470 https://doi.org/10.1144/SP470.6.
Lutz, R., Franke, D., Berglar, K., Heyde, I., Schreckenberger, B., Klitzke, P., Geissler, W. H., 2018. Evidence for mantle exhumation since the early evolution of the slow-spreading Gakkel Ridge, Arctic Ocean. J. Geodyn. https://doi.org/10.1016/j.jog.2018.01.014.
Maher, J., Harmon, D., 2001. Manifestations of the Cretaceous High Arctic large igneous province in Svalbard. J. Geol. 109 (1), 91–104. https://doi.org/10.1086/317960.
Manum, S.B., Throndsen, T., 1978. Rank of coal and dispersed organic matter and its geological bearing in the Spitsbergen Tertiary. Norsk Polarinstitutt Årbok 1977, 159–177.
Marín, D., Escalona, A., Grundvåg, S.-A., Nøhr-Hansen, H., Kairanov, B., 2018. Effects of adjacent fault systems on drainage patterns and evolution of uplifted rift shoulders: the Lower Cretaceous in the Loppa High, southwestern Barents Sea. Mar. Pet. Geol. 94, 212–229. https://doi.org/10.1016/j.marpetgeo.2018.04.009.
Marín, D., Helleren, S., Escalona, A., Olaussen, S., Cedeño, A., Nøhr-Hansen, H., Ohm, S., 2020. The Middle Jurassic to lowermost Cretaceous in the SW Barents Sea: Interplay between tectonics, coarse-grained sediment supply and organic matter preservation. Basin Res. https://doi.org/10.1111/bre.12504.
Marshall, C., Uguna, J., Large, D.J., Meredith, W., Jochmann, M., Friis, B., Vane, C., Spiro, B.F., Snape, C.E., Orheim, A., 2015. Geochemistry and petrology of palaeocene coals from Spitzbergen—Part 2: Maturity variations and implications for local and regional burial models. Int. J. Coal Geol. 143, 1–10. https://doi.org/10.1016/j.coal.2015.03.013.
Matthews, K.J., Maloney, K.T., Zahirovic, S., Williams, S.E., Seton, M., Müller, R.D., 2016. Global plate boundary evolution and kinematics since the late Paleozoic. Glob. Planet. Chang. 146, 226–250. https://doi.org/10.1016/j.gloplacha.2016.10.002.
Medvedev, S., Hartz, E.H., 2015. Evolution of topography of post-Devonian Scandinavia: Effects and rates of erosion. Geomorphology 231, 229–245. https://doi.org/10.1016/j.geomorph.2014.12.010.
Medvedev, S., Hartz, E.H., Faleide, J.I., 2018. Erosion-driven vertical motions of the circum Arctic: Comparative analysis of modern topography. J. Geodyn. 119, 62–81. https://doi.org/10.1016/j.jog.2018.04.003.
Medvedev, S., Hartz, E.H., Schmid, D.W., Zakariassen, E., Varhaug, P., 2019. Influence of glaciations on North Sea petroleum systems. Geol. Soc. Lond. Spec. Publ. 494 https://doi.org/10.1144/SP494-2018-183. SP494-2018-183.
Michael, N.A., Whittaker, A.C., Carter, A., Allen, P.A., 2014. Volumetric budget and grain-size fractionation of a geological sediment routing system: Eocene Escanilla Formation, south-central Pyrenees. Geol. Soc. Am. Bull. 126 (3-4), 585–599. https://doi.org/10.1130/B30954.1.
Midtkandal, I., Faleide, J.I., Faleide, T.S., Serck, C.S., Planke, S., Corseri, R., Dimitriou, M., Nystuen, J.P., 2019. Lower Cretaceous Barents Sea strata: epicontinental basin configuration, timing, correlation and depositional dynamics. Geol. Mag. 1–19. https://doi.org/10.1017/S0016756819000918.
Midtkandal, I., Faleide, T.S., Faleide, J.I., Planke, S., Anell, I., Nystuen, J.P., 2019. Nested intrashelf platform clinoforms—Evidence of shelf platform growth exemplified by Lower Cretaceous strata in the Barents Sea. Basin Res. https://doi.org/10.1111/bre.12377.
Minakov, A., 2018. Late Cenozoic lithosphere dynamics in Svalbard: interplay of glaciation, seafloor spreading and mantle convection. J. Geodyn. https://doi.org/10.1016/j.jog.2018.09.009.
Minakov, A., Faleide, J.I., Glebovsky, V.Y., Mjelde, R., 2012. Structure and evolution of the northern Barents-Kara Sea continental margin from integrated analysis of potential fields, bathymetry and sparse seismic data. Geophys. J. Int. 188 (1), 79–102. https://doi.org/10.1111/j.1365-246X.2011.05258.x.
Mohammedyasin, M., 2017. Two-Dimensional Seismic Interpretation and Petroleum System Modelling in the Hammerfest Basin, SW Barents Sea. J. Geol. Geophys. 6 (273), 2. https://doi.org/10.4172/2381-8719.1000273.
Mosar, J., Lewis, G., Torsvik, T., 2002. North Atlantic sea-floor spreading rates: implications for the Tertiary development of inversion structures of the Norwegian–Greenland Sea. J. Geol. Soc. 159 (5), 503–515. https://doi.org/10.1144/0016-764901-135.
Müller, R.D., Zahirovic, S., Williams, S.E., Cannon, J., Seton, M., Bower, D.J., Tetley, M. G., Heine, C., Le Breton, E., Liu, S., 2019. A global plate model including lithospheric deformation along major rifts and orogens since the Triassic. Tectonics 38 (6), 1884–1907. https://doi.org/10.1029/2018TC005462.
Naber, T., Grasby, S., Cuthbertson, J., Rayner, N., Tegner, C., 2020. New Constraints on the Age, Geochemistry, and Environmental Impact of High Arctic Large Igneous Province magmatism: Tracing the Extension of the Alpha Ridge onto Ellesmere Island, Canada. GSA Bulletin. https://doi.org/10.1130/B35792.1.

Nikishin, A.M., Petrov, E.I., Cloetingh, S., Freiman, S.I., Malyshev, N.A., Morozov, A.F., Posamentier, H.W., Verzhbitsky, V.E., Zhukov, N.N., Startseva, K., 2019. Geological structure and history of the Arctic Ocean based on new geophysical data: implications for paleoenvironment and paleoclimate. Part 2. Mesozoic to Cenozoic geological evolution. Earth-Sci. Rev., 103034 https://doi.org/10.1016/j.earscirev.2019.103034.

Nøttvedt, A., Berglund, L., Rasmussen, E., Steel, R., 1988. Some aspects of Tertiary tectonics and sedimentation along the western Barents Shelf. Geol. Soc. Lond. Spec. Publ. 39 (1), 421–425. https://doi.org/10.1144/GSL.SP.1988.039.01.37.

NPD, 2014. The 2014 NPD Lithostratigraphic Charts. The Norwegian Petroleum Directorate. Accessed 20-12-2020. https://www.npd.no/en/facts/geology/lithostratigraphy/.

NPD, 2016. Factpages. The Norwegian Petroleum Directorate. Accessed 01-09-2016. https://factpages.npd.no/.

NPD, 2018. Resource Report Exploration 2018. https://www.npd.no/globalassets/1-npd/publikasjoner/ressursrapport-2018/resource-report-2018-engelsk.pdf.

NPD, 2019. Resource Report 2019 Discovery and Fields. https://www.npd.no/globalassets/1-npd/publikasjoner/ressursrapport-2019/resource-report-2019.pdf.

NPD, 2020. FactMaps. The Norwegian Petroleum Directorate. Accessed 10-11-2020. https://factmaps.npd.no/factmaps/3_0/.

Nyberg, B., Helland-Hansen, W., Gawthorpe, R.L., Sandbakken, P., Eide, C.H., Sømme, T., Hadler-Jacobsen, F., Leiknes, S.J.S.G., 2018. Revisiting morphological relationships of modern source-to-sink segments as a first-order approach to scale ancient sedimentary systems. Sediment. Geol. 373, 111–133. https://doi.org/10.1016/j.sedgeo.2018.06.007.

Nyland, B., Jensen, L., Skagen, J., Skarpnes, O., Vorren, T., 1992. Tertiary uplift and erosion in the Barents Sea: magnitude, timing and consequences. In: Larsen, R.M., Brekke, H., Larsen, B.T., Talleras, E. (Eds.), Tectonic Modelling and Its Implication to Petroleum Geology, pp. 153–162. https://doi.org/10.1016/B978-0-444-88607-1.50015-2.

Ohm, S.E., Karlsen, D.A., Austin, T., 2008. Geochemically driven exploration models in uplifted areas: Examples from the Norwegian Barents Sea. AAPG Bull. 92 (9), 1191–1223. https://doi.org/10.1306/06180808028.

Ohm, S.E., Larsen, L., Olaussen, S., Senger, K., Birchall, T., Demchuk, T., Hodson, A., Johansen, I., Titlestad, G.O., Karlsen, D.A., 2019. Discovery of shale gas in organic rich Jurassic successions, Adventdalen, Central Spitsbergen, Norway. Norw. J. Geol. 99 (2) https://doi.org/10.17850/njg007.

Olaussen, S., Senger, K., Braathen, A., Grundvåg, S.-A., Mørk, A., 2019. You learn as long as you drill; research synthesis from the Longyearbyen CO2 Laboratory, Svalbard, Norway. Nor. J. Geol. 99 (2). https://dx.doi.org/10.17850/njg008.

Ostanin, I., Anka, Z., di Primio, R., 2017. Role of faults in hydrocarbon leakage in the Hammerfest Basin, SW Barents Sea: insights from seismic data and numerical modelling. Geosciences 7 (2), 28. https://doi.org/10.3390/geosciences7020028.

Ottesen, D., Dowdeswell, J., Rise, L., 2005. Submarine landforms and the reconstruction of fast-flowing ice streams within a large Quaternary ice sheet: the 2500-km-long Norwegian-Svalbard margin (57–80 N). Geol. Soc. Am. Bull. 117 (7-8), 1033–1050. https://doi.org/10.1130/B25577.1.

Patton, H., Andreassen, K., Bjarnadóttir, L.R., Dowdeswell, J.A., Winsborrow, M., Noormets, R., Polyak, L., Auriac, A., Hubbard, A., 2015. Geophysical constraints on the dynamics and retreat of the Barents Sea ice sheet as a paleobenchmark for models of marine ice sheet deglaciation. Rev. Geophys. 53 (4), 1051–1098. https://doi.org/10.1002/2015RG000495.

Patton, H., Hubbard, A., Andreassen, K., Winsborrow, M., Stroeven, A.P., 2016. The build-up, configuration, and dynamical sensitivity of the Eurasian ice-sheet complex to Late Weichselian climatic and oceanic forcing. Quat. Sci. Rev. 153, 97–121. https://doi.org/10.1016/j.quascirev.2016.10.009.

Patton, H., Hubbard, A., Heyman, J., Alexandropoulou, N., Lasabuda, A., Stroeven, A.P., Hall, A.M., Winsborrow, M., Sugden, D. and Andreassen, K, The profound yet transient nature of glacial erosion. in review.

Pechlivanidou, S., Cowie, P.A., Hannisdal, B., Whittaker, A.C., Gawthorpe, R.L., Pennos, C., Riiser, O.S., 2018. Source-to-sink analysis in an active extensional setting: Holocene erosion and deposition in the Sperchios rift, central Greece. Basin Res. https://doi.org/10.1111/bre.12263.

Petersen, T.G., Thomsen, T., Olaussen, S., Stemmerik, L., 2016. Provenance shifts in an evolving Eurekan foreland basin: the Tertiary Central Basin, Spitsbergen. J. Geol. Soc. 173 (4), 634–648. https://doi.org/10.1144/jgs2015-076.

Piasecka, E.D., Winsborrow, M.C., Andreassen, K., Stokes, C.R., 2016. Reconstructing the retreat dynamics of the Bjørnøyrenna Ice Stream based on new 3D seismic data from the central Barents Sea. Quat. Sci. Rev. 151, 212–227. https://doi.org/10.1016/j.quascirev.2016.09.003.

Piepjohn, K., von Gosen, W., Tessensohn, F., 2016. The Eurekan deformation in the Arctic: an outline. J. Geol. Soc. 173 (6), 1007–1024. https://doi.org/10.1144/jgs2016-081.

Poirier, A., Hillaire-Marcel, C., 2011. Improved Os-isotope stratigraphy of the Arctic Ocean. Geophys. Res. Lett. 38 (14) https://doi.org/10.1029/2011GL047953.

Prestvik, T., 1977. Cenozoic plateau lavas of Spitsbergen—A geochemical study. Arbok. Norsk Polarinstituitt 129–143.

Prøis, B.M., 2015. Late Paleocene-Earliest Eocene Prograding System in the SW Barents Sea. University of Oslo. http://urn.nb.no/URN:NBN:no-49739.

Rasmussen, E., Fjeldskaar, W., 1996. Quantification of the Pliocene-Pleistocene erosion of the Barents Sea from present-day bathymetry. Glob. Planet. Chang. 12 (1), 119–133. https://doi.org/10.1016/0921-8181(95)00015-1.

Raymo, M.E., Ruddiman, W.F., 1992. Tectonic forcing of late Cenozoic climate. Nature 359 (6391), 117–122. https://doi.org/10.1038/359117a0.

Rebesco, M., Wåhlin, A., Laberg, J.S., Schauer, U., Beszczynska-Möller, A., Lucchi, R.G., Noormets, R., Accettella, D., Zarayskaya, Y., Diviacco, P., 2013. Quaternary contourite drifts of the Western Spitsbergen margin. Deep-Sea Res. I Oceanogr. Res. Pap. 79, 156–168. https://doi.org/10.1016/j.dsr.2013.05.013.

Redfield, T., Osmundsen, P., 2013. The long-term topographic response of a continent adjacent to a hyperextended margin: a case study from Scandinavia. Geol. Soc. Am. Bull. 125 (1-2), 184–200. https://doi.org/10.1130/B30691.1.

Richardsen, G., Vorren, T.O., Tørudbakken, B.O., 1993. Post-Early Cretaceous uplift and erosion in the southern Barents Sea: a discussion based on analysis of seismic interval velocities. Nor. Geol. Tidsskr. 73 (1), 3–20. NGT_73_1_003-020.pdf.

Riis, Fridtjof, 1992. Dating and measuring of erosion, uplift and subsidence in Norway and the Norwegian shelf in glacial periods. Norsk Geologisk Tidsskrift 72 (3), 325–331.

Riis, F., 1996. Quantification of Cenozoic vertical movements of Scandinavia by correlation of morphological surfaces with offshore data. Glob. Planet. Chang. 12 (1-4), 331–357. https://doi.org/10.1016/0921-8181(95)00027-5.

Riis, F., Fjeldskaar, W., 1992. On the magnitude of the Late Tertiary and Quaternary erosion and its significance for the uplift of Scandinavia and the Barents Sea. In: Larsen, R.M., Brekke, H., Larsen, B.T., Taleraas, E. (Eds.), Structural and Tectonic Modelling and its Application to Petroleum Geology. Norw. Petrol. Soc., pp. 163–185. https://doi.org/10.1016/B978-0-444-88607-1.50016-4

Riis, F., Jensen, L.N., 1992. Introduction: measuring uplift and erosion—Proposal for a terminology. Nor. Geol. Tidsskr. 72 (3), 223–228. NGT_72_3_Spec_Issue.pdf.

Ritter, U., Duddy, I.R., Mork, A., Johansen, H., Arne, D.C., 1996. Temperature and uplift history of Bjornoya (Bear Island), Barents Sea. Pet. Geosci. 2 (2), 133–144. https://doi.org/10.1144/petgeo.2.2.133.

Rydningen, T.A., Laberg, J.S., Kolstad, V., 2016. Late Cenozoic evolution of high-gradient trough mouth fans and canyons on the glaciated continental margin offshore Troms, northern Norway—Paleoclimatic implications and sediment yield. Geol. Soc. Am. Bull. 128 (3-4), 576–596. https://doi.org/10.1130/B31302.1.

Rydningen, T.A., Høgseth, G., Lasabuda, A.P.E., Laberg, J.S., Safronova, P.A., 2020. An Early Neogene—Early Quaternary Contourite Drift System on the SW Barents Sea Continental Margin, Norwegian Arctic. G-cubed. https://doi.org/10.1029/2020GC009142.

Ryseth, A., Augustson, J.H., Charnock, M., Haugerud, O., Knutsen, S.-M., Midbøe, P.S., Opsal, J.G., Sundsbø, G., 2003. Cenozoic stratigraphy and evolution of the Sørvestsnaget Basin, southwestern Barents Sea. Nor. J. Geol. 83 (2), 107–130. NJG_83_107-130.pdf.

Safronova, P.A., Andreassen, K., Laberg, J.S., Vorren, T.O., 2012. Development and post-depositional deformation of a Middle Eocene deep-water sandy depositional system in the Sørvestsnaget Basin, SW Barents Sea. Mar. Pet. Geol. 36 (1), 83–99. https://doi.org/10.1016/j.marpetgeo.2012.06.007.

Safronova, P.A., Henriksen, S., Andreassen, K., Laberg, J.S., Vorren, T.O., 2014. Evolution of shelf-margin clinoforms and deep-water fans during the middle Eocene in the Sorvestsnaget Basin, southwest Barents Sea. AAPG Bull. 98 (3), 515–544. https://doi.org/10.1306/08221312208.

Sattar, N., Juhlin, C., Koyi, H., Ahmad, N., 2017. Seismic stratigraphy and hydrocarbon prospectivity of the Lower Cretaceous Knurr Sandstone lobes along the southern margin of Loppa High, Hammerfest Basin, Barents Sea. Mar. Pet. Geol. 85, 54–69. https://doi.org/10.1016/j.marpetgeo.2017.04.008.

Sclater, J.G., Christie, P.A., 1980. Continental stretching: An explanation of the post-Mid-Cretaceous subsidence of the central North Sea Basin. J. Geophys. Res. Solid Earth 85 (B7), 3711–3739. https://doi.org/10.1029/JB085iB07p03711.

Senger, K., Tveranger, J., Ogata, K., Braathen, A., Planke, S., 2014. Late Mesozoic magmatism in Svalbard: a review. Earth-Sci. Rev. 139, 123–144. https://doi.org/10.1016/j.earscirev.2014.09.002.

Senger, K., Brugmans, P., Grundvåg, S.-A., Jochmann, M.M., Nøttvedt, A., Olaussen, S., Skotte, A., Smyrak-Sikora, A., 2019. Petroleum, coal and research drilling onshore Svalbard: a historical perspective. Nor. J. Geol. 99 (3) https://doi.org/10.17850/njg99-3-1.

Senger, K., Birchall, T., Betlem, P., Ogata, K., Ohm, S., Olaussen, S., Paulsen, R.S., 2020. Resistivity of reservoir sandstones and organic rich shales on the Barents Shelf: implications for interpreting CSEM data. Geosci. Front. https://doi.org/10.1016/j.gsf.2020.08.007.

Smelror, M., Petrov, O., Larssen, G.B., Werner, S., 2009. Geological history of the Barents Sea. Norges Geol. Undersøkelse 1–135.

Solheim, A., Faleide, J.I., Andersen, E.S., Elverhøi, A., Forsberg, C.F., Vanneste, K., Uenzelmann-Neben, G., Channell, J.E., 1998. Late Cenozoic seismic stratigraphy and glacial geological development of the East Greenland and Svalbard–Barents Sea continental margins. Quat. Sci. Rev. 17 (1-3), 155–184. https://doi.org/10.1016/S0277-3791(97)00068-1.

Sømme, T.O., Helland-Hansen, W., Martinsen, O.J., Thurmond, J.B., 2009. Relationships between morphological and sedimentological parameters in source-to-sink systems: a basis for predicting semi-quantitative characteristics in subsurface systems. Basin Res. 21 (4), 361–387. https://doi.org/10.1111/j.1365-2117.2009.00397.x.

Sømme, T.O., Martinsen, O.J., Thurmond, J.B., 2009. Reconstructing morphological and depositional characteristics in subsurface sedimentary systems: an example from the Maastrichtian–Danian Ormen Lange system, Møre Basin, Norwegian Sea. AAPG Bull. 93 (10), 1347–1377. https://doi.org/10.1306/06010909038.

Sømme, T.O., Martinsen, O.J., Lunt, I., 2013. Linking offshore stratigraphy to onshore paleotopography: The Late Jurassic–Paleocene evolution of the south Norwegian margin. Geol. Soc. Am. Bull. 125 (7-8), 1164–1186. https://doi.org/10.1130/B30747.1.

Steel, R., Gjelberg, J., Helland-Hansen, W., Nøttvedt, A., 1985. The Tertiary strike-slip basins and orogenic belt of Spitsbergen. In: Biddle, K.T., Christie-Blick, N. (Eds.), Strike-Slip Deformation, Basin Formation, and Sedimentation. Soc. Econ. Paleo. and Mineral. (SEPM). https://doi.org/10.2110/pec.85.37.

Stephenson, R., Schiffer, C., Peace, A., Nielsen, S.B., Jess, S., 2020. Late Cretaceous-Cenozoic basin inversion and palaeostress fields in the North Atlantic-western Alpine-Tethys realm: implications for intraplate tectonics. Earth-Sci. Rev., 103252 https://doi.org/10.1016/j.earscirev.2020.103252.

Storvoll, V., Bjørlykke, K., Mondol, N.H., 2005. Velocity-depth trends in Mesozoic and Cenozoic sediments from the Norwegian Shelf. AAPG Bull. 89 (3), 359–381. https://doi.org/10.1306/10150404033.

Straume, E.O., Gaina, C., Medvedev, S., Nisancioglu, K.H., 2020. Global Cenozoic Paleobathymetry with a focus on the Northern Hemisphere Oceanic Gateways. Gondwana Res. https://doi.org/10.1016/j.gr.2020.05.011.

Sweeney, J.J., Burnham, A.K., 1990. Evaluation of a simple model of vitrinite reflectance based on chemical kinetics. AAPG Bull. 74 (10), 1559–1570. https://doi.org/10.1306/0C9B251F-1710-11D7-8645000102C1865D.

Talwani, M., Eldholm, O., 1977. Evolution of the Norwegian-Greenland sea. Geol. Soc. Am. Bull. 88 (7), 969–999. https://doi.org/10.1130/0016-7606(1977)88<969:EOTNS>2.0.CO;2.

Tegner, C., Storey, M., Holm, P.M., Thorarinsson, S., Zhao, X., Lo, C.-H., Knudsen, M.F., 2011. Magmatism and Eurekan deformation in the High Arctic large igneous province: 40Ar–39Ar age of Kap Washington Group volcanics, North Greenland. Earth Planet. Sci. Lett. 303 (3-4), 203–214. https://doi.org/10.1016/j.epsl.2010.12.047.

Thyberg, B., Jahren, J., Winje, T., Bjørlykke, K., Faleide, J.I., 2009. From mud to shale: Rock stiffening by micro-quartz cementation. First Break 27 (2). https://doi.org/10.3997/1365-2397.2009003.

Torske, T., 1972. Tertiary oblique uplift of Western Fennoscandia; crustal warping in connection with rifting and break-up of the Laurasian continent. Norges Geologiske Undersøkelse Bull. 273, 43–48.

Treiman, A.H., 2012. Eruption age of the Sverrefjellet volcano, Spitsbergen Island, Norway. Polar Res. 31 (1), 17320 https://doi.org/10.3402/polar.v31i0.17320.

Tripati, A., Darby, D., 2018. Evidence for ephemeral middle Eocene to early Oligocene Greenland glacial ice and pan-Arctic sea ice. Nat. Commun. 9 (1), 1–11. https://doi.org/10.1038/s41467-018-03180-5.

Vågnes, E., 1997. Uplift at thermo-mechanically coupled ocean – Continent transforms: modeled at the Senja Fracture Zone, southwestern Barents Sea. Geo-Mar. Lett. 17 (1), 100–109. https://doi.org/10.1007/s003670050014.

Vågnes, E., Amundsen, H.E.F., 1993. Late Cenozoic uplift and volcanism on Spitsbergen: caused by mantle convection? Geology 21 (3), 251–254. https://doi.org/10.1130/0091-7613(1993)021<0251:LCUAVO>2.3.CO;2.

Vassmyr, S., 1989. Barents Sea Conference Workshop. Harstad. Abstract.

Veire, H., Granli, J., Berger, P., Lewis, O., Hohner, M., Kvist-Lassen, T., Smith, P., Stuberg, L., 2016. The Wisting Discovery-Integrating Acoustic Measurements at Different Scales. 78th EAGE Conf. Exhib. 2016 2016 (1), 1–5. https://doi.org/10.3997/2214-4609.201601552.

Vogt, P., Taylor, P., Kovacs, L., Johnson, G., 1979. Detailed aeromagnetic investigation of the Arctic Basin. J. Geophys. Res. Solid Earth 84 (B3), 1071–1089. https://doi.org/10.1029/JB084iB03p01071.

Vorren, T.O., Laberg, J.S., 1997. Trough mouth fans—Palaeoclimate and ice-sheet monitors. Quat. Sci. Rev. 16 (8), 865–881. https://doi.org/10.1016/S0277-3791(97)00003-6.

Vorren, T., Lebesbye, E., Andreassen, K., Larsen, K.-B., 1989. Glacigenic sediments on a passive continental margin as exemplified by the Barents Sea. Mar. Geol. 85 (2), 251–272. https://doi.org/10.1016/0025-3227(89)90156-4.

Vorren, T.O., Richardsen, G., Knutsen, S.-M., Henriksen, E., 1991. Cenozoic erosion and sedimentation in the western Barents Sea. Mar. Pet. Geol. 8 (3), 317–340. https://doi.org/10.1016/0264-8172(91)90086-G.

Waghorn, K.A., Vadakkepuliyambatta, S., Plaza-Faverola, A., Johnson, J.E., Bünz, S., Waage, M., 2020. Crustal processes sustain Arctic abiotic gas hydrate and fluid flow systems. Sci. Rep. 10 (1), 1–14. https://doi.org/10.1038/s41598-020-67426-3.

Walderhaug, O., 1996. Kinetic modeling of quartz cementation and porosity loss in deeply buried sandstone reservoirs. AAPG Bull. 80 (5), 731–745. https://doi.org/10.1306/64ED88A4-1724-11D7-8645000102C1865D.

Wangen, M., 2010. Physical Principles of Sedimentary Basin Analysis. Cambridge University Press. https://doi.org/10.1017/CBO9780511711824.

Weissel, J.K., Karner, G.D., 1989. Flexural uplift of rift flanks due to mechanical unloading of the lithosphere during extension. J. Geophys. Res. Solid Earth 94 (B10), 13919–13950. https://doi.org/10.1029/JB094iB10p13919.

Wilkinson, M., 2017. Cenozoic erosion of the Scottish Highlands–Orkney–Shetland area: implications for uplift and previous sediment cover. J. Geol. Soc. 174 (2), 209–216. https://doi.org/10.1144/jgs2016-064.

Williamson, M.-C., Kellett, D., Miggins, D., Koppers, A., Carey, R., Oakey, G., Weis, D., Jokat, W., Massey, E., 2019. Age and Eruptive Style of Volcanic Rocks Dredged from the Alpha Ridge, Arctic Ocean. Geophys. Res. Abstr. 21.

Wood, R., Edrich, S., Hutchison, I., 1989. Influence of North Atlantic Tectonics on the Large-Scale Uplift of the Stappen High and Loppa High, Western Barents Shelf: Chapter 36: North Sea and Barents Shelf. AAPG Mem. 36, 559–566. https://doi.org/10.1306/M46497C36.

Zattin, M., Andreucci, B., de Toffoli, B., Grigo, D., Tsikalas, F., 2016. Thermochronological constraints to late Cenozoic exhumation of the Barents Sea Shelf. Mar. Pet. Geol. 73, 97–104. https://doi.org/10.1016/j.marpetgeo.2016.03.004.

Zieba, K.J., Grøver, A., 2016. Isostatic response to glacial erosion, deposition and ice loading. Impact on hydrocarbon traps of the southwestern Barents Sea. Mar. Pet. Geol. 78, 168–183. https://doi.org/10.1016/j.marpetgeo.2016.09.009.

Zieba, K.J., Felix, M., Knies, J., 2016. The Pleistocene contribution to the net erosion and sedimentary conditions in the outer Bear Island Trough, western Barents Sea. Arktos 2 (1), 23. https://doi.org/10.1007/s41063-016-0022-3.

Zieba, K.J., Omosanya, K.O., Knies, J., 2017. A flexural isostasy model for the Pleistocene evolution of the Barents Sea bathymetry. Nor. J. Geol. 97 (1) https://doi.org/10.17850/njg97-1-01.